

A D/A-000 285

A SURFACE FORMULATION FOR CHARACTERISTIC  
MODES OF MATERIAL BODIES

Yu Chang, et al

Syracuse University

Prepared for:

Office of Naval Research

October 1974

DISTRIBUTED BY:



National Technical Information Service  
U. S. DEPARTMENT OF COMMERCE

## UNCLASSIFIED

SECURITY CLASSIFICATION OF THIS PAGE (When Data Entered)

REPORT DOCUMENTATION PAGE		READ INSTRUCTIONS BEFORE COMPLETING FORM
1. REPORT NUMBER TR-74-7	2. GOVT ACCESSION NO.	3. RECIPIENT'S CATALOG NUMBER <b>AD/A-000 285</b>
4. TITLE (and Subtitle) <b>A SURFACE FORMULATION FOR CHARACTERISTIC MODES OF MATERIAL BODIES</b>		5. TYPE OF REPORT & PERIOD COVERED Technical Report No. 2
		6. PERFORMING ORG. REPORT NUMBER
7. AUTHOR(s) Yu Chang Roger F. Harrington		8. CONTRACT OR GRANT NUMBER(s) N00014-67-A-0378-0006
9. PERFORMING ORGANIZATION NAME AND ADDRESS Dept. of Electrical and Computer Engineering Syracuse University Syracuse, New York 13210		10. PROGRAM ELEMENT, PROJECT, TASK AREA & WORK UNIT NUMBERS NR-371-885
11. CONTROLLING OFFICE NAME AND ADDRESS Department of the Navy Office of Naval Research Arlington, Virginia 22217		12. REPORT DATE October 1974
		13. NUMBER OF PAGES
14. MONITORING AGENCY NAME & ADDRESS (if different from Controlling Office)		15. SECURITY CLASS. (of this report) Unclassified
		15a. DECLASSIFICATION/DOWNGRADING SCHEDULE
16. DISTRIBUTION STATEMENT (of this Report)  Approved for public release; distribution unlimited.		
17. DISTRIBUTION STATEMENT (of the abstract entered in Block 20, if different from Report)		
18. SUPPLEMENTARY NOTES Reproduced by NATIONAL TECHNICAL INFORMATION SERVICE U S Department of Commerce Springfield VA 22151		
19. KEY WORDS (Continue on reverse side if necessary and identify by block number) Characteristic Modes Computer Programs Electromagnetic Scattering Material Bodies Two-dimensional Fields		
20. ABSTRACT (Continue on reverse side if necessary and identify by block number)  A theory of characteristic modes for material bodies is developed using equivalent surface currents. This is in contrast to the alternative approach using induced volume currents. The mode currents form a weighted orthogonal set over the material body surface, and the mode fields form an orthogonal set over the sphere at infinity. The characteristic modes of material bodies		

**UNCLASSIFIED**

**SECURITY CLASSIFICATION OF THIS PAGE(When Data Entered)**

have most of the properties of those for perfectly conducting bodies. Formulas for the use of these modes in electromagnetic scattering problems are given. A procedure for computing the characteristic modes is developed, and applied to two-dimensional bodies. Illustrative examples of the computation of characteristic currents and scattering cross sections are given for cylinders of different material constants.

**UNCLASSIFIED**

**SECURITY CLASSIFICATION OF THIS PAGE(When Data Entered)**

## ABSTRACT

A theory of characteristic modes for material bodies is developed using equivalent surface currents. This is in contrast to the alternative approach using induced volume currents. The mode currents form a weighted orthogonal set over the material body surface, and the mode fields form an orthogonal set over the sphere at infinity. The characteristic modes of material bodies have most of the properties of those for perfectly conducting bodies. Formulas for the use of these modes in electromagnetic scattering problems are given. A procedure for computing the characteristic modes is developed, and applied to two-dimensional bodies. Illustrative examples of the computation of characteristic currents and scattering cross sections are given for cylinders of different material constants.

## CONTENTS

	Page
<b>ABSTRACT-----</b>	iii
<b>CHAPTER 1 INTRODUCTION-----</b>	1
1.1 Background-----	1
1.2 The Fundamental Operator Equation-----	2
1.3 Format-----	7
<b>CHAPTER 2 MATRIX FORMULATION-----</b>	9
2.1 Method of Moments-----	9
2.2 Expansion Functions and the Evaluation of [Z] Matrix Elements-----	13
2.3 Evaluations of [B] and [C] Matrix Elements-----	24
2.4 Evaluation of [Y] Matrix Elements-----	31
2.5 Excitation Matrix, Measurement Matrix, and Scattering Cross Sections-----	34
<b>CHAPTER 3 CHARACTERISTIC MODES - A SURFACE FORMULATION-----</b>	42
3.1 Theoretical Development-----	42
3.2 Characteristic Equation and Modal Representation-----	46
3.3 Linear Measurement-----	49
3.4 Characteristic Fields and Scattering Cross Sections-----	50
3.5 Computational Considerations-----	53
<b>CHAPTER 4 COMPUTATIONAL RESULTS-----</b>	60
<b>CHAPTER 5 DISCUSSION-----</b>	103
<b>APPENDIX A MATRIX ELEMENTS FOR PARALLEL POLARIZATION-----</b>	106
<b>APPENDIX B COMPUTER PROGRAMS-----</b>	108
<b>REFERENCES-----</b>	118

CHAPTER 1  
INTRODUCTION

1.1 Background

Characteristic modes have long been used in the analysis of radiation and scattering by dielectric and/or magnetic bodies whose surfaces coincide with coordinate surfaces in coordinate systems for which the Helmholtz equation is separable. From consideration of the scattering matrix, Garbacz [1] has shown that similar modes must exist for any material body. An extensive theory for perfectly conducting bodies was given in reference [1], but the dielectric and magnetic body case was not developed. An alternative treatment of the characteristic modes for perfectly conducting bodies, starting from the impedance operator for the conducting surface, has been given by Harrington and Mautz [2]. The computation of such modes has also been considered by Harrington and Mautz [3]. A theory of characteristic modes for dielectric bodies, magnetic bodies, and for bodies both dielectric and magnetic, has been developed by Harrington, Mautz, and Chang [4]. In this work, a theory of characteristic modes for material bodies is developed using equivalent surface currents. This is in contrast to the approach used in [4], which used the induced volume currents.

The modes are defined by a weighted eigenvalue equation in such a way that both the generalized network matrix [5] and the scattering matrix [1], [2] for the body are diagonalized. The presentation given in this work leads to explicit formulas for determining the mode currents and fields of two-dimensional objects. The formulas remain the same for dielectric bodies, magnetic bodies, and

for bodies both dielectric and magnetic. In particular, the scattering problem of a two dimensional material cylinder will be presented. This formulation of the problem is applicable to any general material body. Details are worked out only for two-dimensional problems.

### 1-2 The Fundamental Operator Equation

Let the material body be represented as in Figure 1-1.

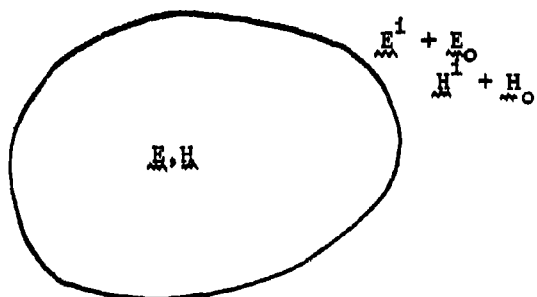


Figure 1-1. A general material body.

$\underline{\underline{H}}^1$ ,  $\underline{\underline{E}}^1$  = incident fields (Wavy underline denotes vector

$\underline{\underline{E}}$ ,  $\underline{\underline{H}}$  = inside fields      quantitics.)

$\underline{\underline{E}}_0$ ,  $\underline{\underline{H}}_0$  = outside fields

The problem of Figure 1-1 can be viewed as a linear superposition of two cases,

(I) zero field inside

(II) zero field outside.

These two cases are illustrated in Figure 1-2.

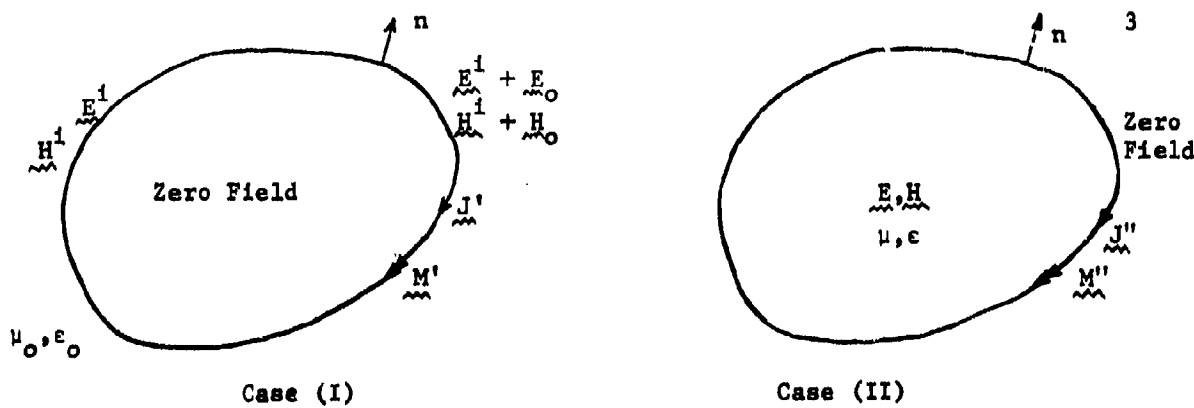


Figure 1-2. A decomposition of the original problem.

In case (I), let  $\mu_0, \epsilon_0$  be the material constants in the zero-field region, and similarly in case (II), let  $\mu, \epsilon$  be the material constants in the zero-field region. Having done so, radiation formulas [6] for unbounded space can be employed. The  $J$  and  $M$  are equivalent surface currents [6]. Since there are no actual surface currents, the following conditions should be satisfied by the equivalent currents

$$J' + J'' = 0 \quad (1-1)$$

$$M' + M'' = 0 \quad (1-2)$$

Equations (1-1) and (1-2) come from the fact that tangential components of fields are continuous across the interface in the original problem. Note that

$$\tilde{E}_0 = -j\omega A' - \nabla \phi'_e - \frac{1}{\epsilon_0} \nabla \times F' + \tilde{E}^i \quad (1-3)$$

$$\tilde{H}_0 = -j\omega F' - \nabla \phi'_m + \frac{1}{\mu_0} \nabla \times A' + \tilde{H}^i \quad (1-4)$$

and

$$\underline{\underline{E}} = -j\omega \underline{\underline{A}}'' - \nabla \phi_e'' - \frac{1}{\epsilon_0} \nabla \times \underline{\underline{F}}'' \quad (1-5)$$

$$\underline{\underline{H}} = -j\omega \underline{\underline{F}}'' - \nabla \phi_m'' + \frac{1}{\mu_0} \nabla \times \underline{\underline{A}}'' \quad (1-6)$$

and

$$\underline{\underline{E}}^s = -j\omega \underline{\underline{A}}' - \nabla \phi_e' - \frac{1}{\epsilon_0} \nabla \times \underline{\underline{F}}' \quad (1-7)$$

$$\underline{\underline{H}}^s = -j\omega \underline{\underline{F}}' - \nabla \phi_m' + \frac{1}{\mu_0} \nabla \times \underline{\underline{A}}' \quad (1-8)$$

where  $\underline{\underline{E}}^s$  and  $\underline{\underline{H}}^s$  are scattered fields, and

$\underline{\underline{A}}$  = vector potential due to electric current

$\underline{\underline{F}}$  = vector potential due to magnetic current

$\phi_e$  = scalar potential due to electric charge

$\phi_m$  = scalar potential due to magnetic charge

Primed quantities refer to case (I)

doubly primed quantities refer to case (II)

In terms of general operator notations, the following equations are obtained

$$\begin{bmatrix} L_{11}' & L_{12}' \\ L_{21}' & L_{22}' \end{bmatrix} \begin{bmatrix} J' \\ M' \end{bmatrix} = \begin{bmatrix} \underline{\underline{E}}^s \\ \underline{\underline{H}}^s \end{bmatrix} \quad (1-9)$$

$$\begin{bmatrix} L_{11}'' & L_{12}'' \\ L_{21}'' & L_{22}'' \end{bmatrix} \begin{bmatrix} J'' \\ M'' \end{bmatrix} = \begin{bmatrix} \underline{\underline{E}} \\ \underline{\underline{H}} \end{bmatrix} \quad (1-10)$$

where the definitions of the operators are obvious when comparing equations (1-9) and (1-10) with (1-5) to (1-8). Note that the tangential fields are continuous at the boundary surface, i.e.

$$\mathbf{n} \times (\mathbf{E}^S + \mathbf{E}^I - \mathbf{E}) = 0 \quad (1-11)$$

$$\mathbf{n} \times (\mathbf{H}^S + \mathbf{H}^I - \mathbf{H}) = 0 \quad (1-12)$$

where  $\mathbf{n}$  = unit normal pointing outward, or

$$-\mathbf{n} \times \mathbf{E}^S + \mathbf{n} \times \mathbf{E} = \mathbf{n} \times \mathbf{E}^I \quad (1-13)$$

$$-\mathbf{n} \times \mathbf{H}^S + \mathbf{n} \times \mathbf{H} = \mathbf{n} \times \mathbf{H}^I \quad (1-14)$$

The following equations are obtained by substituting equations (1-9) and (1-10) into (1-13) and (1-14).

$$-\mathbf{n} \times L'_{11}(J') - \mathbf{n} \times L'_{12}(M') + \mathbf{n} \times L''_{11}(J'') + \mathbf{n} \times L''_{12}(M'') = \mathbf{n} \times \mathbf{E}^I \quad (1-15)$$

$$-\mathbf{n} \times L'_{21}(J') - \mathbf{n} \times L'_{22}(M') + \mathbf{n} \times L''_{21}(J'') + \mathbf{n} \times L''_{22}(M'') = \mathbf{n} \times \mathbf{H}^I \quad (1-16)$$

By equations (1-1) and (1-2), it follows that

$$-\mathbf{n} \times [(L'_{11} + L''_{11})J'] - \mathbf{n} \times [(L'_{12} + L''_{12})M'] = \mathbf{n} \times \mathbf{E}^I \quad (1-17)$$

$$-\mathbf{n} \times [(L'_{21} + L''_{21})J'] - \mathbf{n} \times [(L'_{22} + L''_{22})M'] = \mathbf{n} \times \mathbf{H}^I \quad (1-18)$$

Define all the operators to be tangential operators; the above two equations can be put into standard matrix form as:

$$\begin{bmatrix} -(L'_{11} + L''_{11}) & -(L'_{12} + L''_{12}) \\ -(L'_{21} + L''_{21}) & -(L'_{22} + L''_{22}) \end{bmatrix} \begin{bmatrix} J' \\ M' \end{bmatrix}_{\tan} = \begin{bmatrix} E^1 \\ H^1 \end{bmatrix}_{\tan} \quad (1-19)$$

The  $[ ]_{\tan}$  means the tangential components of the bracketed quantity on the boundary surface. Let

$$Le' = -L'_{11}, \quad Le'' = -L''_{11}, \quad L'_m = -L'_{22}, \quad L''_m = -L''_{22}$$

and define

$$-C'(M') = -\frac{1}{\epsilon_0} \nabla \times F' = L'_{12}(M')$$

$$-C''(M') = -\frac{1}{\epsilon_0} \nabla \times F'' = L''_{12}(M')$$

$$C'(J') = \frac{1}{\mu_0} \nabla \times A' = L'_{21}(J')$$

$$C''(J') = \frac{1}{\mu_0} \nabla \times A'' = L''_{21}(J')$$

Hence equation (1-19) becomes

$$\begin{bmatrix} Le' + Le'' & C' + C'' \\ -(C' + C'') & Lm' + Lm'' \end{bmatrix} \begin{bmatrix} J' \\ M' \end{bmatrix}_{\tan} = \begin{bmatrix} E^1 \\ H^1 \end{bmatrix}_{\tan} \quad (1-20)$$

It is convenient to rearrange equation (1-20) into the form

$$\begin{bmatrix} Le & -jC \\ -jC & Lm \end{bmatrix} \begin{bmatrix} J \\ jM \end{bmatrix} = \begin{bmatrix} E^i \\ jH^i \end{bmatrix} \quad (1-21)$$

where

$$\begin{aligned} Le &= Le' + Le'' & J &= J' \\ Lm &= Lm' + Lm'' & M &= M' \\ C &= C' + C'' \end{aligned}$$

and the subscript "tan" has been dropped for brevity. Equation (1-21) is simply the familiar operator equation expressed below.

$$L(\underline{f}) = \underline{g} \quad (1-22)$$

$L$  is a tangential operator on the surface of the material body, and

$$L = \begin{bmatrix} Le & -jC \\ -jC & Lm \end{bmatrix}; \quad \underline{f} = \begin{bmatrix} J \\ jM \end{bmatrix}; \quad \underline{g} = \begin{bmatrix} E^i \\ jH^i \end{bmatrix}$$

### 1-3 Format

In this work the impressed magnetic field is assumed to be axially-directed (perpendicular polarization). The derivation of all the formulas for an impressed axially-directed electric field (parallel polarization) will not be given in the main body of this work, in order to conserve space, however, explicit formulas will be provided in Appendix A. A list of computer programs will be given in Appendix B.

The content of this work is as follows. In Chapter 2, the operator equation is reduced to a matrix equation suitable for numerical computation.

The reduction is accomplished by using the method of moments for perpendicular polarization. The equivalent surface currents can be obtained by matrix inversion. A concise theory of characteristic modes for material bodies, based on the surface formulation, and explicit formulas for obtaining the modal solutions are given in Chapter 3. Chapter 4 is a presentation of calculations made for cylinders of different material constants using both the matrix inversion method and the modal method. Chapter 5 is a discussion of the results. The computations presented in this work were performed on an IBM System 370, Model 155 digital computer. The computer programs are written in FORTRAN IV.

CHAPTER 2  
MATRIX FORMULATION

The determination of equivalent surface currents requires the solution of the following inhomogeneous equation

$$\mathbf{L}(\mathbf{f}) = \mathbf{g} \quad (2-1)$$

where  $\mathbf{L}$  is the matrix of operators

$$\mathbf{L} = \begin{bmatrix} \mathbf{L}_e & -j\mathbf{C} \\ -j\mathbf{C} & \mathbf{L}_m \end{bmatrix} \quad (2-2)$$

and

$$\mathbf{f} = \begin{bmatrix} \mathbf{J} \\ \mathbf{jM} \end{bmatrix} \quad \mathbf{g} = \begin{bmatrix} \mathbf{E}^1 \\ \mathbf{jH}^1 \end{bmatrix} \quad (2-3)$$

This chapter presents the reduction of equation (2-1) to matrix form by the method of moments.

### 2.1 Method of Moments

To apply the method of moments, an appropriate inner product for the problem is ( $\sim$  indicates transpose)

$$\begin{aligned} \langle \mathbf{f}, \mathbf{g} \rangle &= \iint_S \mathbf{f}^\top \mathbf{g} \, ds \\ &= \iint_S (\mathbf{J} \cdot \mathbf{E} - \mathbf{H} \cdot \mathbf{M}) \, ds \end{aligned} \quad (2-4)$$

A solution by the method of moments is obtained as follows. Define electric expansion and testing functions as

$$\begin{aligned} \tilde{f}_n^e &= \begin{bmatrix} J_n \\ \sim \\ 0 \end{bmatrix} & \tilde{w}_n^e &= \begin{bmatrix} w_n^e \\ \sim \\ 0 \end{bmatrix} \end{aligned} \quad (2-5)$$

and magnetic expansion and testing functions as

$$\begin{aligned} \tilde{f}_n^m &= \begin{bmatrix} 0 \\ M_n \\ \sim \end{bmatrix} & \tilde{w}_n^m &= \begin{bmatrix} 0 \\ W_n^m \\ \sim \end{bmatrix} \end{aligned} \quad (2-6)$$

The expansion for  $f$  is then of the form

$$f = \sum_n (I_n \tilde{f}_n^e + V_n \tilde{f}_n^m) \quad (2-7)$$

where the  $I_n$  and  $V_n$  are constants to be determined.

The inner product of each  $\{\tilde{w}_n^e\}$  with equation (2-1) yields

$$\langle \tilde{w}_n^e, L(f) \rangle = \langle \tilde{w}_n^e, g \rangle \quad (2-8)$$

where

$$\begin{aligned} \langle \tilde{w}_n^e, L(f) \rangle &= \langle \tilde{w}_n^e, \sum_n (I_n \tilde{L}(f_n^e) + V_n \tilde{L}(f_n^m)) \rangle \\ &= \sum_n I_n \langle \tilde{w}_n^e, \tilde{L}(f_n^e) \rangle \\ &\quad + \sum_n V_n \langle \tilde{w}_n^e, \tilde{L}(f_n^m) \rangle \\ &= \sum_n I_n \iint_s \tilde{w}_n^e \cdot \tilde{L}(J_n) ds + \sum_n V_n \iint_s \tilde{w}_n^e \cdot (-jC)(M_n) ds \quad (2-9) \end{aligned}$$

and

$$\langle \tilde{w}_n^e, g \rangle = \iint_s \tilde{w}_n^e \cdot E^i ds \quad (2-10)$$

Similarly, the inner product of each  $\{W_m^m\}$  with equation (2-1) yields

$$\langle \overset{\text{m}}{\underset{\sim}{W_m^m}}, L(f_n) \rangle = \langle \overset{\text{m}}{\underset{\sim}{W_m^m}}, g \rangle \quad (2-11)$$

and

$$\begin{aligned} \langle \overset{\text{m}}{\underset{\sim}{W_m^m}}, L(f_n) \rangle &= \sum_n I_n \iint_s \overset{\text{m}}{\underset{\sim}{W_m^m}} \cdot (-jC) (\overset{\text{n}}{\underset{\sim}{J_n}}) ds \\ &\quad + \sum_n V_n \iint_s \overset{\text{m}}{\underset{\sim}{W_m^m}} \cdot L_m (\overset{\text{n}}{\underset{\sim}{M_n}}) ds \end{aligned} \quad (2-12)$$

$$\langle \overset{\text{m}}{\underset{\sim}{W_m^m}}, g \rangle = \iint_s \overset{\text{m}}{\underset{\sim}{W_m^m}} \cdot jH^i ds \quad (2-13)$$

Equation (2-8) and Equation (2-11) can be placed in matrix form

$$\begin{bmatrix} [Z] & [B] \\ [C] & [Y] \end{bmatrix} \begin{bmatrix} [I] \\ [V] \end{bmatrix} = \begin{bmatrix} [V^i] \\ [I^i] \end{bmatrix} \quad (2-14)$$

where

$$Z_{mn} = \iint_s \overset{\text{e}}{\underset{\sim}{W_m^e}} \cdot L_e (\overset{\text{n}}{\underset{\sim}{J_n}}) ds \quad (2-15)$$

$$B_{mn} = \iint_s \overset{\text{e}}{\underset{\sim}{W_m^e}} \cdot (-jC) (\overset{\text{n}}{\underset{\sim}{M_n}}) ds \quad (2-16)$$

$$C_{mn} = \iint_s \overset{\text{m}}{\underset{\sim}{W_m^m}} \cdot (-jC) (\overset{\text{n}}{\underset{\sim}{J_n}}) ds \quad (2-17)$$

$$Y_{mn} = \iint_s \overset{\text{m}}{\underset{\sim}{W_m^m}} \cdot L_m (\overset{\text{n}}{\underset{\sim}{M_n}}) ds \quad (2-18)$$

$$\mathbf{V}_m^i = \iint_s \mathbf{W}_m^e \cdot \mathbf{E}^i ds \quad (2-19)$$

$$\mathbf{I}_m^i = \iint_s \mathbf{W}_m^m \cdot j\mathbf{H}^i ds \quad (2-20)$$

Choose  $\mathbf{J}_n^a = \mathbf{W}_n^e$ . Note that  $[Z]$  is obviously symmetric, already shown by Harrington and Mautz. With the choice  $\mathbf{M}_n^m = \mathbf{W}_n^m$ ,  $[Y]$  is the dual of  $[Z]$ , magnetic instead of electric, so the symmetric nature of  $[Y]$  can be easily established. It is known that  $C(\mathbf{M}_n^m)$  gives rise to an electric field and  $C(\mathbf{J}_n^a)$  will produce a magnetic field. Observe that by reciprocity

$$\iint_s (\mathbf{E}^a \cdot \mathbf{J}^b - \mathbf{H}^a \cdot \mathbf{M}^b) ds = \iint_s (\mathbf{E}^b \cdot \mathbf{J}^a - \mathbf{H}^b \cdot \mathbf{M}^a) ds \quad (2-21)$$

Now, consider

- (i) In situation "a" only electric sources
- (ii) In situation "b" only magnetic sources.

It follows that

$$\iint_s (-\mathbf{H}^a \cdot \mathbf{M}^b) ds = \iint_s (\mathbf{E}^b \cdot \mathbf{J}^a) ds \quad (2-22)$$

Hence

$$\mathbf{B}_{mn} = C_{nm} \quad (2-23)$$

Consequently,  $[C]$  is the transpose of  $[B]$ , or

$$[B] = \tilde{[C]} \quad \text{with} \quad \begin{aligned} \mathbf{J}_n^a &= \mathbf{W}_n^e \\ \mathbf{M}_n^m &= \mathbf{W}_n^m \end{aligned} \quad (2-24)$$

To this point the matrix formulation is completely general and has been achieved without reference to specific excitation, expansion functions, and testing functions. Note that every one of the operators  $L_e$ ,  $C$ , and  $L_m$  is composed of two parts as indicated by equation (1-21), and consequently every matrix element in  $[Z]$ ,  $[B]$ ,  $[C]$  and  $[Y]$  has two parts; one is due to the primed operator, and the other is due to the doubly primed operator.

## 2.2 Expansion Functions and the Evaluation of [Z] Matrix Element

In this section, the incident field is the axially directed magnetic field,  $\tilde{H}_z^1$ . Before going into any specific excitation for the scattering problem, some general considerations about the evaluation of different types of matrix elements will be presented as follows.

Note that the original problem, the scattering from material bodies, has been decomposed into two cases, and their associated operators are of the same functional form. For instance, the expression for  $L_e''(\tilde{J})$  will be identical to  $L_e'(\tilde{J})$  except for the constitutive constants,  $\mu$  and  $\epsilon$ . For the sake of brevity, only  $L_e'$  will be considered. Once  $L_e'(\tilde{J})$  is known,  $L_e''(\tilde{J})$  is obtained by replacing  $\epsilon_0$  and  $\mu_0$  by  $\epsilon$  and  $\mu$ , respectively.

By equation (2-15)

$$Z_{mn} = \int_{\text{body}} \tilde{w}_m \cdot (\tilde{j}\omega \tilde{A}_n + \nabla \tilde{\phi}_n) d\ell \quad (2-25)$$

where

$\tilde{A}_n$  = magnetic vector potential due to  $\tilde{J}_n$

$\tilde{\phi}_n$  = scalar potential due to  $\tilde{\sigma}_n$ , surface charge

Applying the one dimensional divergence theorem to the vector  $\phi_n \overset{\sim}{W_m}$ , and noting that

$$\int_c \nabla \cdot \phi_n \overset{\sim}{W_m} d\ell = \phi_n \int_c \nabla \cdot \overset{\sim}{W_m} d\ell + \overset{\sim}{W_m} \cdot \nabla \phi_n d\ell \quad (2-26)$$

the following relationship is obtained

$$\int_c \nabla \phi_n \cdot \overset{\sim}{W_m} d\ell = - \int_c \phi_n \nabla \cdot \overset{\sim}{W_m} d\ell \quad (2-27)$$

Define  $\sigma_m$  such that

$$\sigma_m = - \frac{1}{j\omega} \nabla \cdot \overset{\sim}{W_m} \quad (2-28)$$

Observe that equation (2-28) has the form of the continuity equation if  $\overset{\sim}{W_m}$  and  $\sigma_m$  are interpreted as current and charge, respectively. An alternative form for the [Z] matrix element can be obtained by substituting equations (2-27) and (2-28) into equation (2-25). The new form is computationally more attractive.

$$Z_{mn} = j\omega \int_c (\overset{\sim}{W_m} \cdot \overset{\sim}{A_n} + \sigma_m \phi_n) d\ell \quad (2-29)$$

Define the two-dimensional Green's function  $G(r, r')$ .

$$G(r, r') = \frac{1}{4j} H_0^{(2)}(k|r - r'|) \quad (2-30)$$

and

$$\overset{\sim}{A}(r) = \mu \int_c J(r') G(r, r') d\ell' \quad (2-31)$$

$$\phi(r) = \frac{1}{\epsilon} \int_c q(r') G(r, r') d\ell' \quad (2-32)$$

where  $q$  is related to  $J$  by the equation of continuity

$$\nabla \cdot J = -j\omega q \quad (2-33)$$

After substituting equations (2-31), (2-32), and (2-33) into equation (2-29), the expression for  $Z_{mn}$  becomes

$$\begin{aligned} Z_{mn} &= j\omega \int_C \left( \int_C [W_m \cdot \mu J_n(r') + \frac{\sigma_m}{\epsilon} q_n(r')] G(r, r') dr' \right) dr \\ &= \int_C \int_C [j\omega \mu W_m \cdot J_n + \frac{1}{j\omega \epsilon} (\nabla \cdot W_m)(\nabla \cdot J_n)] G(r, r') dr' dr \quad (2-34) \end{aligned}$$

Note that the primed symbols refer to source location variation, while the unprimed symbols relate to variation in field point location.

The specific formulation proceeds by dividing the contour C into N segments, not necessarily equal in length. There are N segments and N+1 points,

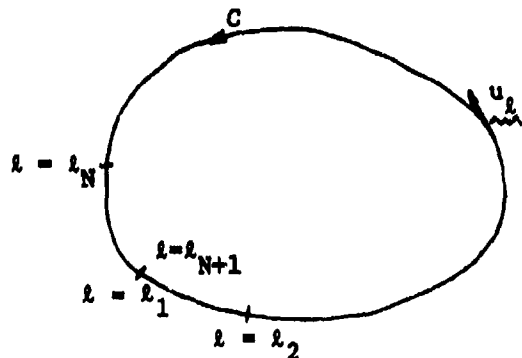


Fig. 2-1. A cross sectional contour.

and  $\ell$  is the path length proceeding counterclockwise around contour C.

The sets of expansion and testing functions are chosen as triangle functions for both electric and magnetic surface currents.

$$\underline{\underline{w}_k} = T(\ell - \ell_k) \underline{\underline{u}_k} \quad k=1, 2, \dots, N \quad (2-35)$$

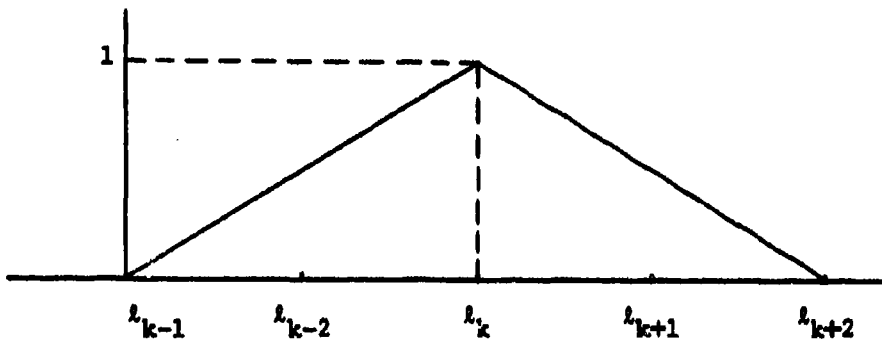


Fig. 2-2. A triangle function.

where  $\underline{\underline{u}_k}$  is the unit vector tangent to C path length value  $\ell$ , and T is the triangle function defined by

$$T(t - t_k) = \begin{cases} 1 - \frac{t - t_k}{t_{k+2} - t_k} & t_k \leq t \leq t_{k+2} \\ 1 + \frac{t - t_k}{t_k - t_{k-2}} & t_{k-2} \leq t \leq t_k \\ 0 & t \geq t_{k+2} \\ 0 & t_{k-2} \geq t \end{cases} \quad (2-36)$$

or

$$T(t - t_k) = \begin{cases} 1 - \frac{t - t_k}{t_{k+2} - t_k} & 0 \leq t - t_k \leq t_{k+2} - t_k \\ 1 + \frac{t - t_k}{t_k - t_{k-2}} & -(t_k - t_{k-2}) \leq t - t_k \leq 0 \\ 0 & t - t_k \geq t_{k+2} - t_k \\ 0 & -(t_k - t_{k-2}) \geq t - t_k \end{cases} \quad (2-37)$$

Let  $\Delta t_k = t_{k+1} - t_k$  then

$$T(t - t_k) = \begin{cases} 1 - \frac{t - t_k}{\Delta t_k + \Delta t_{k+1}} & \sigma \leq t - t_k \leq \Delta t_k + \Delta t_{k+1} \\ 1 + \frac{t - t_k}{\Delta t_{k-2} + \Delta t_{k-1}} & -(\Delta t_{k-2} + \Delta t_{k-1}) \leq t - t_k \leq 0 \\ 0 & t - t_k \geq \Delta t_k + \Delta t_{k+1} \\ 0 & -(\Delta t_{k-2} + \Delta t_{k-1}) \geq t - t_k \end{cases} \quad (2-38)$$

and

$$\Delta t_0 = \Delta t_N$$

Now,  $Z_{mn}$  can be written as

$$\begin{aligned}
 Z_{mn} &= \int \int [j\omega \mu W_m \cdot J_n + \frac{1}{j\omega \epsilon} (\nabla \cdot W_m) (\nabla' \cdot J_n)] G d\ell' d\ell \\
 &= \int_{\ell_{m-2}}^{\ell_{m+2}} \int_{\ell_{n-2}}^{\ell_{n+2}} [j\omega \mu T(\ell - \ell_m) T(\ell' - \ell_n) (u_k \cdot u'_k) \\
 &\quad + \frac{1}{j\omega \epsilon} T'(\ell' - \ell_n) T'(\ell - \ell_n)] G d\ell' d\ell \quad (2-39)
 \end{aligned}$$

The subscript m indicates the mth triangle testing function and the subscript n indicates the nth triangle expansion function.  $T'$  is the derivative of the triangle function.

$$T'(\ell - \ell_k) = \begin{cases} -\frac{1}{\ell_{k+2} - \ell_k} & \ell_k \leq \ell \leq \ell_{k+2} \\ \frac{1}{\ell_k - \ell_{k-2}} & \ell \geq \ell_{k+2} \\ 0 & \ell \geq \ell_{k+2} \\ 0 & \ell_{k-2} \geq \ell \end{cases} \quad (2-40)$$

or

$$T'(\ell - \ell_k) = \begin{cases} \frac{1}{\Delta \ell_k + \Delta \ell_{k+1}} & 0 \leq \ell - \ell_k \leq 0 \Delta \ell_k + \Delta \ell_{k+1} \\ \frac{1}{\Delta \ell_{k-2} + \Delta \ell_{k-1}} & -(\Delta \ell_{k-2} + \Delta \ell_{k-1}) \leq \ell - \ell_k \leq 0 \\ 0 & \ell - \ell_k \geq \Delta \ell_k + \Delta \ell_{k+1} \\ 0 & -(\Delta \ell_{k-2} + \Delta \ell_{k-1}) \geq \ell - \ell_k \end{cases} \quad (2-41)$$

The triangle function is approximated by four pulses with amplitudes  $h_{k-2}$ ,  $h_{k-1}$ ,  $h_k$ , and  $h_{k+1}$  as shown below

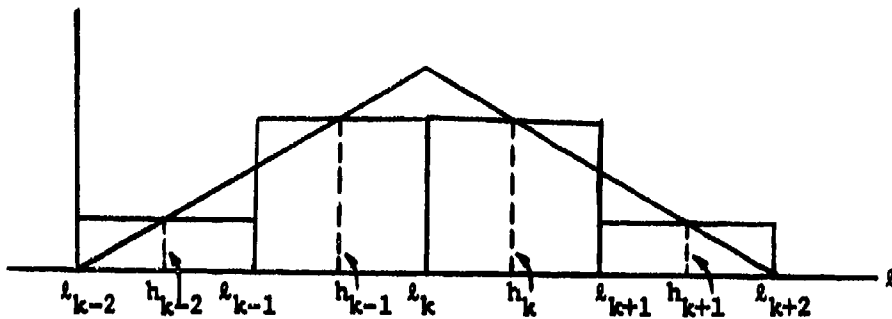


Fig. 2-3. A four-pulse approximation

where

$$h_{k-2} = \frac{\frac{1}{2} \Delta l_{k-2}}{\Delta l_{k-2} + \Delta l_{k-1}}$$

$$h_{k-1} = \frac{\Delta l_{k-2} + \frac{1}{2} \Delta l_{k-1}}{\Delta l_{k-2} + \Delta l_{k-1}}$$

$$h_k = \frac{\frac{1}{2} \Delta l_k + \Delta l_{k+1}}{\Delta l_k + \Delta l_{k+1}}$$

$$h_{k+1} = \frac{\frac{1}{2} \Delta l_{k+1}}{\Delta l_k + \Delta l_{k+1}} \quad (2-42)$$

The derivative  $T'$  of the Triangle function can be represented graphically as

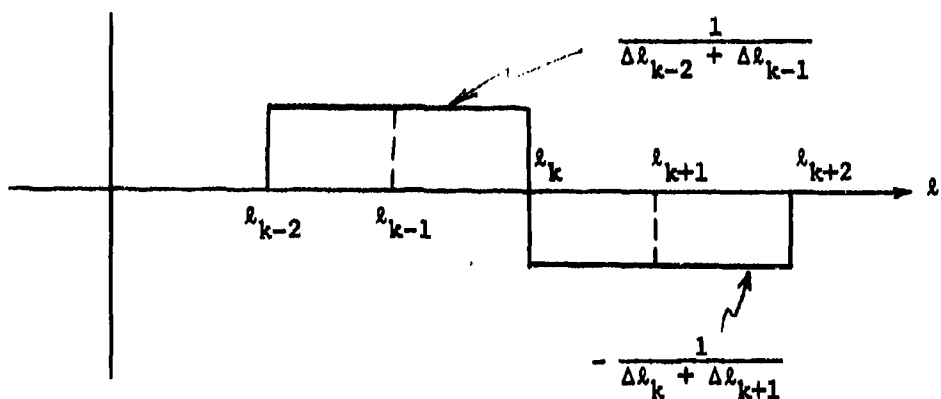


Fig. 2-4. The derivative of a triangle function.

Consider the contour interval spanned by the expansion or testing triangle function as shown in Fig. 2-5.

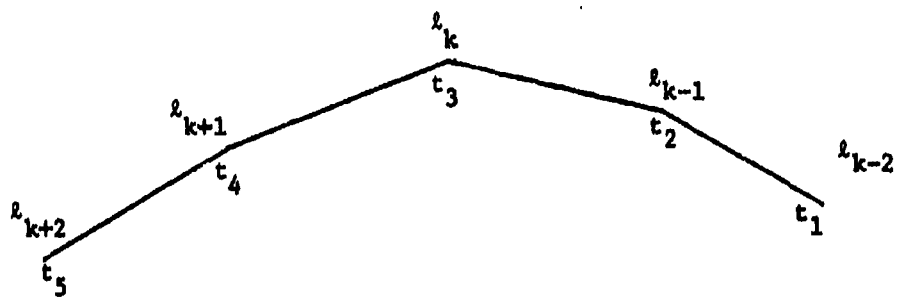


Fig. 2-5. Straight line representation of the contour.

To evaluate the integrals in equation (2-39) each such portion of the contour is replaced by straight line segments drawn between the points on the actual contour defined by  $\ell_1, \ell_2, \dots, \ell_{N+1}$ . The integration variables in equation (2-39) are taken along these straight line segments. For the nth expansion function, the index  $p=1, 2, 3, 4$  is associated with the four pulse intervals for increasing path length. Similarly, the index  $q=1, 2, 3, 4$  is defined for the mth testing function. Equation (2-39) can be put in the following form

$$z_{mn} = \sum_{q=1}^4 \sum_{p=1}^4 \int_{t_q}^{t_{q+1}} \int_{t_p}^{t_{p+1}} [j\omega\mu T_p T_q (u_p \cdot u_q) + \frac{1}{j\omega\epsilon} T'_q T'_p] G d\ell_p d\ell_q \quad (2-43)$$

Note that  $T_p$  and  $T_q$  are the amplitudes of the pth and qth pulses, respectively. The unit vectors  $u_p$  and  $u_q$  are parallel to the straight lines of the pth and qth intervals in the direction of increasing path length. Observe that each of the sixteen terms on the right hand side of equation (2-43) results from one of two situations. Either the pth and qth intervals coincide, or they do not. These two situations will be considered separately.

#### (i) Noncoincident intervals

In this situation each integral in equation (2-44) is approximated by the product of its integrand evaluated at the interval midpoint times the interval length. Hence equation (2-44) becomes

$$z_{mn} = \sum_{q=1}^4 \sum_{p=1}^4 \Delta t_p \Delta t_q [j\omega \mu T_p T_q \underbrace{u_p}_{\sim\sim} \underbrace{u_q}_{\sim\sim} + \frac{1}{j\omega \epsilon} T'_p T'_q] \frac{H_o^{(2)}(kR_{pq})}{4j} \quad (2-44)$$

$\Delta t_p$  and  $\Delta t_q$  are determined by

$$\Delta t_k = t_{k+1} - t_k \quad (k = 1, 2, 3, 4)$$

and  $R_{pq}$  is the distance between the midpoints of the pth and qth pulses.

### (ii) Coincident intervals

For coincident pth and qth intervals the integral evaluations proceed as follows. The q integral is approximated by the product of the integrand, sampled at the midpoint of the interval, times the interval length. The p integral is then evaluated as an improper integral.

The small argument approximation for  $H_o^{(2)}(kR)$  is

$$H_o^{(2)}(kR) \approx 1 - j \frac{2}{\pi} \log \left( \frac{\gamma kR}{2} \right) \quad (2-46)$$

where  $\log \gamma$  is Euler's constant. Then for coincident pulse intervals

$$\begin{aligned} & \int_{t_q}^{t_{q+1}} \int_{t_p}^{t_{p+1}} [j\omega \mu T_p T_q \underbrace{u_p}_{\sim\sim} \underbrace{u_q}_{\sim\sim} + \frac{1}{j\omega \epsilon} T'_p T'_q] \frac{H_o^{(2)}(kR)}{4} dt_p dt_q \\ &= \frac{1}{4} \Delta t_q [j\omega \mu T_p T_q + \frac{1}{j\omega \epsilon} T'_p T'_q] \int_{t_p}^{t_{p+1}} H_o^{(2)}(kR) dt_p \end{aligned} \quad (2-47)$$

Note that the integrand is singular at the midpoint. The improper integral can be treated as:

$$\begin{aligned}
 \int_{t_p}^{t_{p+1}} H_0^{(2)}(kR) dt &= \int_{-\Delta t_p/2}^{\Delta t_p/2} [1 - j \frac{2}{\pi} \log (\frac{\gamma k |x|}{2})] dx \\
 &= \lim_{\epsilon \rightarrow 0} \int_{-\Delta t_p/2}^{-\epsilon} [1 - j \frac{2}{\pi} \log (-\frac{\gamma k x}{2})] dx \\
 &\quad + \lim_{\epsilon \rightarrow 0} \int_{\epsilon}^{\Delta t_p/2} [1 - j \frac{2}{\pi} \log (\frac{\gamma k x}{2})] dx \\
 &= \Delta t_p [1 - j \frac{2}{\pi} \log \frac{\gamma k \Delta t_p}{4\epsilon}] \tag{2-48}
 \end{aligned}$$

Therefore  $Z_{mn}$  can be expressed as

$$Z_{mn} = \frac{1}{4} \sum_{q=1}^4 \sum_{p=1}^4 \Delta t_p \Delta t_q [\omega \mu T_p T_q (u_p \cdot u_q) - \frac{1}{\omega \epsilon} T_p' T_q' Z] \tag{2-49}$$

where

$$Z = \begin{cases} H_0^{(2)}(kR_{pq}) & \text{noncoincident intervals} \\ 1 - j \frac{2}{\pi} \log \frac{\gamma k \Delta t_p}{4\epsilon} & \text{coincident intervals} \end{cases}$$

Equation (2-49) is used to compute the two parts of each matrix element, with  $\epsilon_0$ ,  $\mu_0$ , and  $k_0$  in one part and  $\epsilon, \mu$ , and  $k$  in the other. It can be readily observed that the use of equation (2-49) will lead to a symmetric  $[Z]$  matrix.

### 2.3 Evaluation of [B] and [C] Matrix Elements

Matrix elements for [B] are expressed by equation (2-16)

$$B_{mn} = \int_c \underbrace{w_m^e}_{\sim\sim} \cdot (-jC) \underbrace{M_n}_{\sim\sim} dl \quad (2-50)$$

Because of the discontinuity of the curl operator at the boundary, care should be exercised in evaluating equation (2-50). The Green's function is singular, and a simple interchange of differentiation and integration is not always possible. Note that the operator C consists of two kinds of operators, namely, C' and C''. C' is for the outside field, and C'' for the inside field, with respect to the material body. In the following development, the symbol C can be either C' or C'' unless stated otherwise. Since the incident field,  $\underbrace{H^i}_{\sim\sim}$  in the present case, is considered to be axially directed, there will be a circumferentially directed electric current and an axially directed magnetic current.

Let

$$\underbrace{w_m^e}_{\sim\sim} = T(\ell - \ell_k) \underbrace{u_\ell}_{\sim\sim} \quad (2-51)$$

and

$$\underbrace{M_n}_{\sim\sim} = T(\ell - \ell_k) \underbrace{u_z}_{\sim\sim}$$

Hence, equation (2-51) takes the form

$$\begin{aligned} B_{mn} &= -\frac{1}{4} \int T(\ell - \ell_m) \underbrace{u_\ell}_{\sim\sim} \cdot \nabla \times \underbrace{u_z}_{\sim\sim} \int T(\ell' - \ell_n) H_o^{(2)}(kR) d\ell' d\ell \\ &= -\frac{1}{4} \sum_{q=1}^4 \sum_{p=1}^4 \int_{t_q}^{t_{q+1}} T_q \underbrace{u_\ell}_{\sim\sim} \cdot \nabla \times \underbrace{u_z}_{\sim\sim} \int_{t_p}^{t_{p+1}} T_p H_o^{(2)}(kR) d\ell' d\ell \end{aligned} \quad (2-52)$$

Since  $T_p$  and  $T_q$  are constant between  $t_p$  and  $t_{p+1}$ ,  $t_q$  and  $t_{q+1}$ , respectively, hence they can be taken outside the integral signs, so

$$B_{mn} = -\frac{1}{4} \sum_{q=1}^4 \sum_{p=1}^4 T_p T_q \int_{t_q}^{t_{q+1}} u_x \cdot \nabla \times u_z \int_{t_p}^{t_{p+1}} H_0^{(2)}(kR) dt' dt \quad (2-53)$$

Again, two situations will be treated separately.

(i) Non-coincident p and q intervals

The Hankel function is continuous and differentiable. After performing the indicated curl operation in equation (2-53), and noting that  $u_x$  refers to q coordinates, then

$$B_{mn} = -\frac{1}{4} \sum_{q=1}^4 \sum_{p=1}^4 \Delta t_p \left\{ \frac{\partial H_0^{(2)}(kR_{pq})}{\partial y_q} \Delta x_q - \frac{\partial H_0^{(2)}(kR_{pq})}{\partial x_q} \Delta y_q \right\} T_p T_q \quad (2-54)$$

where

$$R_{pq} = [(x_q - x_p)^2 + (y_q - y_p)^2]^{1/2} \quad (2-55)$$

and

$$\frac{\partial H_0^{(2)}(kR)}{\partial x} = -kH_1^{(2)}(kR) \frac{x - x_p}{R} \quad (2-56)$$

$$\frac{\partial H_0^{(2)}(kR)}{\partial y} = -kH_1^{(2)}(kR) \frac{y - y_p}{R} \quad (2-57)$$

Hence

$$B_{mn} = -\frac{1}{4} \sum_{q=1}^4 \sum_{p=1}^4 \Delta t_p \frac{-T_p T_q k H_1^{(2)}(kR)}{R} [-(y_p - y_q) \Delta x_q + (x_p - x_q) \Delta y_q] \quad (2-58)$$

Equation (2-58) is obtained through the application of triangle expansion and testing function employing a four-pulse approximation to the triangle, and the integrand was evaluated at the midpoint of each pulse interval.

(ii) Coincident p and q

Note that in this case, the method used in evaluating the improper integral for [Z] can not be applied here because the curl operator is not continuous across the boundary, for instance

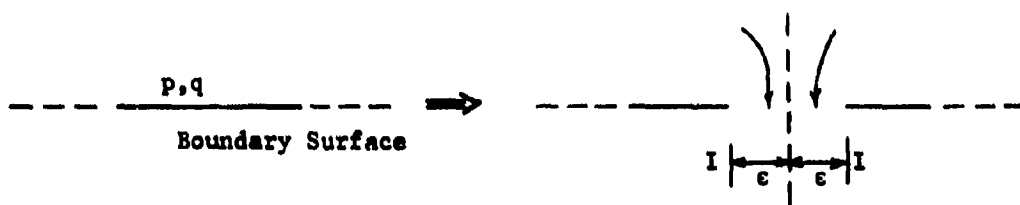


Fig. 2-6 Boundary Surface

By visualizing a current sheet that flows into the paper as shown in Fig. 2-6, it is evident that the tangential field component will decidedly be zero as  $\epsilon \rightarrow 0$ .

A better way is to find the field at a point above the boundary surface, then find the limit as it approaches the boundary surface from above. Before performing the limiting process, the integrals in equation (2-53) becomes

$$\int_{t_q}^{t_{q+1}} \underbrace{u_x}_{\sim} \cdot \nabla \times \underbrace{u_y}_{\sim} \int_{t_p}^{t_{p+1}} H_o^{(2)}(kR) d\ell' d\ell$$

$$= \Delta t_p \int_{t_q}^{t_{q+1}} \left[ u_x \frac{\partial H_o^{(2)}(kR)}{\partial y_q} - u_y \frac{\partial H_o^{(2)}(kR)}{\partial x_q} \right] \cdot [u_x dx_q + u_y dy_q]$$

Note that in equation (2-58)  $\underbrace{u_x}_{\sim}$  refers to the q-coordinates and the p-integral is evaluated as the product of the integrand sampled at the midpoint of the p-interval times the interval length.

A local coordinate system is constructed for the evaluation of the improper integral as  $R \rightarrow 0$ . A local coordinate system is shown in Fig. 2-7.

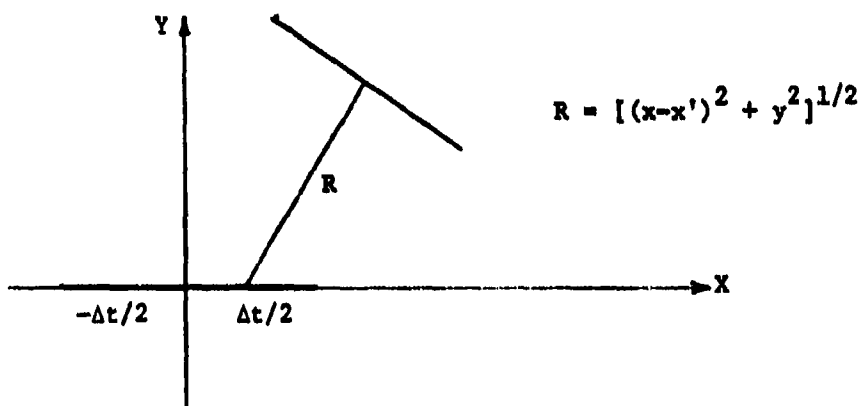


Fig. 2-7. A local coordinate system.

Next, consider the term

$$\int_{-\Delta t/2}^{\Delta t/2} \frac{\partial H_0^{(2)}(kR)}{\partial y} dx' \quad (2-59)$$

and noting that

$$\frac{\partial H_0^{(2)}(kR)}{\partial y} = -k H_1^{(2)}(kR) \frac{\partial R}{\partial y} \quad (2-60)$$

By using small argument approximation for  $H_1^{(2)}(kR)$

$$H_1^{(2)}(kR) \approx J_1(kR) - jN_1(kR) \\ \approx \frac{kR}{2} + j \frac{2}{\pi} \frac{1}{kR} \quad (2-61)$$

equation (2-59) becomes

$$\int_{-\Delta t/2}^{\Delta t/2} \frac{\partial H_0^{(2)}(kR)}{\partial y} dx' = -k \int_{-\Delta t/2}^{\Delta t/2} \left[ \frac{kR}{2} + j \frac{2}{\pi kR} \right] \frac{\partial R}{\partial y} dx' \\ = -\frac{k^2}{2} y \Delta t - j \frac{2}{\pi} \left[ \tan^{-1} \left( \frac{\Delta t}{2} - x \right) - \tan^{-1} \left( -\frac{\Delta t}{2} - x \right) \right] \quad (2-62)$$

Note that as  $x \rightarrow 0$ ,  $y \rightarrow 0$ , the improper integral approaches  $-j2$ .

Finally the expression for  $B_{mn}$  can be stated as follows.

$$B_{mn} = -\frac{1}{4} \sum_{q=1}^4 \sum_{p=1}^4 \Delta t_p T_p T_q B \quad (2-63)$$

where

$$B = - \frac{kH_1^{(2)}(kR_{pq})}{R_{pq}} [ - (y_p - y_q)\Delta x_q + (x_p - x_q)\Delta y_q ]$$

(non-coincident)

$$B = - j2 \quad \text{(coincident)}$$

Equation (2-63) is used to compute the two parts of each [B] matrix element, R in one part (due to primed operator) and k in the other (due to doubly primed operator). Since C' is an outside operator and C'' is an inside operator, the values of B for the coincidental case will have opposite signs. Hence the coincidental-pulse-interval situation contributes nothing to the values of the matrix elements.

In spite of the fact that  $[C] = \widetilde{[B]}$ , it is advantageous to evaluate  $C_{mn}$  explicitly. The procedures involved will be essentially the same as in evaluating  $B_{mn}$ . Recall equation (2-17), and it can be expressed in greater detail as

$$C_{mn} = \int_C \underset{\sim\sim}{W_m^m} \cdot (-jC) \underset{\sim\sim}{(J_n)_n} dt$$

A specific form, suitable for computational purposes is developed in a manner similar to that used for  $B_{mn}$ . Considerations governing the choices of expansion and testing functions are the same as those discussed at the beginning of this section. Note that the electric surface current, in the present case, is circumferentially directed.

$$\underset{\sim\sim}{W_m^m} = T(\ell - \ell_k) \underset{\sim\sim}{u_z} \quad (2-65)$$

$$\underset{\sim\sim}{(J_n)_n} = T(\ell - \ell_k) \underset{\sim\sim}{u_\ell}$$

where  $T$  is defined by equation (2-38) and  $\underline{u}_z$  is the unit vector in the direction of the axis;  $\underline{u}_z$  is the unit vector along the cross-sectional contour.  $C_{mn}$  can be expressed as

$$C_{mn} = -\frac{1}{4} \sum_{q=1}^4 \sum_{p=1}^4 \int_{t_q}^{t_{q+1}} T_q \underline{u}_z \cdot \nabla \times \underline{u}_z \int_{t_p}^{t_{p+1}} T_p H_o^{(2)}(kR) d\ell' d\ell \quad (2-66)$$

The evaluation of the integrals appearing in equation (2-66) is facilitated by approximating the triangle function by four pulses. The index  $p = 1, 2, 3, 4$  is associated with each pulse, respectively, for the  $n$ th expansion function, while the index  $q = 1, 2, 3, 4$  is similarly defined for the  $m$ th testing function. Since  $T_p$  is constant between  $t_p$  and  $t_{p+1}$  and  $T_q$  is constant between  $t_q$  and  $t_{q+1}$ , they can be taken outside the integral signs.  $\underline{u}_z$  is the unit vector along the contour with respect to  $p$  coordinates. Hence

$$\begin{aligned} C_{mn} &= -\frac{1}{4} \sum_{q=1}^4 \sum_{p=1}^4 T_p T_q \Delta t_q \int_{t_p}^{t_{p+1}} \underline{u}_z \cdot \nabla \times [\underline{u}_x dx_p H_o^{(2)}(kR) \\ &\quad + \underline{u}_y dy_p H_o^{(2)}(kR)] \\ &= -\frac{1}{4} \sum_{q=1}^4 \sum_{p=1}^4 T_p T_q \Delta t_q \left[ \int_{t_p}^{t_{p+1}} \left[ \frac{\partial H_o^{(2)}(kR)}{\partial x_q} dy_p - \frac{\partial H_o^{(2)}(kR)}{\partial y_q} dx_p \right] \right] \quad (2-67) \end{aligned}$$

Note that the integral

$$\int_{t_p}^{t_{p+1}} \left[ \frac{\partial H_o^{(2)}(kR)}{\partial x_q} dy_p - \frac{\partial H_o^{(2)}(kR)}{\partial y_q} dx_p \right] \quad (2-68)$$

can be evaluated just like in the previous  $B_{mn}$  case. It follows that equation (2-68) becomes

$$-kH_1^{(2)}(kR_{pq}) \left[ -\frac{x_p - x_q}{R_{pq}} \Delta y_p + \frac{y_p - y_q}{R_{pq}} \Delta x_p \right] \quad (2-69)$$

For coincident p-pulse and q-pulse intervals, the evaluation of the improper integral is identical to that developed for  $B_{mn}$ . To this point, the matrix elements for [C] can be conveniently specified as

$$C_{mn} = -\frac{1}{4} \sum_{q=1}^4 \sum_{p=1}^4 \Delta t_q T_p T_q C \quad (2-70)$$

where

$$C = -\frac{kH_1^{(2)}(kR_{pq})}{R_{pq}} \left[ -(x_p - x_q) \Delta y_p + (y_p - y_q) \Delta x_p \right] \quad (\text{noncoincident intervals})$$

$$C = -j2 \quad (\text{coincident intervals})$$

Equation (2-70) is used to compute the two parts of each [C] matrix elements; one part is due to the outside operator  $C'$ , and the other is due to the inside operator  $C''$ . Again, for the coincidental-pulse-interval situation, the net contribution, to the value of each matrix element, is zero, because the two values of C in equation (2-70) have opposite signs.

#### 2.4 Evaluation of [Y] Matrix Elements

The only expression left to be developed is that for the [Y] matrix elements. By equation (2-18)

$$\begin{aligned} Y_{mn} &= \int_C \underbrace{W_m^m}_{\sim\sim} \cdot \underbrace{L_m(M_n^m)}_{\sim\sim} d\ell \\ &= \int \underbrace{W_m^m}_{\sim\sim} \cdot \underbrace{(j\omega F_n^m + v\phi_n^m)}_{\sim\sim} d\ell \end{aligned} \quad (2-71)$$

The superscript,  $m$ , indicates magnetic quantities. By equations (2-26) to (2-28), the following is obtained

$$Y_{mn} = j\omega \int_C \left( \underline{W}_m \cdot \underline{F}_n + \sigma_m \phi_n^m \right) d\underline{l} \quad (2-72)$$

In this case all the currents are axially directed. The expansion and testing functions are chosen as

$$\underline{W}_k = \underline{M}_k = T(l - l_k) \underline{u}_z \quad (2-73)$$

where  $T$  is the triangle function defined by equation (2-38), and  $\underline{u}_z$  is the unit vector in the axial direction. The continuity equation in this case is

$$\sigma_n = -\frac{1}{j\omega} \nabla \cdot \underline{M}_n \quad (2-74)$$

Note that  $\underline{M}_n$  is  $\underline{u}_z$  directed, so

$$\nabla \cdot \underline{M}_n = 0 \quad (2-75)$$

and it follows that

$$\sigma_n = 0 \quad \text{and} \quad \phi_n^m = 0 \quad (2-76)$$

Therefore

$$\begin{aligned} Y_{mn} &= j\omega \int_C \underline{W}_m^m \cdot \underline{A}_n^m d\underline{l} \\ &= \frac{\omega \epsilon}{4} \int_C \int_C (\underline{W}_m^m \cdot \underline{M}_n^{(2)}) H_o^{(2)}(kr) d\underline{l}' d\underline{l} \end{aligned} \quad (2-77)$$

where the unprimed integration is taken over field points and the primed integration over the source points. A specific form is developed in a manner similar to that used for  $Z_{mn}$ . Equation (2-77) can be expressed

in greater detail as

$$Y_{mn} = \frac{w\epsilon}{4} \int_{t_{m-2}}^{t_{m+2}} \int_{t_{n-2}}^{t_{n+2}} [T(t-t_m) T(t'-t_m') H_o^{(2)}(kR)] dt' dt \quad (2-78)$$

The evaluation of the integrals appearing in equation (2-78) is carried out by approximating the triangle function by four pulses as shown in Fig. 2-3. Equation (2-78) can be written as

$$Y_{mn} = \frac{w\epsilon}{4} \sum_{q=1}^4 \sum_{p=1}^4 \int_{t_q}^{t_{q+1}} \int_{t_p}^{t_{p+1}} T_p T_q H_o^{(2)}(kR) dt' dt \quad (2-79)$$

The indices p and q have the usual meaning.  $T_p$  and  $T_q$  have already been defined by equation (2-42). Each of the sixteen terms contributing to  $Y_{mn}$  falls into one of two categories. Either the p-pulse and q-pulse intervals coincide, or they do not. If the latter is true, each integral is approximated by the product of its integrand sampled at the interval midpoint times the interval length. The expression for  $Y_{mn}$  becomes

$$Y_{mn} = \frac{w\epsilon}{4} \sum_{q=1}^4 \sum_{p=1}^4 T_p T_q \Delta t_p \Delta t_q H_o^{(2)}(kR_{pq}) \quad (2-80)$$

As previously stated,  $\Delta t_p$  and  $\Delta t_q$  are defined by equation (2-45) and  $R_{pq}$  is the distance between the midpoints of the p-pulse and q-pulse intervals. For coincident p-pulse and q-pulse intervals, the improper integral and its evaluation are the same as those in  $Z_{mn}$ . Hence

$$\int_{t_q}^{t_{q+1}} \int_{t_p}^{t_{p+1}} T_p T_q H_o^{(2)}(kR) dt' dt \\ = T_p T_q \Delta t_p \Delta t_q [1 - j \frac{2}{\pi} \log(\frac{\gamma k \Delta t}{4e})] \quad (2-81)$$

where  $\log \gamma =$  Euler's constant

$$e = 2.718 \dots$$

The final expression for  $Y_{mn}$  is

$$Y_{mn} = \frac{\omega e}{4} \sum_{q=1}^4 \sum_{p=1}^4 T_p T_q \Delta t_p \Delta t_q Y \quad (2-82)$$

where

$$Y = H_o^{(2)}(kR_{pq}) \quad (\text{non-coincident intervals})$$

$$= [1 - j \frac{2}{\pi} \log(\frac{\gamma k \Delta t}{4e})] \quad (\text{coincident intervals})$$

## 2.5 Excitation Matrix, Measurement Matrix, and Scattering Cross Section

The matrix elements of the excitation matrix are represented by two expressions, equations (2-19) and (2-20). It is important to realize that the transformation of (2-19) and (2-20) into computable forms depends on the type and polarization of the impressed field. In the case under consideration, the excitation is assumed to be a z-directed magnetic field of unit magnitude. The incident field is given by

$$\underline{\underline{H}}_z^i(\rho) = e^{-jk_z \cdot \rho} \quad (2-83)$$

The wave number vector  $k$  points in the direction of travel of the incident wave. A coordinate system for the evaluation of the excitation matrix

elements is shown in Fig. 2-8.

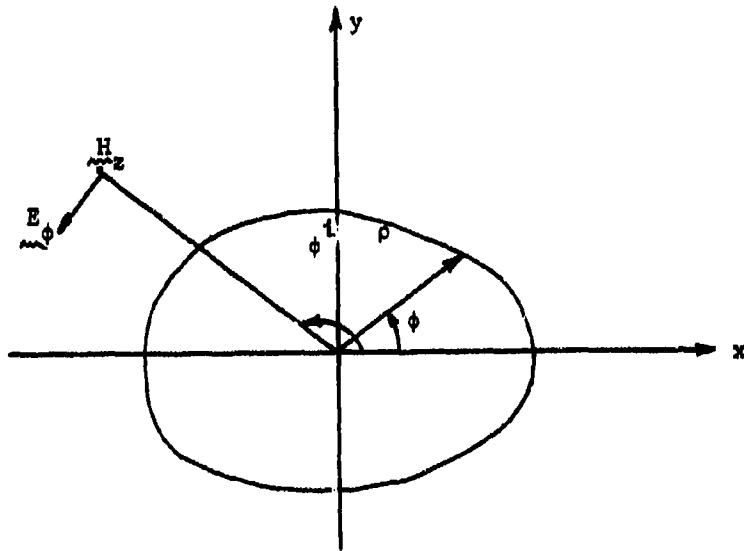


Fig. 2-8. Incident field.

Equation (2-19) will be considered first. The testing function is

$$\underline{\underline{w}}_m^a = T(\lambda - \lambda_k) \underline{\underline{u}}_k \quad (2-84)$$

For plane wave excitation the  $\phi$ -directed electric field, associated with the z-directed magnetic field defined by equation (2-83), is

$$\begin{aligned} \underline{\underline{E}}^i &= -\eta \underline{\underline{u}}_\phi e^{-jkz} \cdot \underline{\underline{u}}_k \\ &= -\eta (-\underline{\underline{u}}_x \sin \phi^i + \underline{\underline{u}}_y \cos \phi^i) e^{jk(x_{mp} \cos \phi^i + y_{mp} \sin \phi^i)} \end{aligned} \quad (2-85)$$

where  $\underline{\underline{u}}_\phi$  =  $\phi$ -directed unit vector

$\underline{\underline{u}}_x$  = x-directed unit vector

$\underline{\underline{u}}_y$  = y-directed unit vector

$\phi^i$  = incident angle

$x_{mp}, y_{mp}$  = midpoint coordinates of each straight line segment

$n$  = intrinsic wave impedance

By using four-pulse approximations for the triangle testing functions, equation (2-19) can be expressed as

$$v_m^i = \sum_{p=1}^4 \int_{t_p}^{t_{p+1}} \tilde{u}_z T_p \cdot E^i(\rho) d\rho \quad (2-86)$$

Note that the excitation matrix element  $v_m^i$  is given as the component of  $E^i(\rho)$  tangent to the contour for the  $m$ th triangle. The integral in equation (2-86) is evaluated as the tangential field component of  $E^i$  sampled at the midpoint of each  $p$ -pulse interval. Hence

$$v_m^i = -n \sum_{p=1}^4 T_p \{ e^{jk(x_{mp} \cos \phi^i + y_{mp} \sin \phi^i)} [-\Delta x \sin \phi^i + \Delta y \cos \phi^i] \} \quad (2-87)$$

where  $\Delta x$  and  $\Delta y$  are the rectangular components of the pulse interval. A portion of the contour is shown in Fig. 2-9 which illustrates how equation (2-87) is obtained.

Equation (2-20) can be evaluated in a similar manner. The testing functions are triangle functions, and each triangle function is represented by equation (2-39) and chosen to be z-directed.

$$\tilde{w}_k = T(l - l_k) \tilde{u}_z \quad (2-88)$$

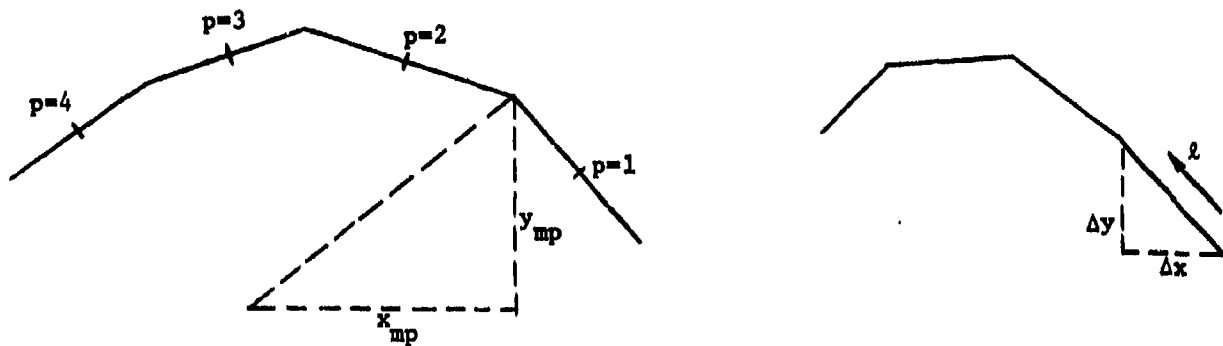


Fig. 2-9. A partial contour.

The evaluation of (2-20) is quite straightforward and the procedures are identical to those used in the evaluation of  $V_m^1$ . Hence

$$I_m^1 = j \sum_{p=1}^4 T_p \Delta t_p e^{jk(x_{mp} \cos \phi^1 + y_{mp} \sin \phi^1)} \quad (2-89)$$

The distant scattered field can be evaluated by reciprocity. A z-directed magnetic current filament at  $\rho_0$  of strength  $M_p$  is adjusted to produce the unit plane wave incident on the material body

$$\underline{\underline{H}}^1 = \underline{\underline{u}}_z e^{jk(x_n \cos \phi^8 + y_n \sin \phi^8)} \quad (2-90)$$

Note that  $M_p$  produces a  $\phi$ -directed  $\underline{\underline{E}}^1$  and a z-directed  $\underline{\underline{H}}^1$

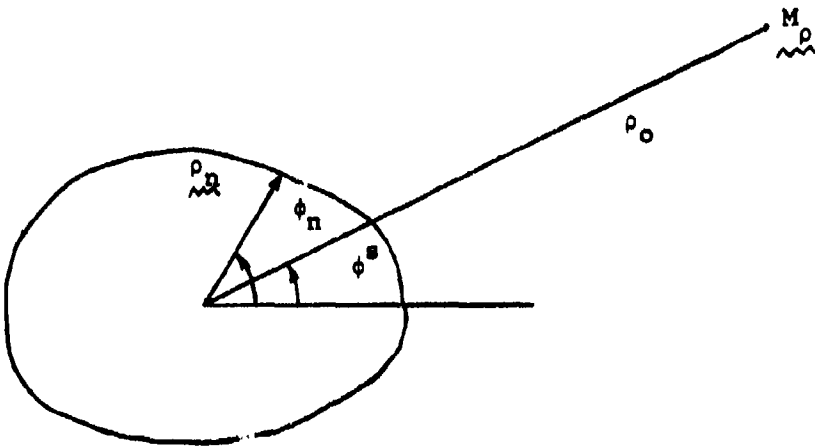


Fig. 2-10. A two-dimensional contour and z-directed magnetic current filament.

By reciprocity it is evident that

$$-\mathbf{H}_0 = \frac{1}{M} \int_C (\mathbf{E}^i \cdot \mathbf{n} - \mathbf{H}^i \cdot \mathbf{M}) d\ell \quad (2-91)$$

or

$$-\mathbf{H}_0 = \frac{1}{M_p} \int_C \begin{bmatrix} \mathbf{E}^i \\ \mathbf{jH}^i \end{bmatrix} d\ell \quad (2-92)$$

where

$$\mathbf{f} = \begin{bmatrix} \mathbf{J} \\ \mathbf{jM} \end{bmatrix}$$

Equation (2-7) can be expressed in matrix form as

$$\mathbf{f} = \begin{bmatrix} [\mathbf{I}_n] & [\mathbf{J}_n] \\ [\mathbf{V}_n] & [\mathbf{M}_n] \end{bmatrix} \quad (2-93)$$

With the help of equation (2-93), a new form for equation (2-92) is

$$-H_p = \frac{1}{M_p} [D] \begin{bmatrix} [I_n] \\ [V_n] \end{bmatrix} \quad (2-94)$$

Note that  $[I_n]$  and  $[V_n]$  are column matrices, and the matrix  $[D]$  is

$$[D] = \left[ \left( \int_C \frac{E^i}{\lambda} \cdot [\widetilde{J}_n] d\lambda \right) \left( \int_C [\widetilde{M}_n] \cdot jH^i d\lambda \right) \right] \quad (2-95)$$

The values of  $I_n$  and  $V_n$  can be obtained from equation (2-14) by matrix inversion. The constant  $1/M_p$  is that needed to produce a plane wave of unit amplitude at the origin, which is

$$\begin{aligned} \frac{1}{M_p} &= -\frac{k^2}{4\omega\mu} H_0^{(2)}(k\rho_0) \\ &= -\frac{\omega\epsilon}{4} H_0^{(2)}(k\rho_0) \end{aligned} \quad (2-96)$$

Redefine equation (2-95) as

$$[D] = \{[D^e] \ [D^m]\} \quad (2-97)$$

where

$$D_n^e = \int_C \frac{E^i}{\lambda} \cdot [\widetilde{J}_n] d\lambda \quad (2-98)$$

$$D_n^m = \int_C jH^i \cdot [\widetilde{M}_n] d\lambda \quad (2-99)$$

The evaluation of the integrals in equation (2-98) and (2-99) is straightforward, and the procedures involved are completely analogous to

those used in the evaluation of  $V_m^i$  and  $I_m^i$ . Only the results will be given here

$$D_n^e = -n \sum_{p=1}^4 T_p e^{jk(x_{np} \cos \phi^s + y_{np} \sin \phi^s)} [-\Delta x \sin \phi^s + \Delta y \cos \phi^s] \quad (2-100)$$

$$D_n^m = j \sum_{p=1}^4 T_p \Delta t_p e^{jk(x_{np} \cos \phi^s + y_{np} \sin \phi^s)} \quad (2-101)$$

The scattered field can be expressed as

$$H_\rho = \frac{\omega \epsilon}{4} H_0^{(2)}(k\rho_0) [[D_m^e][D_n^m]] \begin{bmatrix} [I_n] \\ [V_n] \end{bmatrix} \quad (2-102)$$

or

$$H_\rho = \frac{\omega \epsilon}{4} H_0^{(2)}(k\rho_0) [[D_n^e][D_n^m]] \begin{bmatrix} [Z] & [B] \\ [C] & [Y] \end{bmatrix}^{-1} \begin{bmatrix} [V_n^i] \\ [I_n^i] \end{bmatrix} \quad (2-103)$$

In the scattering problem, the bistatic scattering cross section  $\sigma$  is a parameter of interest. It is defined as the width for which the incident wave carries sufficient power to produce the field  $E_\rho$ ,  $H_\rho$  by omnidirectional radiation. It may be expressed as

$$\sigma(\phi^s) = 2\pi \rho_0 \lim_{\rho_0 \rightarrow \infty} \left| \frac{E_\rho(\phi^s)}{\rho_0} \right|^2$$

or

$$= 2\pi \rho_0 \lim_{\rho_0 \rightarrow \infty} \left| H_\rho(\phi^s) \right|^2 \quad (2-104)$$

The large argument approximation for  $H_0^{(2)}(kR)$  is

$$H_0^{(2)}(x) \xrightarrow{x \rightarrow \infty} \sqrt{\frac{2i}{\pi x}} e^{-jx} \quad (2-107)$$

The expression for the scattering cross section can be stated as

$$\begin{aligned} \sigma &= \lim_{\rho_0 \rightarrow \infty} 2\pi\rho_0 \left| \frac{w_0}{4} \sqrt{\frac{2}{\pi k\rho_0}} h \right|^2 \\ &= \frac{k}{4\pi} |h|^2 \end{aligned} \quad (2-106)$$

where

$$h = \begin{vmatrix} [D] & \begin{bmatrix} [Z] & [B] \\ [C] & [Y] \end{bmatrix}^{-1} & \begin{bmatrix} [V_n^i] \\ [I_n^i] \end{bmatrix} \end{vmatrix}$$

CHAPTER 3  
CHARACTERISTIC MODES - A SURFACE FORMULATION

### 3.1 Theoretical Development

The treatment of characteristic modes for perfectly conducting bodies, starting from the impedance operator for the conducting surface, has been given by Harrington and Mautz [2]. In terms of the polarization current and the magnetization current, a volume formulation of the characteristic mode theory for dielectric and magnetic bodies has also been treated [4]. In this chapter a theory of characteristic modes for material bodies (dielectric, magnetic, or both) based on a surface formulation is developed. The appropriate operator formulation of the problem is

$$\begin{bmatrix} Le & N \\ N & Lm \end{bmatrix} \begin{bmatrix} J \\ jM \end{bmatrix} = \begin{bmatrix} E^i \\ jH^i \end{bmatrix} \quad (3-1)$$

To emphasize the symmetric nature of the matrix of operators, the off-diagonal operators are denoted by a single symbol, N. Define the following rise vectors

$$f = \begin{bmatrix} J \\ jM \end{bmatrix}, \quad g = \begin{bmatrix} E \\ jH \end{bmatrix} \quad (3-2)$$

and the matrix of operators

$$T = \begin{bmatrix} Le & N \\ N & Lm \end{bmatrix} \quad (3-3)$$

where  $N = -jC$ .

Equation (3-1) can then be written as

$$\tilde{T}f = \frac{i}{\tilde{g}}$$

Define the symmetric product

$$\begin{aligned} \langle f, g \rangle &= \iint_S \tilde{f} \tilde{g} ds \\ &= \iint_S (J \cdot E - M \cdot H) ds \end{aligned} \quad (3-4)$$

which, for  $f$  a source quantity and  $g$  a field quantity, is reaction. The product

$$\begin{aligned} \langle f^*, g \rangle &= \iint_S \tilde{f}^* g ds \\ &= \iint_S (J^* \cdot E + M^* \cdot H) ds \end{aligned} \quad (3-5)$$

is a suitable inner product for the Hilbert space of functions  $\tilde{f}, \tilde{g}$  in  $S$ .

If  $f$  is a source quantity and  $g$  a field quantity, the real part of (3-5) is time average power, but the imaginary part of (3-5) differs from the usual imaginary power. It is easy to show that  $T$  is symmetric, that is,

$\langle f_1, Tf_2 \rangle = \langle f_2, Tf_1 \rangle$  by reciprocity. The operator  $T$  can be expressed in terms of its Hermitian parts as  $T = T_1 + jT_2$  where

$$T_1 = \frac{1}{2} (T + T^*) = \begin{bmatrix} R & N_1 \\ N_1 & G \end{bmatrix} \quad (3-6)$$

$$T_2 = \frac{1}{2j} (T - T^*) = \begin{bmatrix} X & N_2 \\ N_2 & B \end{bmatrix} \quad (3-7)$$

Here  $N_1$  and  $N_2$  are the Hermitian parts of  $N$ ,  $R$  and  $X$  are the Hermitian parts of  $Z$ ,  $G$  and  $B$  are the Hermitian parts of  $Y$ .

By equation (1-9), the fields due to  $J$  and  $M$  can be expressed as

$$\begin{bmatrix} J \\ jM \end{bmatrix} = - \begin{bmatrix} E \\ jH \end{bmatrix}; \quad L' = \begin{bmatrix} Le' & -jC' \\ -jC' & Lm' \end{bmatrix} \quad (3-8)$$

As far as radiation is concerned, the contribution due to the doubly primed operators is zero. The power radiated by any  $\underline{\underline{J}}$  and  $\underline{\underline{M}}$  on  $S$  is given by

$$\begin{aligned} \text{Re}(P_S) &= -\text{Re} \iint_{\text{mm}} (E \cdot \underline{\underline{J}}^* + M \cdot \underline{\underline{H}}^*) ds \\ &= -\text{Re} \iint_{\text{mm}} (E \cdot \underline{\underline{J}}^* + M^* \cdot \underline{\underline{H}}) ds \\ &= \text{Re} \left\langle \underline{\underline{f}}^*, T \underline{\underline{f}} \right\rangle \end{aligned} \quad (3-9)$$

Hence the time average power delivered by a source  $f$  is

$$\text{Re}(P_S) = \text{Re} \left\langle \underline{\underline{f}}^*, T \underline{\underline{f}} \right\rangle \quad (3-10)$$

The imaginary part of  $\left\langle \underline{\underline{f}}^*, T \underline{\underline{f}} \right\rangle$  is not simply related to reactive power.

Using six-vector notation, we formulate a theory of characteristic modes which parallels that of the volume formulation [4]. The eigenvalue equation defining the modes is

$$\sum_{\text{nn}} T_2(f_n) = \lambda_n \sum_{\text{nn}} T_1(f_n) \quad (3-11)$$

where  $T_1$  and  $T_2$  are real symmetric operators. Hence, all eigenvalues  $\lambda_n$  are real and all characteristic sources  $f_n$  may be chosen real. In expanded form

$$\tilde{f}_n = \begin{bmatrix} J_n \\ \sim \\ jM_n \end{bmatrix} \quad (3-12)$$

which, for characteristic sources, implies that  $M_n$  is imaginary and  $J_n$  is real. The characteristic sources can be normalized to radiate unit power, and the usual orthogonality relationships expressed as

$$\begin{aligned} \langle \tilde{f}_m^*, T_1 \tilde{f}_n \rangle &= \langle \tilde{f}_m, T_1 \tilde{f}_n \rangle = \delta_{mn} \\ \sim &\quad \sim \quad \sim & \sim \\ \langle \tilde{f}_m^*, T_2 \tilde{f}_n \rangle &= \langle \tilde{f}_m, T_2 \tilde{f}_n \rangle = \lambda_n \delta_{mn} \\ \sim &\quad \sim \quad \sim & \sim \\ \langle \tilde{f}_m^*, T_f \tilde{f}_n \rangle &= \langle \tilde{f}_m, T_f \tilde{f}_n \rangle = (1 + j\lambda_n) \delta_{mn} \end{aligned} \quad (3-13)$$

where  $\delta_{mn}$  is the Kronecker delta. The field

$$\tilde{s}_n = \begin{bmatrix} E_n \\ \sim \\ jH_n \end{bmatrix} \quad (3-14)$$

due to a source  $\tilde{f}_n$  is called a characteristic field. In the radiation zone the characteristic field is of the form of an outward traveling wave, and it is completely characterized by either  $E_n$  or  $H_n$ .

Let  $\tilde{f}_m$  and  $\tilde{f}_n$  be two characteristic sources. By equation (3-13), the following expression is true.

$$\begin{aligned} \langle \tilde{f}_m^*, T_f \tilde{f}_n \rangle &= \langle \begin{bmatrix} J_m & jM_m \\ \sim & \sim \end{bmatrix} \begin{bmatrix} L_e & N \\ N & L_m \end{bmatrix} \begin{bmatrix} J_n \\ \sim \\ jM_n \end{bmatrix} \rangle \\ &= 0 \quad \text{for } m \neq n \end{aligned} \quad (3-15)$$

Equation (3-13) is essentially

$$\iint (\tilde{J}_m \cdot \tilde{E}_n - \tilde{H}_n \cdot \tilde{M}_m) ds = 0 \quad (3-16)$$

where  $\tilde{E}_n$  and  $\tilde{H}_n$  are produced by  $f_n$ . Because  $J_m$  is real and  $M_m$  is imaginary, we have

$$\operatorname{Re} \iint_{\text{boundary}} (\tilde{J}_m^* \cdot \tilde{E}_n + \tilde{H}_n^* \cdot \tilde{M}_m) ds = 0 \quad (3-17)$$

It follows that

$$\operatorname{Re} \iint_{\text{boundary}} (\tilde{E}_n \cdot \tilde{J}_m^* + \tilde{H}_n^* \cdot \tilde{M}_m) ds = 0 \quad (3-18)$$

which means that the real part of the cross power is zero. In the radiation zone the characteristic waves are of the form of outward traveling wave, i.e.

$$\tilde{E}_n = n \tilde{H}_n \times n \quad (3-19)$$

where  $n$  is the unit radial vector on  $S_\infty$ . The real part of the cross power can be expressed as

$$\operatorname{Re} \iint_{\text{boundary}} \tilde{E}_m \times \tilde{H}_n^* \cdot ds = \operatorname{Re} \iint_{\text{boundary}} \frac{\tilde{E}_m \cdot \tilde{E}_n^*}{n} ds = 0 \quad (3-20)$$

The real part of the cross power between  $j(\tilde{E}_n, \tilde{H}_n)$  and  $(\tilde{E}_m, \tilde{H}_m)$  is also zero. Hence,

$$\frac{1}{n} \iint_{\text{boundary}} \tilde{E}_m \cdot \tilde{E}_n^* ds = n \iint_{\text{boundary}} \tilde{H}_m \cdot \tilde{H}_n^* ds = \delta_{mn} \quad (3-21)$$

### 3.2 Characteristic Equation and Modal Representation

In the preceding section, the analytical development was based on the interpretation of operators. The reduction of operator equations to matrix equations can be effected in the usual manner by the method of moments.

Let

$$\tilde{f}_n = \sum_j (I_j f_j^e + V_j f_j^m) \quad (3-22)$$

where

$$f_j^e = \begin{bmatrix} W_j^e \\ M_j \\ 0 \end{bmatrix}, \quad f_j^m = \begin{bmatrix} 0 \\ W_j^m \\ M_j \end{bmatrix} \quad (3-23)$$

After substituting equation (3-22) into equation (3-11), the following is obtained.

$$\left\{ \sum_j I_j T_2 f_j^e + \sum_j V_j T_2 f_j^m \right\} = \lambda_n \left\{ \sum_j I_j T_1 f_j^e + \sum_j V_j T_1 f_j^m \right\} \quad (3-24)$$

Perform inner product with electric testing function  $W_i^e$ ,

$$\begin{aligned} & \left\{ \sum_j I_j \langle W_i^e, T_2 f_j^e \rangle + \sum_j V_j \langle W_i^e, T_2 f_j^m \rangle \right\} \\ &= \lambda_n \left\{ \sum_j I_j \langle W_i^e, T_1 f_j^e \rangle + \sum_j V_j \langle W_i^e, T_1 f_j^m \rangle \right\} \quad (3-25) \end{aligned}$$

and with magnetic testing function  $W_i^m$ .

$$\begin{aligned} & \left\{ \sum_j I_j \langle W_i^m, T_2 f_j^e \rangle + \sum_j V_j \langle W_i^m, T_2 f_j^m \rangle \right\} \\ &= \lambda_n \left\{ \sum_j I_j \langle W_i^m, T_1 f_j^e \rangle + \sum_j V_j \langle W_i^m, T_1 f_j^m \rangle \right\} \quad (3-26) \end{aligned}$$

Equation (3-25) and equation (3-26) can be put into one matrix equation.

$$\begin{bmatrix} [X] & [N_2] \\ \widetilde{[N_2]} & [B] \end{bmatrix} \begin{bmatrix} [I] \\ [V] \end{bmatrix}_n = \lambda_n \begin{bmatrix} [R] & [N_1] \\ \widetilde{[N_1]} & [G] \end{bmatrix} \begin{bmatrix} [I] \\ [V] \end{bmatrix}_n \quad (3-27)$$

The definitions of  $[X]$ ,  $[N_2]$ ,  $[B]$ ,  $[R]$ ,  $[N_1]$ ,  $[G]$ ,  $[I]$ , and  $[V]$  are obvious by comparing equation (3-27) with equations (3-25) and (3-26).

Equation (3-27) is the eigenvalue equation which will be used in the actual computation of the modes. In abbreviated form, it becomes

$$[T_2] \underset{\sim}{\underset{\sim}{[f_n]}} = \lambda_n [T_1] \underset{\sim}{\underset{\sim}{[f_n]}} \quad (3-28)$$

Now, with the understanding that  $\lambda_n$  and  $f_n$  can be found, the modal solution for  $f$  can be expressed as

$$\underset{\sim}{\underset{\sim}{f}} = \sum_n a_n \underset{\sim}{\underset{\sim}{f_n}} \quad (3-29)$$

Recall that

$$\underset{\sim}{\underset{\sim}{Tf}} = \underset{\sim}{\underset{\sim}{g^i}} \quad (3-30)$$

After substituting equation (3-29) into equation (3-30) and performing the inner product with  $f_m$ , the following equation results.

$$\sum_n a_n \underset{\sim}{\underset{\sim}{\langle f_m, Tf_n \rangle}} = \underset{\sim}{\underset{\sim}{\langle f_m, g^i \rangle}} \quad (3-31)$$

Apply the orthogonality relationships given in equation (3-13). It follows that

$$a_n = \frac{\underset{\sim}{\underset{\sim}{\langle f_m, g^i \rangle}}}{(1 + j \lambda_n) \underset{\sim}{\underset{\sim}{\langle f_m, Tf_n \rangle}}} \quad (3-32)$$

Explicitly,

$$\underset{\sim}{\underset{\sim}{\langle f_m, g^i \rangle}} = \sum_i I_i \underset{\sim}{\underset{\sim}{\langle f_i^e, g^i \rangle}} + \sum_i V_i \underset{\sim}{\underset{\sim}{\langle f_i^m, g^i \rangle}} \quad (3-33)$$

The matrix equivalents of the orthogonality relationships for the characteristic currents, equation (3-13), are also of interest. For example, that for  $T_1$  is

$$\begin{aligned}
 \langle \underset{\sim}{f}_m, T_1 \underset{\sim}{f}_n \rangle &= \left\langle \sum_i \left( I_i f_i^e + V_i f_i^m \right)_m, T_1 \sum_j \left( I_j f_j^e + V_j f_j^m \right)_n \right\rangle \\
 &= \sum_{i,j} \left\{ I_i I_j \langle \underset{\sim}{f}_i^e, T_1 \underset{\sim}{f}_j^e \rangle + I_i V_j \langle \underset{\sim}{f}_i^e, T_1 \underset{\sim}{f}_j^m \rangle \right. \\
 &\quad \left. + V_i I_j \langle \underset{\sim}{f}_i^m, T_1 \underset{\sim}{f}_j^e \rangle + V_i V_j \langle \underset{\sim}{f}_i^m, T_1 \underset{\sim}{f}_j^m \rangle \right\} \\
 &= [\widetilde{I}]_m [R] [\widetilde{I}]_n + [\widetilde{I}]_m [N_1] [\widetilde{V}]_n \\
 &\quad + [\widetilde{V}]_m [\widetilde{N}_1] [\widetilde{I}]_n + [\widetilde{V}]_m [G] [\widetilde{V}]_n \\
 &= [\widetilde{\underset{\sim}{f}}_m] [T_1] [\underset{\sim}{f}_n] = \delta_{mn} \tag{3-34}
 \end{aligned}$$

where  $\widetilde{\cdot}$  denotes transpose. Similar derivations hold for  $T_2$  and  $T$ .

### 3.3 Linear Measurement

Any scalar  $\rho$  linearly related to the generalized current, i.e. a linear functional of the equivalent electric and magnetic currents, will be called a linear measurement of the current.

Any linear functional of  $f$  can be expressed as

$$\rho = \langle \underset{\sim}{g}^m, \underset{\sim}{f} \rangle \tag{3-35}$$

where  $\underset{\sim}{g}^m$  is a vector function which consists of an electric field and a magnetic field. By equations (3-32) and (3-33), the linear measurement of  $f$  can be stated as

$$\rho = \sum_n \frac{\langle \underset{\sim}{f}_n, \underset{\sim}{g}^i \rangle}{(1 + j\lambda_n) \langle \underset{\sim}{f}_n, T_1 \underset{\sim}{f}_n \rangle} \langle \underset{\sim}{g}^m, \underset{\sim}{f}_n \rangle \tag{3-36}$$

where

$$\sum \langle g^m, f_n \rangle = \sum I_{in} \sum \langle g^m, f_i^e \rangle = \sum v_{in} \sum \langle g^m, f_i^m \rangle \quad (3-37)$$

and define the following

$$K_n^m = \sum \langle g^m, f_n \rangle = \text{modal measurement coefficient} \quad (3-38)$$

$$\sum \langle g^i, f_n \rangle = \text{modal excitation coefficient} \quad (3-39)$$

Equation (3-36) is a symmetric bilinear functional of  $\sum g^i$  (the impressed field) and of  $\sum g^m$  (the measured field). The symmetry of (3-36) is a consequence of the symmetry of the original operator T. Equation (3-36) can be expressed as

$$p = \sum_n \frac{K_n^i K_n^m}{1 + j \lambda_n} \quad (3-40)$$

similarly, in terms of  $K_n^i$  equation (3-32) becomes

$$\alpha_n = \frac{K_n^i}{1 + j \lambda_n} \quad (3-41)$$

and equation (3-29) will take the form

$$\sum f_n = \sum_n \frac{K_n^i}{1 + j \lambda_n} f_n \quad (3-42)$$

### 3.4 Characteristic Fields and Scattering Cross Section

The characteristic fields are linearly related to the characteristic currents,  $f_n$ , and hence can also be expressed in modal form.

$$\sum g_n = \sum_n \frac{K_n^i}{1 + j \lambda_n} g_n \quad (3-43)$$

When  $K_n^1$  and  $f_n$  are known, the field pattern can be obtained by employing equation (3-43). A convenient way is to evaluate the modal measurement coefficient first. In the two-dimensional case, consider a magnetic current filament,  $M = M u_m$  at  $(\rho_m, \phi)$  on  $S_\infty$ . See Fig. 3-1 below.

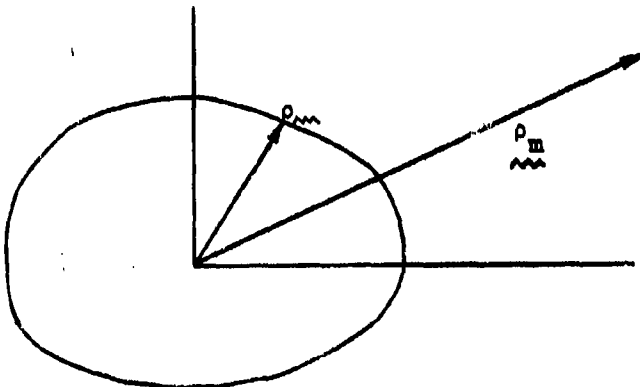


Fig. 3-1. A coordinate system for modal measurement coefficient

By reciprocity, it is readily seen that

$$\int_{S_\infty} H_n \cdot M = \int_{S_\infty} (J_n \cdot E_m - M_n \cdot H_m) ds \quad (3-44)$$

where  $H_n$  is the characteristic field components produced by the mode current  $f_n$ .  $E_m$  and  $H_m$  are the fields due to the magnetic current filament,  $M$ . To simplify the analysis, the magnitude of the magnetic current,  $M$ , is adjusted to produce a plane wave on the material body, i.e.

$$\int_{S_\infty} H_m = u_m e^{-jk_m \cdot r_m} \quad (3-45)$$

$$\int_{S_\infty} E_m = n H_m \times u_{km} \quad (3-46)$$

where  $\eta$  is the wave impedance and  $\hat{u}_{km}$  is the unit vector in the direction of propagation. The right hand side of equation (3-44), in matrix form, is the modal measurement coefficient. Hence,

$$K_n^m = \int_c (\hat{J}_n \cdot \hat{E}_m - \hat{M}_n \cdot \hat{H}_m) dt \quad (3-47)$$

Explicitly, the electric field and the magnetic field can be extracted from equation (3-43) as

$$\hat{E} = \sum_n \frac{K_n^1}{1 + j \lambda_n} \hat{E}_n \quad (3-48)$$

$$\hat{H} = \sum_n \frac{K_n^1}{1 + j \lambda_n} \hat{H}_n \quad (3-49)$$

Since the magnetic field is currently under consideration, only equation (3-49) will be used. The component of the magnetic field on  $\hat{u}_m$  is

$$\begin{aligned} \hat{H} \cdot \hat{u}_m &= \sum_n \frac{K_n^1}{1 + j \lambda_n} \hat{H}_n \cdot \hat{u}_m \\ &= -\frac{1}{M} \sum_n \frac{K_n^1 K_n^m}{1 + j \lambda_n} \\ &= -\frac{\omega \epsilon}{4} H_0^{(2)} (k\rho) \sum_n \frac{K_n^1 K_n^m}{1 + j \lambda_n} \end{aligned} \quad (3-50)$$

Note that  $K_n^1$  is of the same functional form as  $K_n^m$ . Equation (2-98) has been used in deriving equation (3-50).

A commonly used parameter in plane wave scattering problems is the echo area. In two-dimensional problems the quantity "echo width" corresponds to the "echo area" of the three-dimensional problems.

The echo width is defined in equation (2-106).

$$\sigma = 2 \pi \rho_m | \sum_{m=1}^{\infty} H_m \cdot u_m |^2 \quad (3-51)$$

limit  $\rho_m \rightarrow \infty$

By equations (3-50) and (2-106), the following expression for the scattering cross section is obtained.

$$\sigma = \frac{k}{4 n^2} \left| \sum_n \frac{K_n^1 K_n^m}{1 + j \lambda_n} \right|^2 \quad (3-52)$$

### 3.5 Computational Considerations

The solution of the matrix eigenvalue problem, equation (3-28), will be discussed.

$$[T_2] \underbrace{[f]}_{\sim} = \lambda [T_1] \underbrace{[f]}_{\sim} \quad (3-53)$$

Note that the subscript  $n$  has been dropped for brevity. The conventional method for reducing (3-53) to a symmetric unweighted eigenvalue equation requires  $[T_2]$  to be positive definite. In theory  $[T_1]$  is positive semi-definite, but because of numerical inaccuracies it is actually indefinite, with some small negative eigenvalues. If the values of the matrix elements cover a very wide range, scaling will become desirable. The magnitude of the scale factor can be chosen as such that all scaled matrix elements will be brought, as close as possible, to the same order of magnitude. The conventional method will be modified as follows.

Let  $[D]$  be a diagonal matrix. After premultiplying by  $[D]$ , equation (3-47) becomes

$$[D][T_2] \underset{\sim}{[f]} = \lambda [D][T_1] \underset{\sim}{[f]} \quad (3-54)$$

Then observe that

$$\begin{aligned} [D][T_2][D]^{-1}([D]^{-1}\underset{\sim}{[f]}) \\ = \lambda [D][T_1][D]^{-1}([D]^{-1}\underset{\sim}{[f]}) \end{aligned} \quad (3-55)$$

The eigenvalue equation as given by (3-55) will have the same eigenvalues as the original unscaled equation, but the eigenvectors will be different. In other words the eigenvalues are not affected by the diagonal transformation. The original eigenvectors will be modified by [D] inverse. If the scale factor is  $s$ , [D] can be chosen as

$$[D] = \begin{bmatrix} 1/s & 0 \\ 0 & 1 \end{bmatrix} \quad (3-56)$$

By equations (3-27), (3-55), and (3-56), the scaled eigenvalue equation is

$$[T_2^s] \underset{\sim}{[f^s]} = \lambda [T_1^s] \underset{\sim}{[f^s]} \quad (3-57)$$

where

$$[T_2^s] = \begin{bmatrix} [X]/s^2 & [N_2]/s \\ [\widetilde{N}_2]/s & [B] \end{bmatrix} \quad (3-58)$$

$$[T_1^s] = \begin{bmatrix} [R]/s^2 & [N_1]/s \\ [\widetilde{N}_1]/s & [G] \end{bmatrix} \quad (3-59)$$

and

$$[\begin{array}{c} \tilde{f}^s \\ \tilde{\mathbf{v}} \end{array}] = \begin{bmatrix} s[\mathbf{I}] \\ [\mathbf{V}] \end{bmatrix} \quad (3-60)$$

Note that  $[\mathbf{I}]$  and  $[\mathbf{V}]$  ( $\mathbf{J}$  and  $\mathbf{M}$ ) should first be recovered from the scaled eigenvectors before computing the surface currents and the scattered fields.

Rewrite equation (3-57) below

$$[\mathbf{T}_2][\begin{array}{c} \tilde{f} \\ \tilde{\mathbf{r}} \end{array}] = \lambda [\mathbf{T}_1][\begin{array}{c} \tilde{f} \\ \tilde{\mathbf{r}} \end{array}] \quad (3-61)$$

Note that the superscripts have been dropped for brevity. An approximation will be used in finding the eigenvalues and eigenvectors. The eigenvalue equation

$$[\mathbf{T}_1][\begin{array}{c} \tilde{r} \\ \tilde{\mathbf{r}} \end{array}] = \mu [\begin{array}{c} \tilde{r} \\ \tilde{\mathbf{r}} \end{array}] \quad (3-62)$$

is used to find a set of basis functions for the  $\mathbf{T}_1$  vector space. An orthonormal set of vectors can be obtained by using the vectors  $\{\mathbf{r}_1\}$ . Let  $\{\mathbf{U}_1\}$  be the set of orthonormal vectors, and let  $[\mathbf{U}]$  be the orthogonal matrix which diagonalizes  $[\mathbf{T}_1]$  according to

$$[\widetilde{\mathbf{U}}][\mathbf{T}_1][\mathbf{U}] = \begin{bmatrix} \mu_1 0 0 0 \dots \\ 0 \mu_2 0 0 \dots \\ 0 0 \mu_3 0 \dots \\ 0 0 0 \mu_4 \dots \\ \dots \dots \dots \\ \dots \dots \dots \end{bmatrix} \quad (3-63)$$

where the  $\mu_i$  are the eigenvalues of  $[\mathbf{T}_1]$  ordered  $\mu_1 \geq \mu_2 \geq \mu_3 \geq \mu_4 \geq \dots$ . Every column of  $[\mathbf{U}]$  is in  $\{\mathbf{U}_1\}$ . Only the larger  $\mu_i$  can be considered accurate. All  $\mu_i > M\mu_1$  are put in  $[\mu_1]$  where  $M$  is some small positive number set by the estimated accuracy of  $[\mathbf{T}_1]$ . Usually  $M$  is anywhere between  $10^{-3}$  and  $10^{-6}$ . The diagonal matrix  $[\mu]$  is then partitioned as

$$[u] = \begin{bmatrix} [u_1] & [0] \\ [0] & [u_2] \end{bmatrix} \quad (3-64)$$

where

$$[u_1] = \begin{bmatrix} u_1 & & & 0 \\ & u_2 & & \\ & & \ddots & \\ & 0 & & u_m \end{bmatrix} \quad (3-65)$$

$$[u_2] = \begin{bmatrix} u_{m+1} & & & 0 \\ & u_{m+2} & & \\ & & \ddots & \\ & 0 & & u_n \end{bmatrix} \quad (3-66)$$

Now consider

$$f = \sum_{k=1}^n x_k \underbrace{U_k}_{\sim \sim} \quad (3-67)$$

where  $\underbrace{U_k}_{\sim \sim}$  is a column vector of  $[U]$ . This is a valid expansion because the  $\{\underbrace{U_k}_{\sim \sim}\}$  vectors form a basis for  $T_1$  vector space. In matrix form equation (3-67) becomes

$$f = [\underbrace{U}_{\sim \sim}] [\underbrace{x}_{\sim \sim}] \quad (3-68)$$

If  $[u_2]$  is set to zero, it follows that all column vectors of  $[U]$  corresponding to all  $u_k \in [u_2]$  are in the null space of  $T_1$ . This is illustrated in Fig. 3-2.

The expression for  $f$  as given in equation (3-67) can be written as

$$f = \sum_{i=1}^m x_i \underbrace{U_i}_{\sim \sim} + \sum_{k=m+1}^n x_k \underbrace{U_k}_{\sim \sim} \quad (3-69)$$

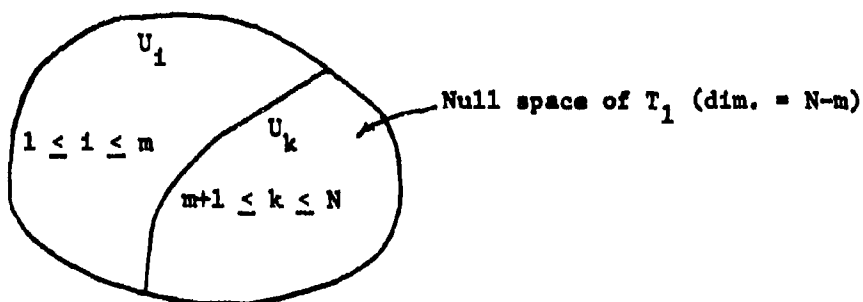


Fig. 3-2.  $T_1$  vector space

The column vector  $\begin{bmatrix} \mathbf{x} \end{bmatrix}$  in equation (3-68) can be partitioned as

$$\begin{bmatrix} \mathbf{x} \end{bmatrix} = \begin{bmatrix} \widetilde{\mathbf{U}} \end{bmatrix} \begin{bmatrix} \mathbf{f} \end{bmatrix} = \begin{bmatrix} \begin{bmatrix} \mathbf{x}_1 \\ \mathbf{x}_2 \end{bmatrix} \end{bmatrix} \quad (3-70)$$

where  $\begin{bmatrix} \mathbf{x}_1 \end{bmatrix}$  and  $\begin{bmatrix} \mathbf{x}_2 \end{bmatrix}$  are column vectors, and they are obtained by partitioning  $\begin{bmatrix} \mathbf{x} \end{bmatrix}$  according to equation (3-69). Premultiply equation (3-61) by  $\begin{bmatrix} \widetilde{\mathbf{U}} \end{bmatrix}$  and use equations (3-63) and (3-68). The result is

$$\begin{bmatrix} \widetilde{\mathbf{U}} \end{bmatrix} \begin{bmatrix} T_2 \end{bmatrix} \begin{bmatrix} \mathbf{U} \end{bmatrix} \begin{bmatrix} \mathbf{x} \end{bmatrix} = \lambda \begin{bmatrix} \mu \end{bmatrix} \begin{bmatrix} \mathbf{x} \end{bmatrix} \quad (3-71)$$

Set  $\begin{bmatrix} \mu_2 \end{bmatrix}$  equal to zero and partition all other matrices conformably. The following two matrix equations are obtained.

$$\begin{bmatrix} A_{11} \end{bmatrix} \begin{bmatrix} \mathbf{x}_1 \end{bmatrix} + \begin{bmatrix} A_{12} \end{bmatrix} \begin{bmatrix} \mathbf{x}_2 \end{bmatrix} = \lambda \begin{bmatrix} \mu_1 \end{bmatrix} \begin{bmatrix} \mathbf{x}_1 \end{bmatrix} \quad (3-72)$$

$$\begin{bmatrix} A_{12} \end{bmatrix} \begin{bmatrix} \mathbf{x}_1 \end{bmatrix} + \begin{bmatrix} A_{22} \end{bmatrix} \begin{bmatrix} \mathbf{x}_2 \end{bmatrix} = 0 \quad (3-73)$$

Note that  $\begin{bmatrix} A \end{bmatrix} = \begin{bmatrix} \widetilde{\mathbf{U}} \end{bmatrix} \begin{bmatrix} T_2 \end{bmatrix} \begin{bmatrix} \mathbf{U} \end{bmatrix}$ . Equation (3-73) can be solved for  $\begin{bmatrix} \mathbf{x}_2 \end{bmatrix}$  and the result substituted into equation (3-72) to get

$$\begin{bmatrix} A_{11} - A_{12} A_{22}^{-1} \widetilde{A}_{12} \end{bmatrix} \begin{bmatrix} \mathbf{x}_1 \end{bmatrix} = \lambda \begin{bmatrix} \mu_1 \end{bmatrix} \begin{bmatrix} \mathbf{x}_1 \end{bmatrix} \quad (3-74)$$

The brackets of submatrices have been dropped to conserve space.

Now  $[\mu_1]$  has only positive diagonal elements as defined by equation (3-65).

Observe that

$$[\mu_1] = [\mu_1^{1/2}] [\mu_1^{1/2}] \quad (3-75)$$

where

$$[\mu_1^{1/2}] = \begin{bmatrix} \mu_1^{1/2} & & & & & \\ & \mu_2^{1/2} & & & & \\ & & \mu_3^{1/2} & & & \\ & & & \ddots & & \\ & & & & & \\ 0 & & & & & \mu_m^{1/2} \end{bmatrix} \quad (3-76)$$

By equations (3-74) and (3-75) a new and unweighted eigenvalue equation is obtained.

$$[B][\tilde{y}] = \lambda [\tilde{y}] \quad (3-77)$$

where

$$[\tilde{y}] = [\mu_1^{1/2}] [\tilde{x}_1] \quad (3-78)$$

$$[B] = [\mu_1^{-1/2}] [A_{11} - A_{12} A_{22}^{-1} \tilde{A}_{12}] [\mu_1^{-1/2}] \quad (3-79)$$

The eigenvalues of equation (3-77) are the smaller eigenvalues of the original equation (3-61), and the eigenvectors of (3-77) give the corresponding eigenvectors of equation (3-61) according to

$$\tilde{f} = [U][\tilde{x}] = [U] \begin{bmatrix} [\delta] \\ [-A_{22}^{-1} A_{12}] \end{bmatrix} [\mu_1^{-1/2}] [\tilde{y}] \quad (3-80)$$

where  $[\delta]$  is the identity matrix.

Once the eigenvalues and the eigencurrents are known, the equivalent surface currents and scattered fields can be obtained by employing appropriate formulas for those quantities.

CHAPTER 4  
RESULTS

The results of far field scattering calculations for some material cylinders are presented in this chapter. Equations used are those developed in Chapter 2 and Chapter 3.

The far field scattering patterns of circular material cylinders have been computed and the results are shown in Figures 4-1 through 4-16, for perpendicular polarization (TE). Figures 4-17 through 4-22 give the results for parallel polarization (TM). All results are compared with exact harmonic series solutions [7]. Figures 4-1 to 4-5 are obtained by using 15 triangle expansion functions. Twenty expansion functions have been used in obtaining Figures 4-6 to 4-22. In all figures the computed scattering cross section are normalized by  $\pi a$ , where "a" is the radius of the cylinder.

The normalized scattering cross sections of square cylinders are shown in Figures 4-23 through 4-27. All computed results are normalized by  $\pi b$ , where "b" is one-half the width of the square cylinder under consideration. Twenty expansions have been used in all computations for square cylinders of different material constants.

Figures 4-28 through 4-30 show the characteristic currents (or mode currents) for circular cylinders of different material constants. Fifteen expansion functions have been used for the computation of mode currents.

For representative computations, consider a circular cylinder with  $ka = 0.7$  (where "a" is the radius of the cylinder,  $\epsilon_r = 9.5$ ,  $\mu_r = 1.0$ ). The contour is approximated by 32 straight lines segments of equal length (the

line segments can be of different length), and 15 expansion functions are used for both electric and magnetic surface currents. Figure 4-28 shows the characteristic currents plotted vs. the contour length variable in terms of a sequence of triangle functions. All the mode currents are composite currents. The first 15 points represent the electric mode current, and the second the magnetic current.

Figure 4-29 shows the characteristic currents for a circular cylinder with  $\epsilon_r = 50.0$ ,  $\mu_r = 1.0$ , and  $ka = 0.7$ . Figure 4-30 shows the characteristic currents for a circular cylinder of  $\epsilon_r = 2.56$ . Note that every mode current is normalized by its maximum magnitude.

For perpendicular polarization (TE), the modal solution for the scattered field agrees extremely well with the scattered field computed directly from matrix inversion. The scattering cross sections using characteristic modes are almost identical to the matrix inversion solutions (the differences are less than 0.001 db).

To be specific, Fig. 4-1 shows the normalized scattering cross section of a circular cylinder with  $\epsilon_r = 9.5$ ,  $\mu_r = 1.0$ , and  $ka = 0.7$  for perpendicular polarization (TE). The computed scattering cross section is in good agreement with harmonic solution [7]. The maximum deviation is 0.65 db. Figure 4-2 gives the normalized scattering cross section of a circular cylinder with  $\epsilon_r = 20.0$ ,  $\mu_r = 1.0$ , and  $ka = 0.7$ , for perpendicular polarization (TE). The maximum deviation from exact harmonic series solution is 0.076 db. Figure 4-3 shows the normalized scattering cross section of a circular cylinder with  $\epsilon_r = 50.0$ ,  $\mu_r = 1.0$ , and  $ka = 0.7$ , for perpendicular polarization (TE). Maximum

deviation from exact harmonic solution is 0.485 db. The scattering cross section shown in Fig. 4-4 is for a circular cylinder with  $\epsilon_r = 100.0$ ,  $\mu_r = 0.01$ , and  $ka = 0.7$  for perpendicular polarization. The computed solution is in excellent agreement with the exact solution. Maximum deviation is 0.01 db. Figure 4-5 gives the normalized scattering cross section of a circular cylinder with  $\epsilon_r = 1000.0$ ,  $\mu_r = 0.001$ , and  $ka = 0.7$ , for perpendicular polarization. Note that the computed result is in excellent agreement with the calculations of a conducting cylinder. Maximum deviation is 0.01 db. The conducting cylinder problem can be viewed as a specialization of the more general material cylinder problem. This is expected to be true even for three-dimensional objects. Figure 4-6 shows the normalized scattering cross section of a circular cylinder with  $\epsilon_r = 9.0$ ,  $\mu_r = 1.0$ , and  $ka = 2.0$ , for perpendicular polarization (TE). Maximum deviation from exact harmonic solution is 1.79 db. Better agreement can be reached, if more expansion functions are used. The scattering cross section given in Fig. 4-7 is for a circular cylinder with  $\epsilon_r = 9.0$ ,  $\mu_r = 1.0$ , and  $ka = 1.0$ , for perpendicular polarization. The agreement with exact solution is excellent. Maximum deviation is 0.013 db. Figure 4-8 shows the normalized scattering cross section of a circular cylinder with  $\epsilon_r = 9.0$ ,  $\mu_r = 100.0$ , and  $ka = 0.7$ , for perpendicular polarization. Agreement with exact solution is very good. Maximum deviation is 0.01 db. Figure 4-9 shows the normalized scattering cross section of a circular cylinder with  $\epsilon_r = 9.0$ ,  $\mu_r = 5.0$ , and  $ka = 0.7$ , for perpendicular polarization. The computed result is in good agreement with exact

solution. Maximum deviation is 0.3 db. The computed scattering cross section of a circular cylinder with  $\epsilon_r = 0.001$ ,  $\mu_r = 1000.0$ , and  $ka = 0.7$ , for perpendicular polarization is shown in Fig. 4-10. Note that the cylinder is highly magnetic. Maximum deviation from exact harmonic solution is 0.001 db. The agreement is excellent. Figure 4-11 shows the normalized scattering cross section of a circular cylinder with  $\epsilon_r = 1.0$ ,  $\mu_r = 1000.0$ , and  $ka = 0.7$ , for perpendicular polarization. Maximum deviation from exact solution is 0.04 db. Figure 4-12 represents the computed scattering cross section of a circular cylinder with  $\epsilon_r = 1.0$ ,  $\mu_r = 10.0$ , and  $ka = 0.7$ , for perpendicular polarization. Maximum deviation from exact solution is 0.04 db. Figure 4-13 shows the computed scattering cross section of a circular cylinder with  $\epsilon_r = 1.0$ ,  $\mu_r = 300$ , and  $ka = 0.7$ , for perpendicular polarization. Maximum deviation from exact harmonic solution is 0.2 db. Figure 4-14 gives the normalized scattering cross section of a circular cylinder with  $\epsilon_r = 2.56$ ,  $\mu_r = 1.0$ , and  $ka = 0.7$ , for perpendicular polarization. Maximum deviation is 0.6 db. Figure 4-15 shows the computed scattering cross section of a circular cylinder with  $\epsilon_r = 1000.0$ ,  $\mu_r = 0.001$ , and  $ka = 0.7$ , for perpendicular polarization. The computed solution is in excellent agreement with exact solution. Maximum deviation is 0.01 db. The computed scattering cross sections of a circular cylinder with  $ka = 0.7$ , are given in Fig. 4-16 for three different sets of material constants; i)  $\epsilon_r = 1000.0$ ,  $\mu_r = 1.0$  ii)  $\epsilon_r = 10000.0$ ,  $\mu_r = 1.0$  iii)  $\epsilon_r = 5.0$ ,  $\mu_r = 10^{-6}$ . All are for perpendicular polarization. Figure 4-17 shows the normalized scattering cross section of a circular cylinder with  $\epsilon_r = 1000.0$ ,  $\mu_r = 0.001$ , and  $ka = 0.7$ , for parallel polarization (TM). The solution agrees excellently with conducting cylinder solution. Maximum deviation is 0.023 db. The normalized scattering

cross section of a circular cylinder with  $\epsilon_r = 2.56$ ,  $\mu_r = 1.0$ , and  $ka = 0.7$ , for parallel polarization is shown in Fig. 4-18. Maximum deviation from exact solution is 0.5 db. Figure 4-19 represents the computed scattering cross section of a circular cylinder with  $\epsilon_r = 20.0$ ,  $\mu_r = 1.0$ , and  $ka = 0.7$ , for parallel polarization. Maximum deviation from exact solution is 0.2 db. Figure 4-20 shows the computed scattering cross section of a circular cylinder with  $\epsilon_r = 50.0$ ,  $\mu_r = 1.0$ , and  $ka = 0.7$ , for parallel polarization. The computed solution is in excellent agreement with exact harmonic solution. Maximum deviation is 0.05 db. Figure 4-21 shows the computed scattering cross section of a circular cylinder with  $\epsilon_r = 4.0$ ,  $\mu_r = 1.0$ , and  $ka = 0.7$ , for parallel polarization. Maximum deviation from exact solution is 0.2 db. Figure 4-22 shows the computed scattering cross section of a circular cylinder with  $\epsilon_r = 9.5$ ,  $\mu_r = 1.0$ , and  $ka = 0.7$ , for parallel polarization. The computed solution is in excellent agreement with exact harmonic solution maximum deviation is 0.01 db. Figure 4-23 shows the computed scattering cross sections of a square cylinder with  $kb = 1.4$ , for two sets of material constants: i)  $\epsilon_r = 1000.0$ ,  $\mu_r = 0.001$  ii)  $\epsilon_r = 1000.0$ ,  $\mu_r = 1.0$ , all for perpendicular polarization. For square cylinders, there are no exact solutions. Figure 4-24 shows the computed scattering cross section of a square cylinder with  $\epsilon_r = 10000.0$ ,  $\mu_r = 0.0001$ , and  $kb = 1.4$ , for perpendicular polarization. The computed solution has been compared with the solution of a conducting square cylinder by using E-field formulation [13]. Maximum deviation is 0.1 db. Figure 4-25 shows the computed scattering cross section of a square cylinder with  $\epsilon_r = 9.0$ ,  $\mu_r = 1.0$ , and  $kb = 1.4$ , for perpendicular polarization. Figure 4-26 shows the computed scattering cross section of a square cylinder with  $\epsilon_r = 100.0$ ,  $\mu_r = 1.0$ , and  $kb = 1.4$ , for

parallel polarization. Figure 4-27 shows the scattering cross section of a square cylinder with  $\epsilon_r = 10000.0$ ,  $\mu_r = 0.0001$ , and  $kb = 1.4$ , for parallel polarization. The computed result is in excellent agreement with conducting square cylinder solution. Figure 4-28 shows the lowest order characteristic currents, plotted as a function of the contour variable. The currents are normalized by choosing their maximum amplitude to be unity. The characteristic currents are for a circular cylinder with  $\epsilon_r = 9.5$ ,  $\mu_r = 1.0$ , and  $ka = 0.7$ , for perpendicular polarization. The electric part of each characteristic current is circumferentially directed and the magnetic part is axially directed. The scattering cross section computed from modal solution is almost identical to that from matrix inversion. Figure 4-29 shows the normalized characteristic currents for a circular cylinder with  $\epsilon_r = 50.0$ ,  $\mu_r = 1.0$ , and  $ka = 0.7$ , for perpendicular polarization. Figure 4-30 gives the normalized characteristic currents for a circular cylinder with  $\epsilon_r = 2.56$ ,  $\mu_r = 1.0$ , and  $ka = 0.7$ , for perpendicular polarization.

The purpose of this work is to show the feasibility that a surface formulation for the theory characteristic modes can be applied to the solution of scattering from material objects. For large cylinders, more expansion functions are needed. No attempt has been made to treat large objects. It is expected that this is one of the important areas for future research. Many questions are still left unanswered in the interpretation and application of characteristic modes to material objects. It is hoped that this work will be of some value to future researchers in their effort to gain a complete understanding of the theory of characteristic modes.

The eigenvalue equation (3-61) is

$$[T_2][f] = \lambda [T_1][f] \quad (4-1)$$

and the expression for the Rayleigh quotient associated with equation (4-1) is

$$\lambda_1 = \frac{[\tilde{f}_1][T_2][f_1]}{[\tilde{f}_1][T_1][f_1]} \quad (4-2)$$

The computed eigenvalues and their corresponding eigenvectors should satisfy equation (4-2). The Rayleigh quotient check is important because it gives some verification to the approximations used in numerical computation.

The quadratic term  $[f_1][T_1][f_1]$  deserves some elaboration since it appears frequently in equations. Note that

$$\begin{aligned} [\tilde{f}][T_1][f] &= [\tilde{x}][\tilde{U}][T_1][U][x] \\ &= [\tilde{x}][u][x] \\ &= [\tilde{x}_1][u_1][x_1] + [\tilde{x}_2][u_2][x_2] \end{aligned} \quad (4-3)$$

It has already been pointed out in Chapter 3 that  $[x_2]$  is the component of an eigencurrent  $f$  that lies within the null space of  $T_1$ , in other words,  $[x_2]$  does not radiate. Since approximations are made in the computational procedures, the eigencurrents will not be absolutely exact. Consequently, the second quadratic term on the right hand side of equation (4-3) will differ from zero, but it should be much smaller than the first quadratic term. To a certain degree, this will give some indication of the accuracy of the computed eigencurrents. The first quadratic term at the right hand side of equation (4-3) can be further expressed as

$$\begin{aligned}
 & \widetilde{[x_1]}[u_1][x_1] \\
 &= \widetilde{[u_1^{-1/2}][y][u_1][u_1^{-1/2}][y]} \\
 &= \widetilde{[y]} \widetilde{[u_1^{-1/2}][u_1][u_1^{-1/2}][y]} \\
 &= \widetilde{[y]}[y] \\
 &= 1 \text{ (if } \{y_i\} \text{ are orthonormal)} \quad (4-4)
 \end{aligned}$$

In numerical computation, approximations are inevitable. Some special analytical manipulations such as those discussed above can often provide added insight to the correctness of the numerical results.

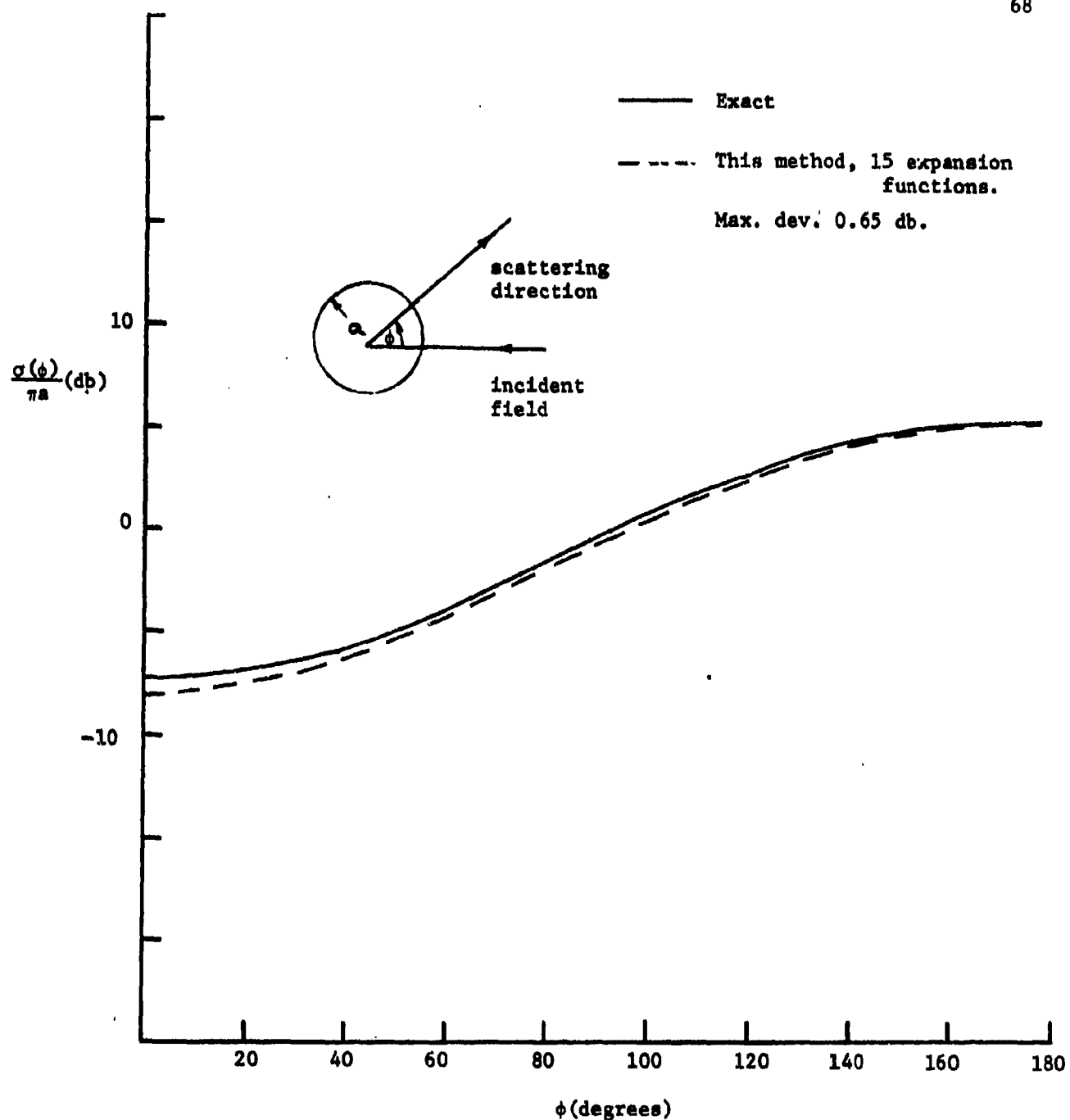


Fig. 4-1. Normalized scattering cross section of a circular cylinder with  $\epsilon_r = 9.5$ ,  $\mu_r = 1.0$ ,  $ka = 0.7$ , perpendicular polarization (TE).

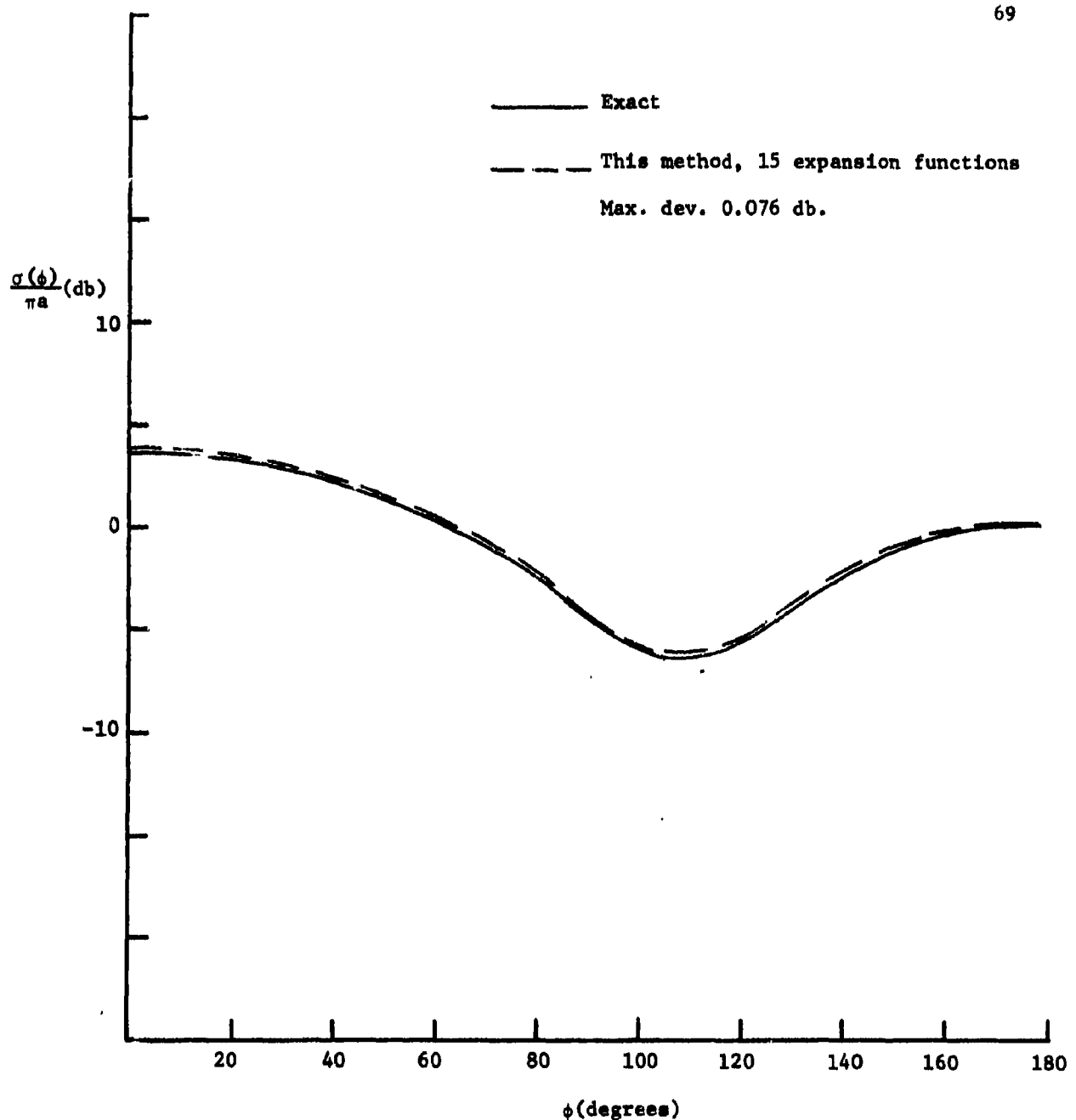


Fig. 4-2. Normalized scattering cross section of a circular cylinder with  $\epsilon_r = 20.0$ ,  $\mu_r = 1.0$ ,  $ka = 0.7$ , perpendicular polarization (TE).

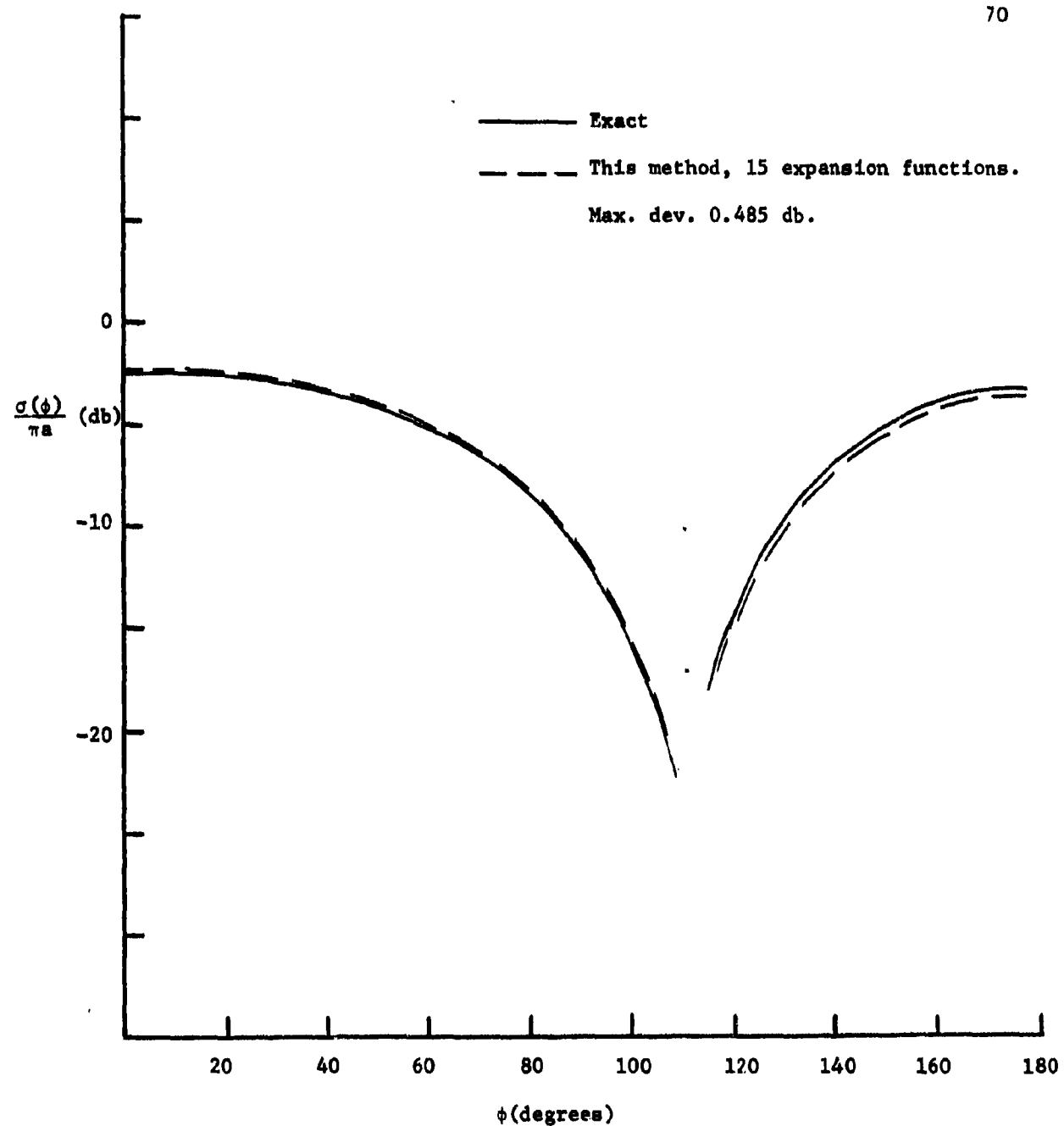


Fig. 4-3. Normalized scattering cross section of a circular cylinder with  $\epsilon_r = 50.0$ ,  $\mu_r = 1.0$ ,  $ka = 0.7$ , perpendicular polarization (TE).

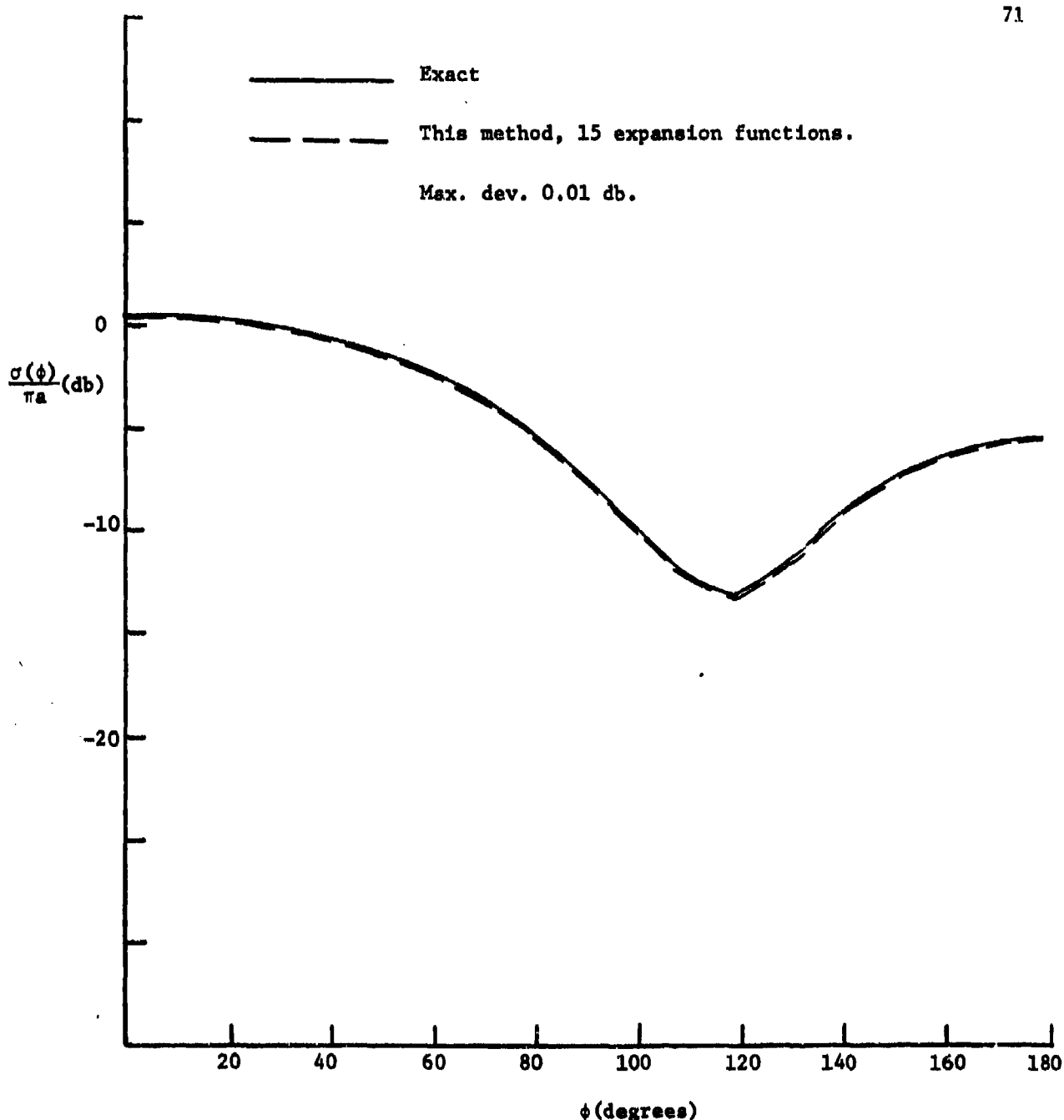


Fig. 4-4. Normalized scattering cross section of a circular cylinder with  $\epsilon_r = 100.0$ ,  $\mu_r = 0.01$ ,  $ka = 0.7$ , perpendicular polarization (TE).

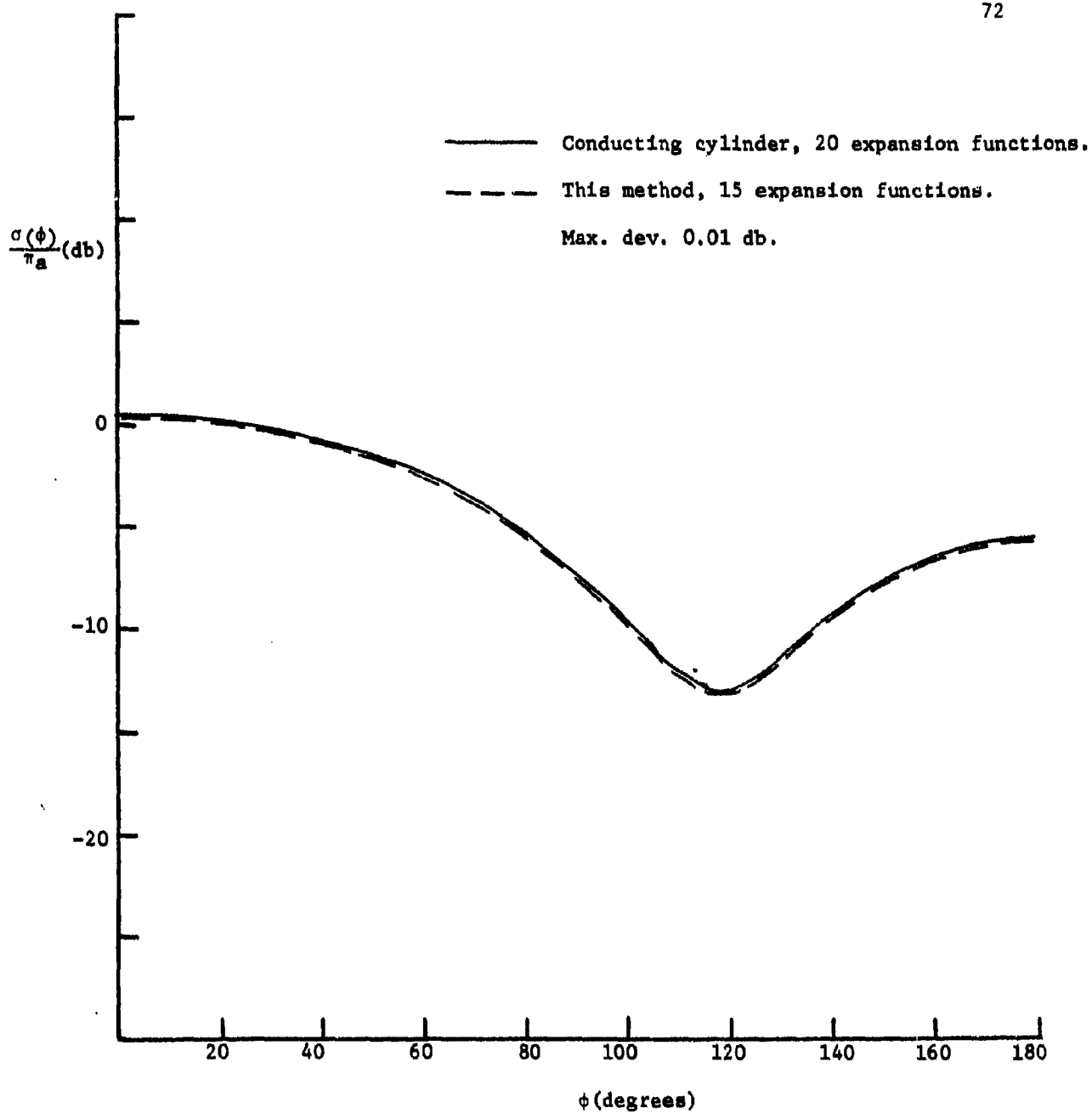


Fig. 4-5. Normalized scattering cross section of a circular cylinder with  $\epsilon_r = 1000.0$ ,  $\mu_r = 0.001$ ,  $ka = 0.7$ , perpendicular polarization (TE).

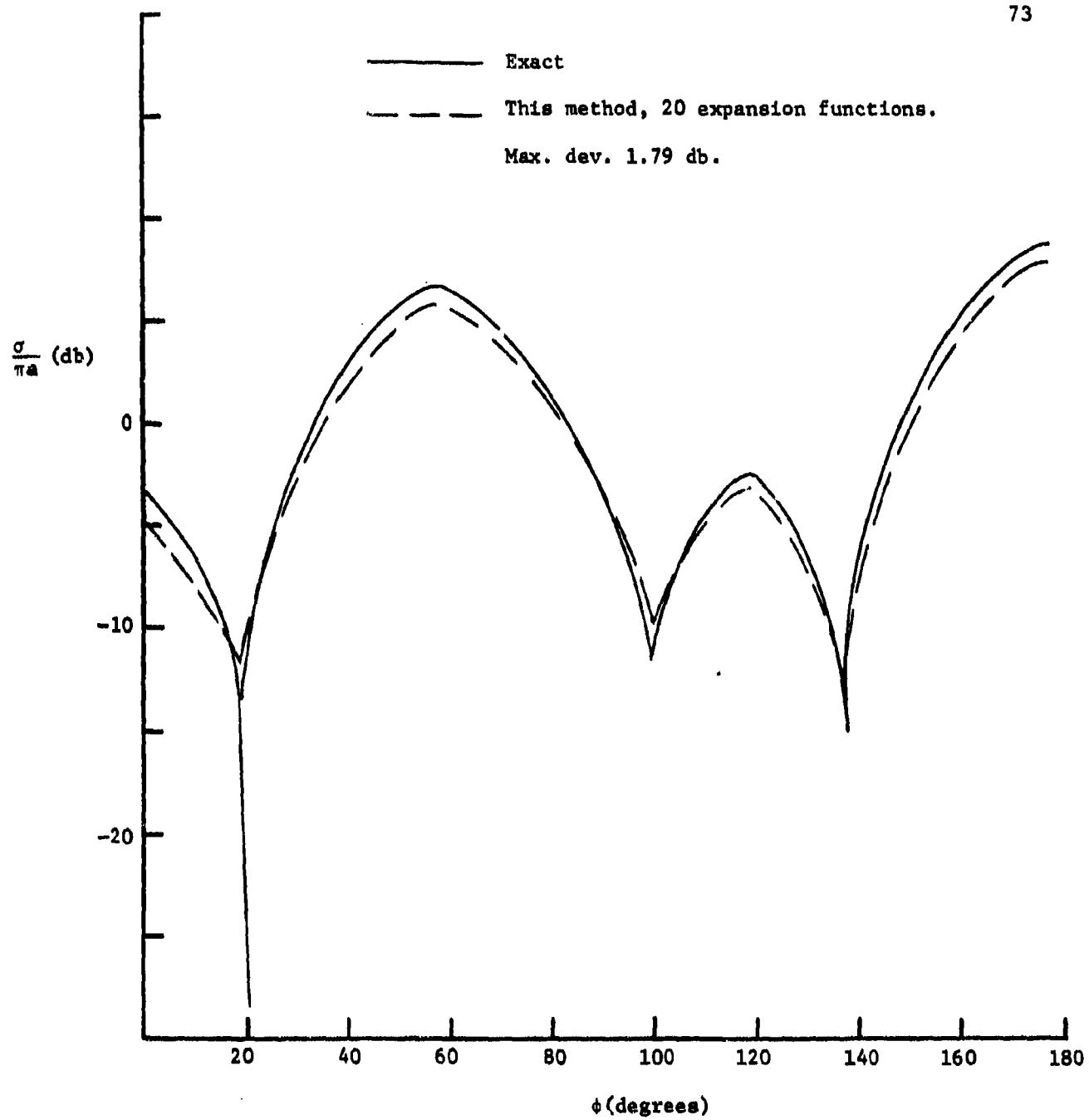


Fig. 4-6. Normalized scattering cross section of a circular cylinder with  $\epsilon_r = 9.0$ ,  $\mu_r = 1.0$ ,  $ka = 2.0$ , perpendicular polarization (TE).

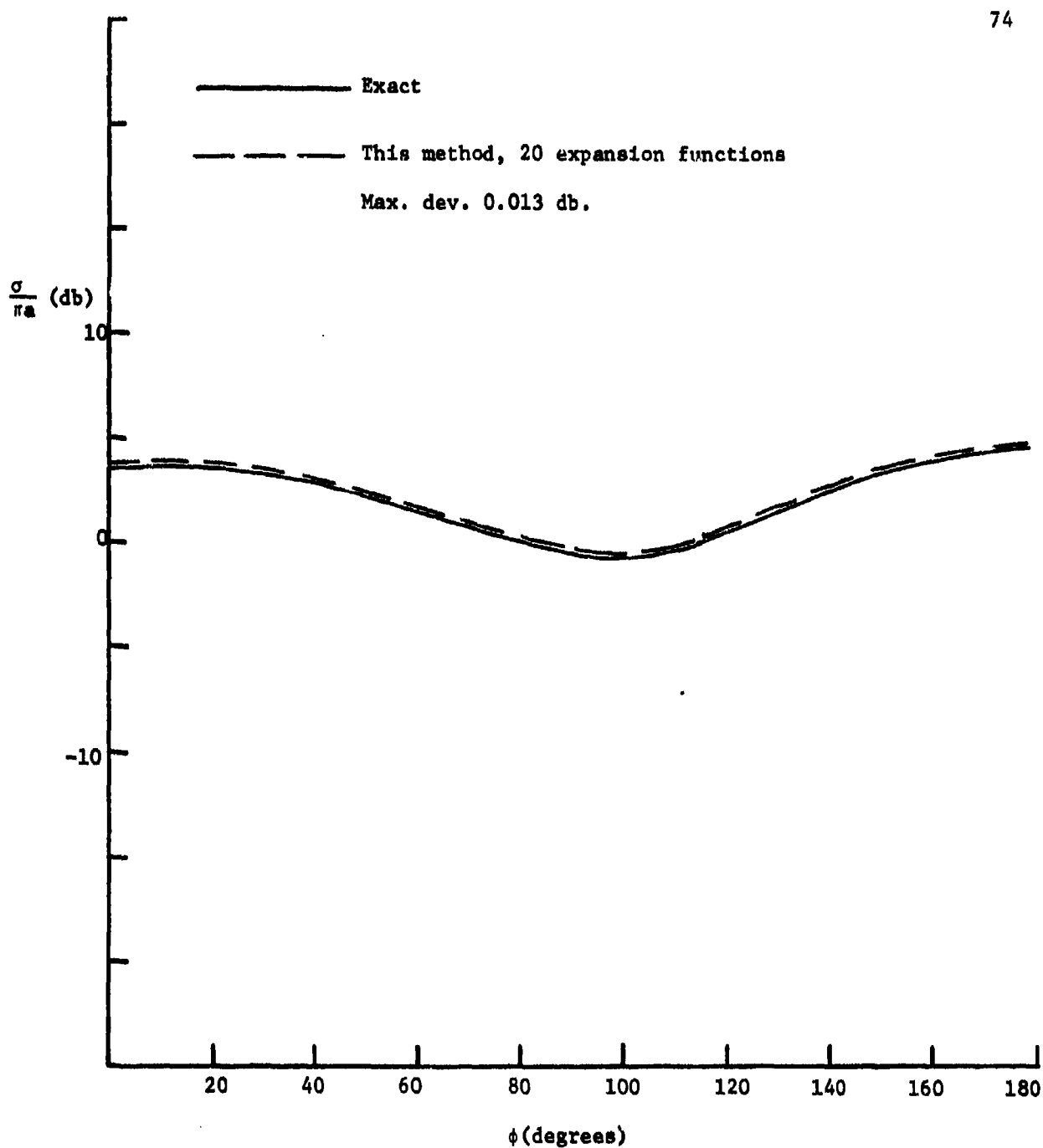


Fig. 4-7. Normalized scattering cross section of a circular cylinder with  $\epsilon_r = 9.0$ ,  $\mu_r = 1.0$ ,  $ka = 1.0$ , perpendicular polarization (TE).

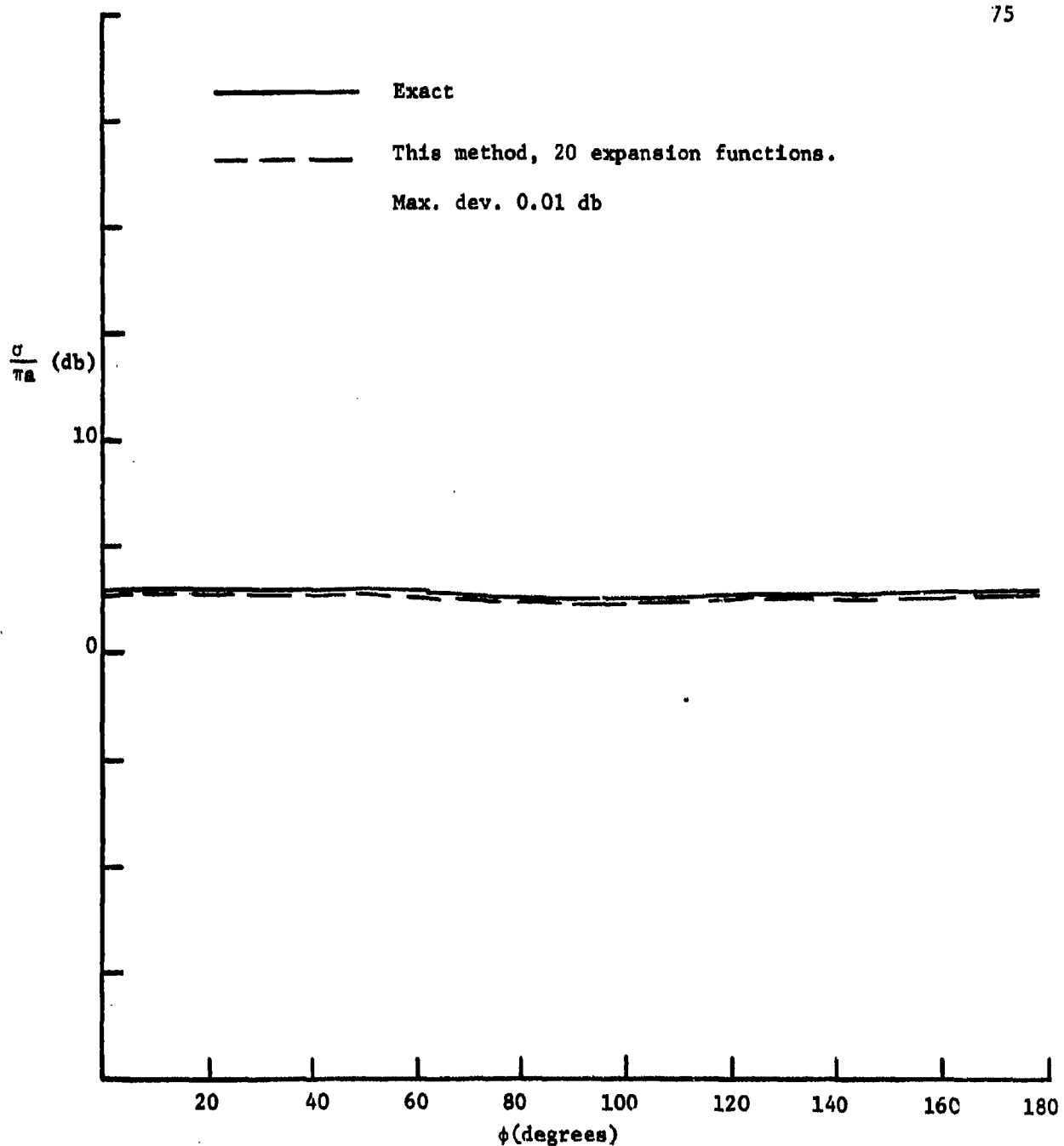


Fig. 4-8. Normalized scattering cross section of a circular cylinder with  $\epsilon_r = 9.0$ ,  $\mu_r = 100.0$ ,  $ka = 0.7$ , perpendicular polarization (TE).

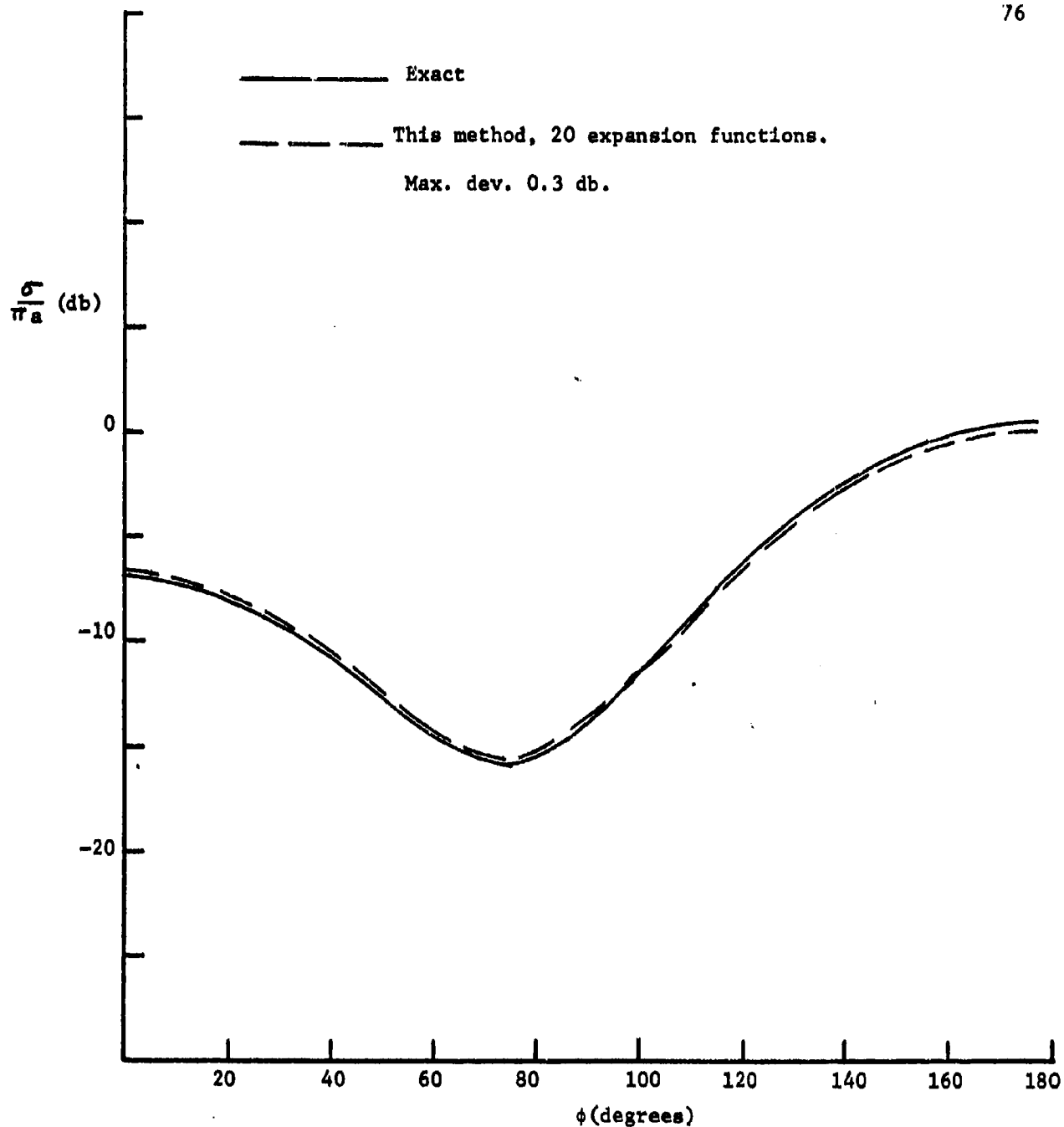


Fig. 4-9. Normalized scattering cross section of a circular cylinder with  $\epsilon_r = 9.0$ ,  $\mu_r = 5.0$ ,  $ka = 0.7$ , perpendicular polarization (TE).

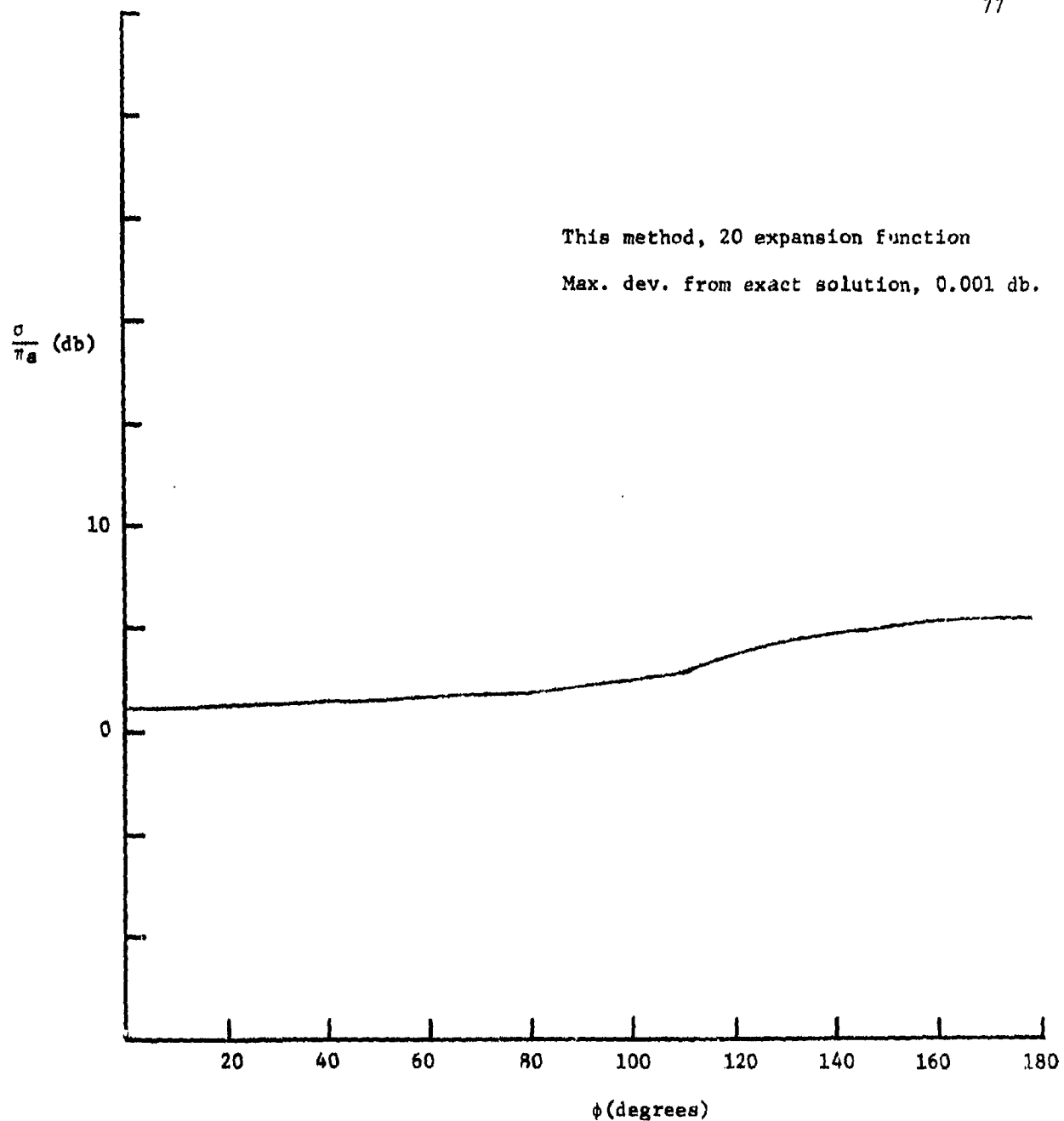


Fig. 4-10. Normalized scattering cross section of a circular cylinder with  $\epsilon_r = 0.001$ ,  $\mu_r = 1000.0$ ,  $ka = 0.7$ , perpendicular polarization (TE).

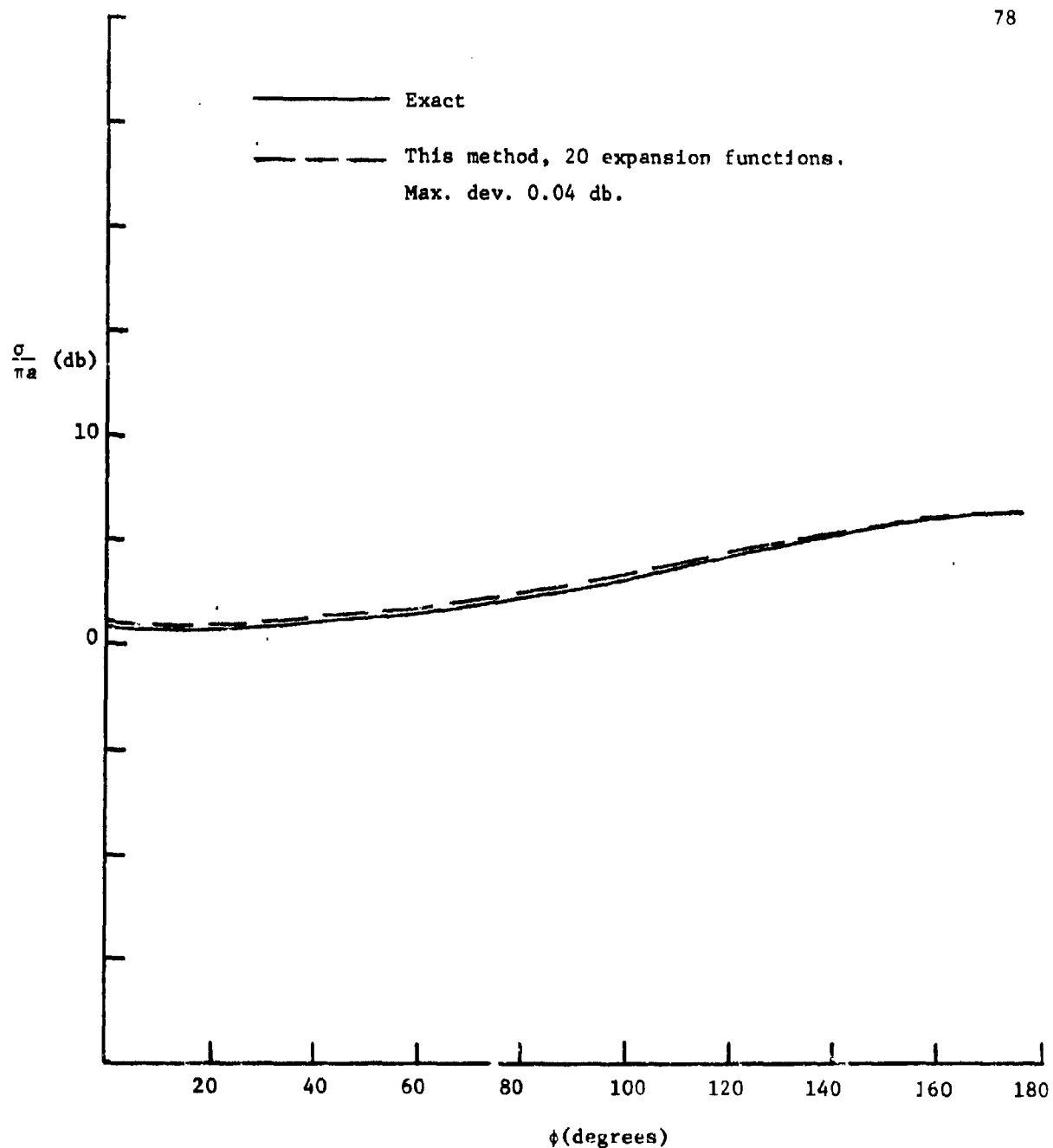


Fig. 4-11. Normalized scattering cross section of a circular cylinder with  $\epsilon_r = 1$ ,  $\mu_r = 1000$ ,  $ka = 0.7$ , perpendicular polarization (TE).

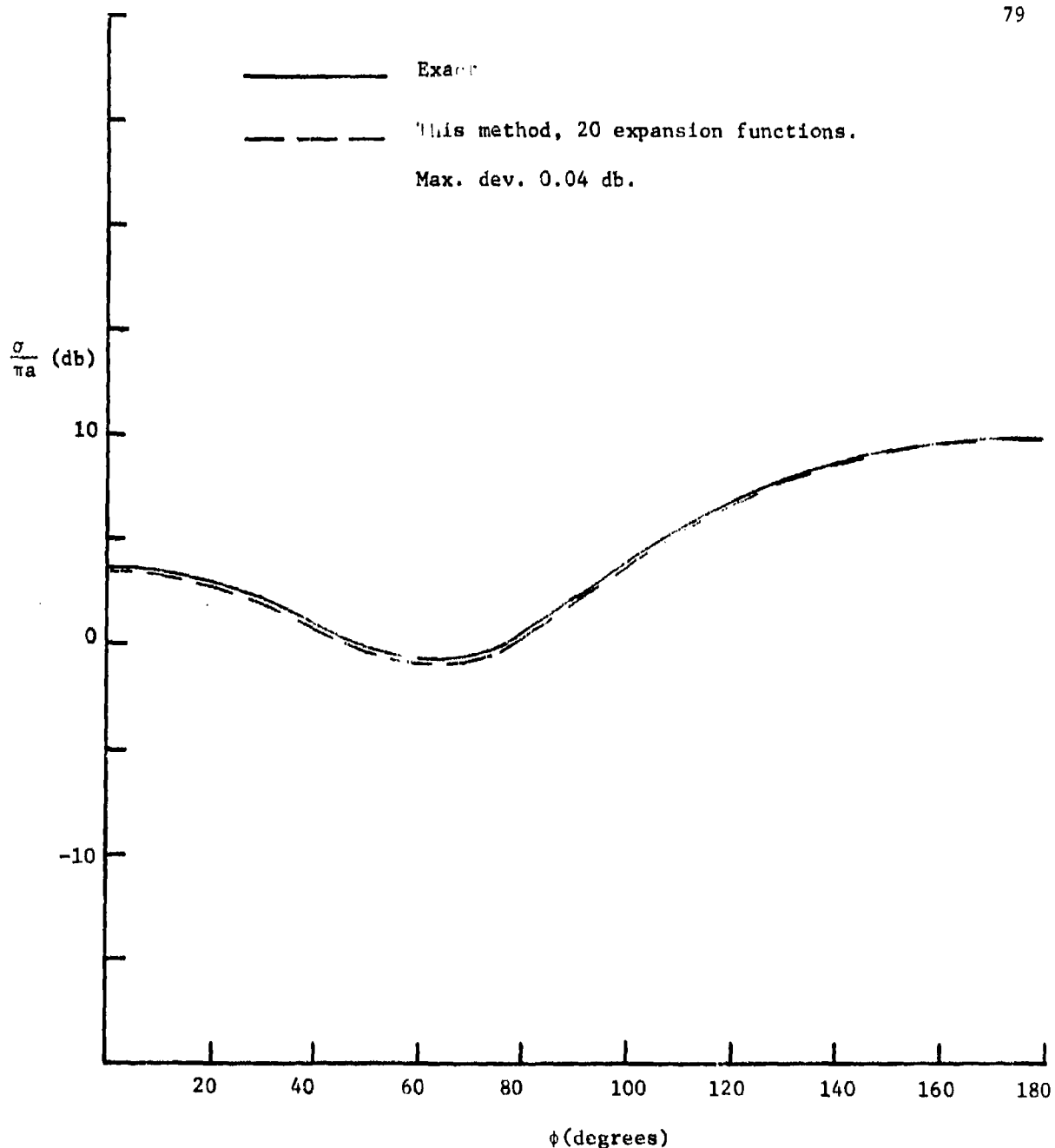


Fig. 4-12. Normalized scattering cross section of a circular cylinder with  $\epsilon_r = 1.0$ ,  $\mu_r = 10.0$ ,  $ka = 0.7$ , perpendicular polarization (TE).

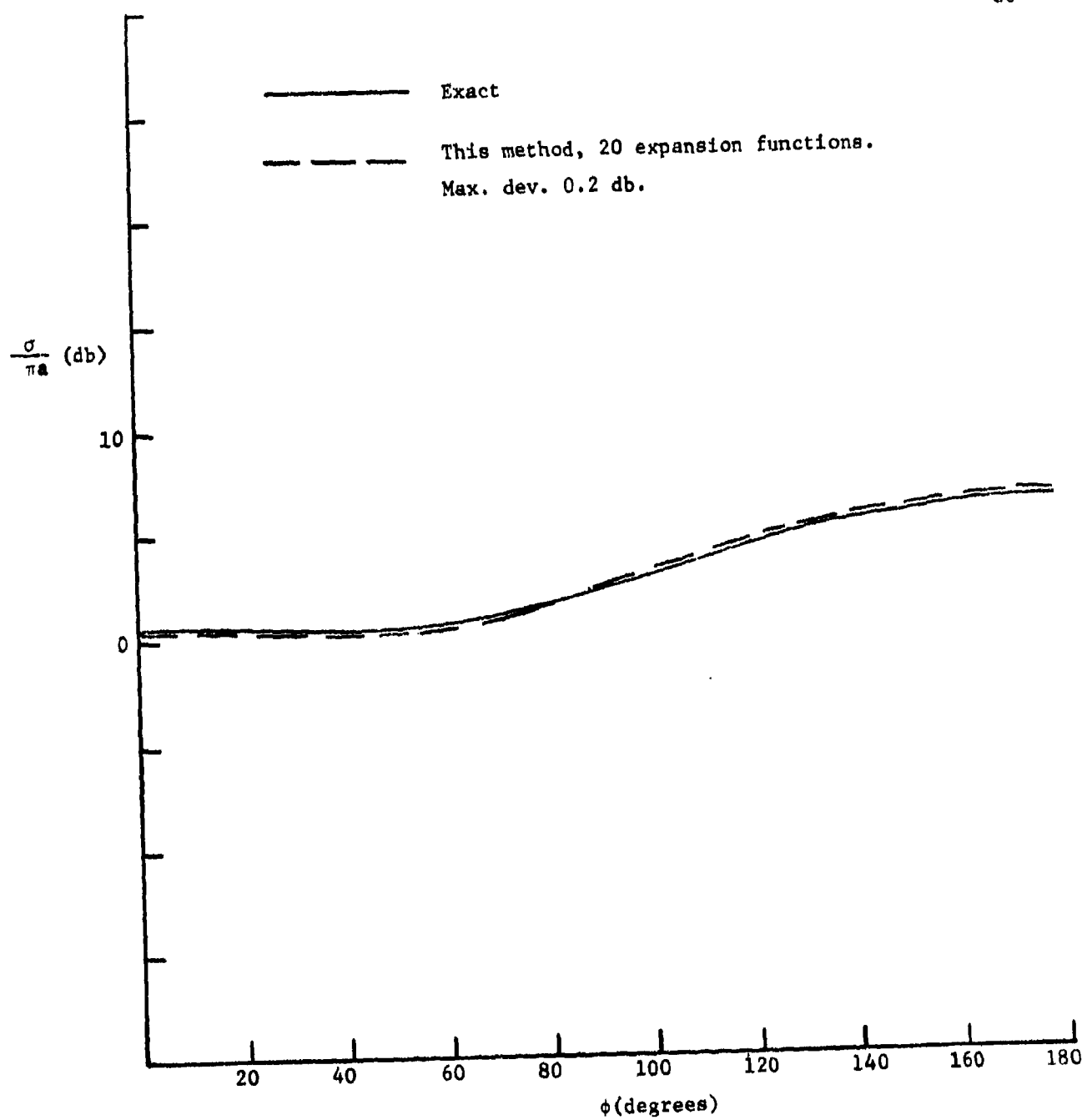


Fig. 4-13. Normalized scattering cross section of a circular cylinder with  $\epsilon_r = 1.0$ ,  $\mu_r = 300$ ,  $ka = 0.7$ , perpendicular polarization (TE).

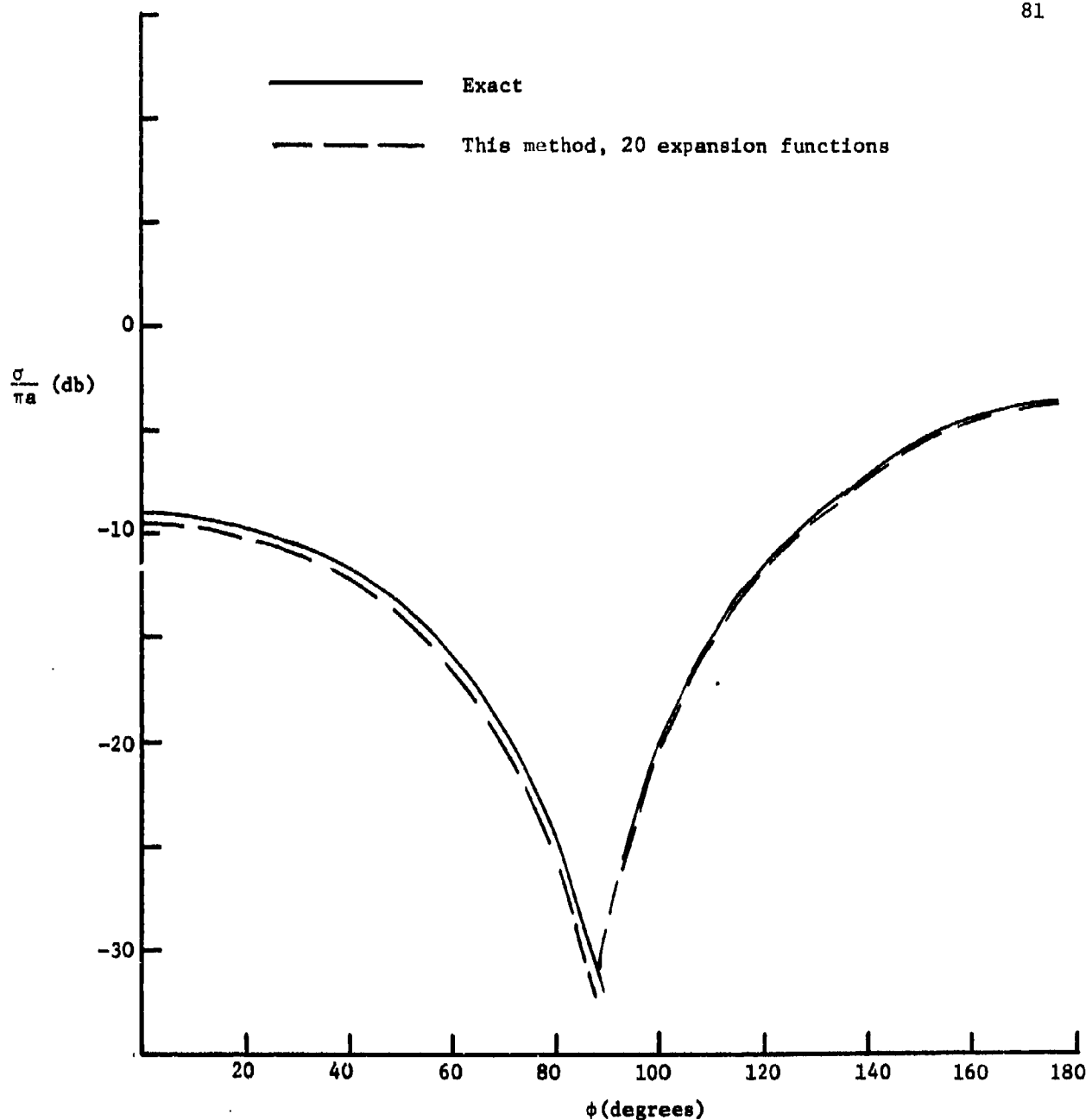


Fig. 4-14. Normalized scattering cross section of a circular cylinder with  $\epsilon_r = 2.56$ ,  $\mu_r = 1.0$ ,  $ka = 0.7$ , perpendicular polarization (TE).

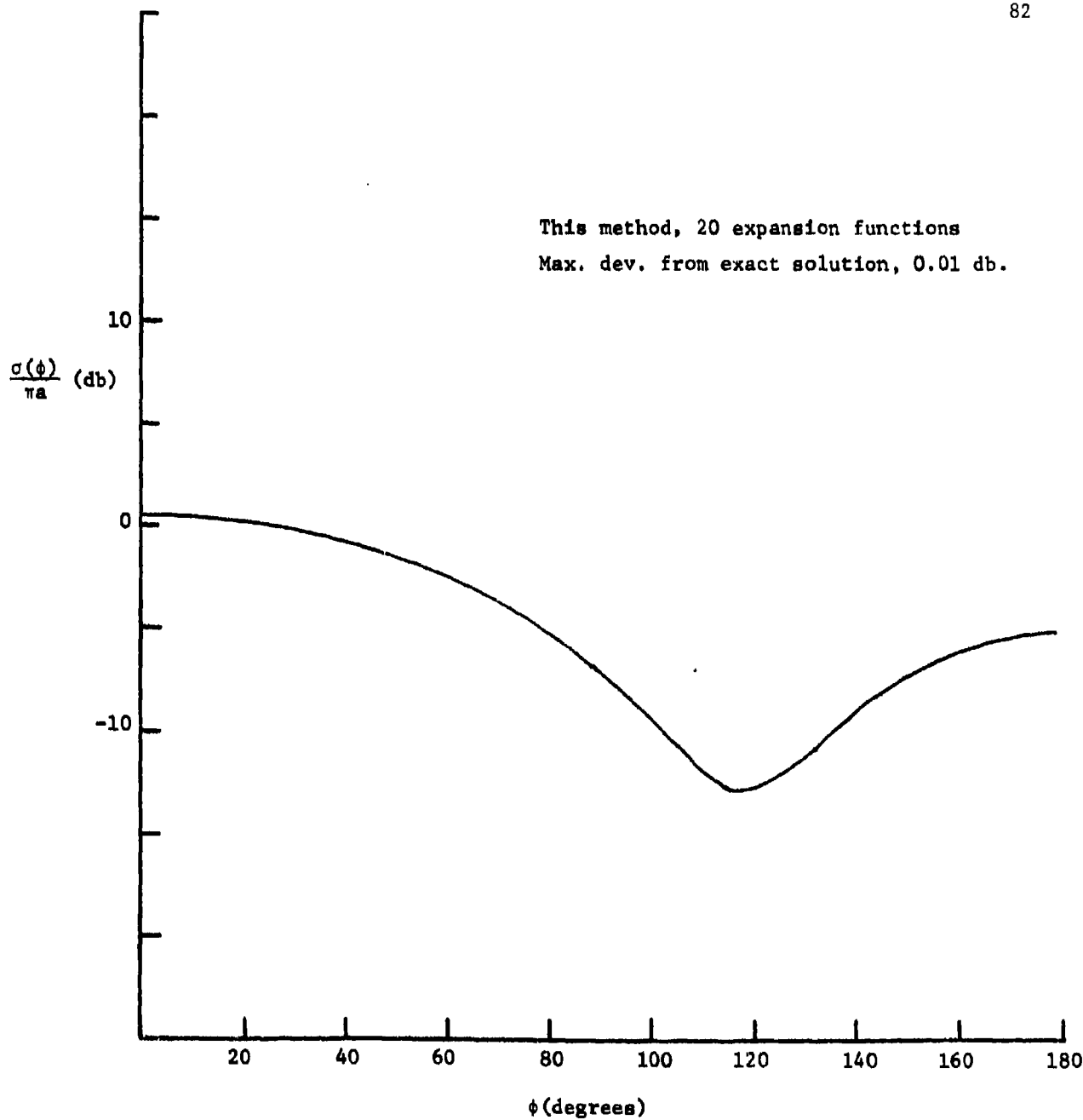


Fig. 4-15. Normalized scattering cross section of a circular cylinder with  $\epsilon_r = 1000.0$ ,  $\mu_r = 0.001$ ,  $ka = 0.7$ , perpendicular polarization (TE).

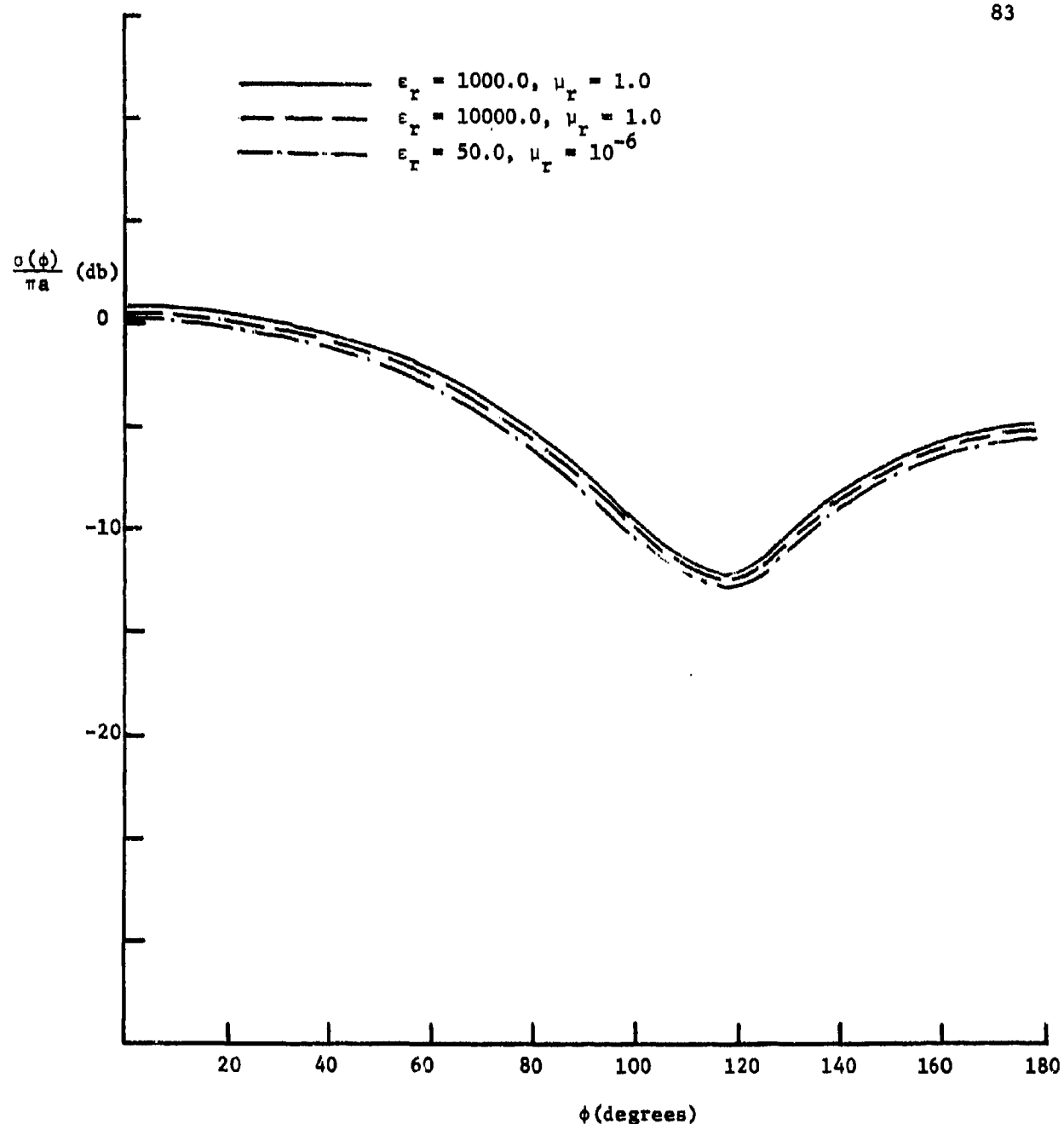


Fig. 4-16. Normalized scattering cross section of a circular cylinder with  $ka = 0.7$ , perpendicular polarization (TE).

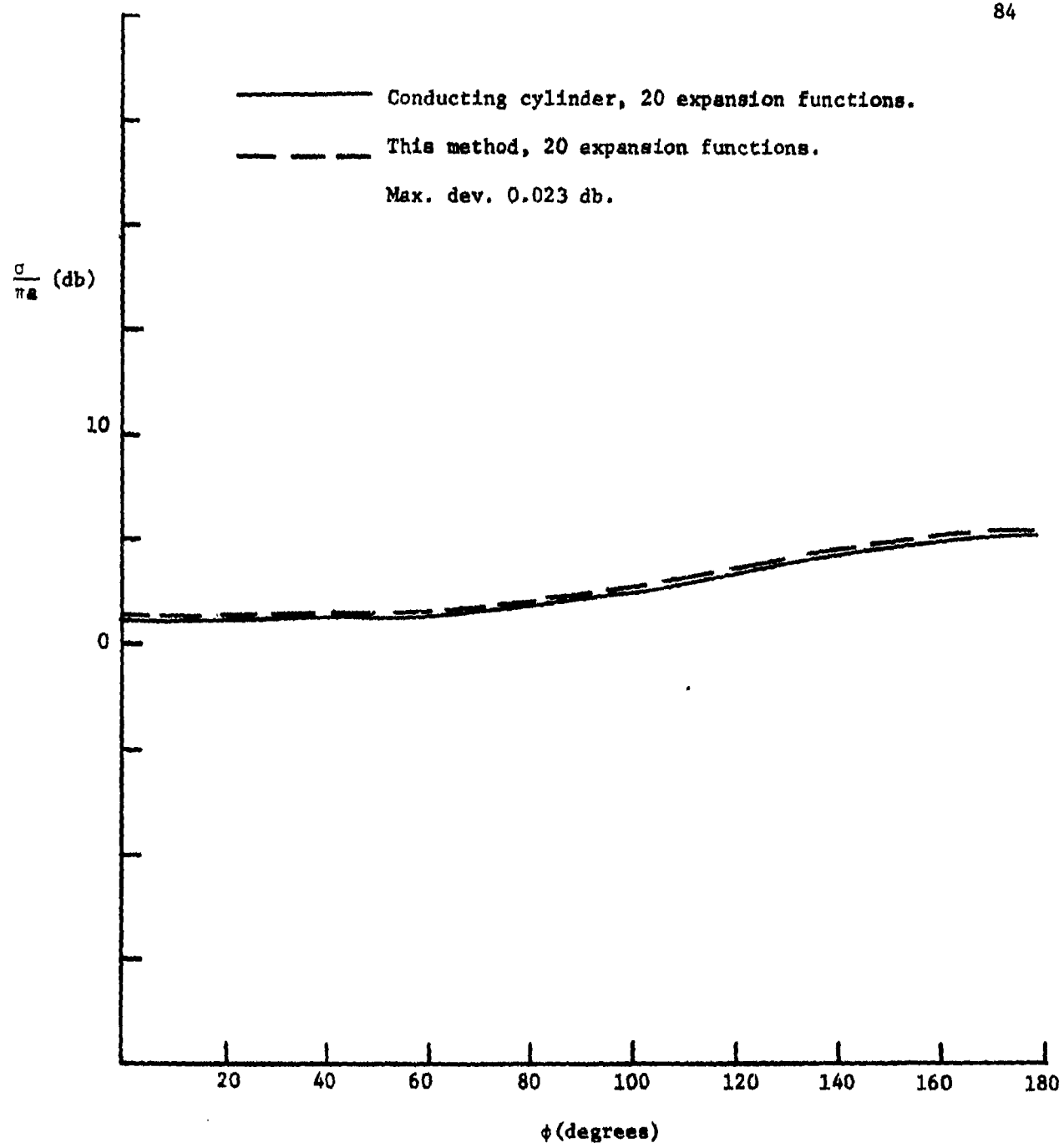


Fig. 4-17. Normalized scattering cross section of a circular cylinder with  $\epsilon_r = 1000.0$ ,  $\mu_r = 0.001$ ,  $ka = 0.7$ , parallel polarization (TM).

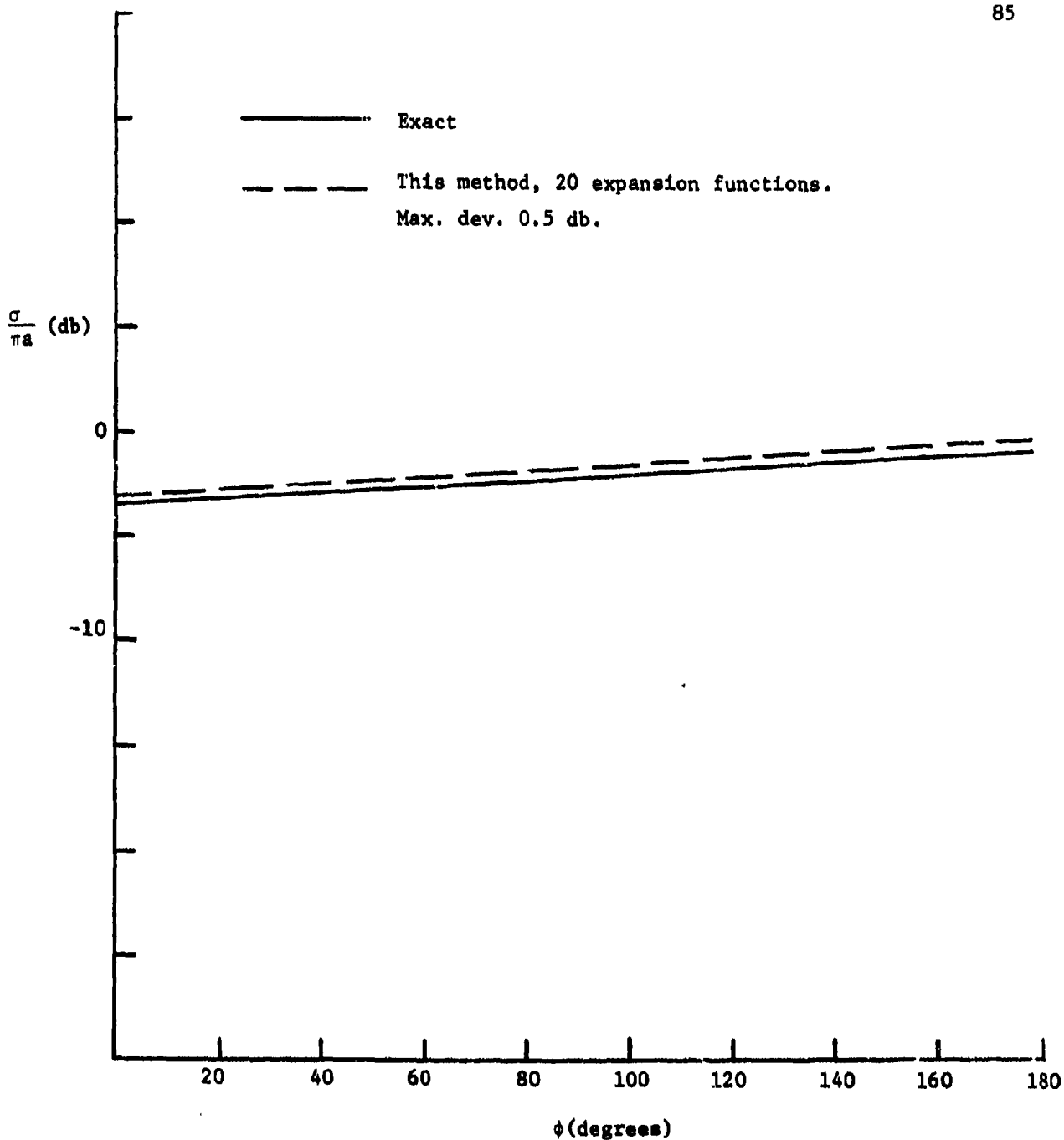


Fig. 4-18. Normalized scattering cross section of a circular cylinder with  $\epsilon_r = 2.56$ ,  $\mu_r = 1.0$ ,  $ka = 0.7$ , parallel polarization (TM).

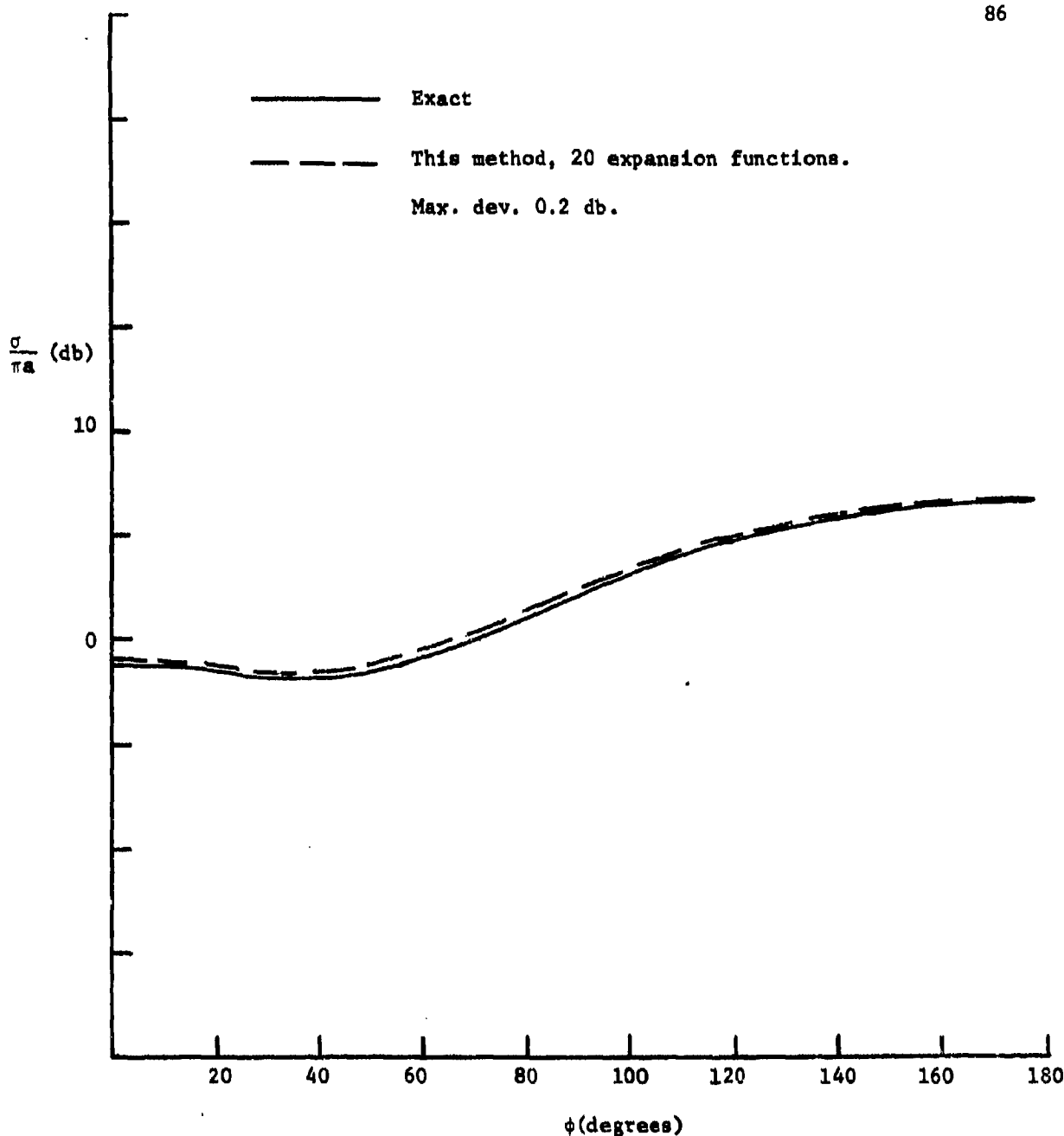


Fig. 4-19. Normalized scattering cross section of a circular cylinder with  $\epsilon_r = 20.0$ ,  $\mu_r = 1.0$ ,  $ka = 0.7$ , parallel polarization (TM).

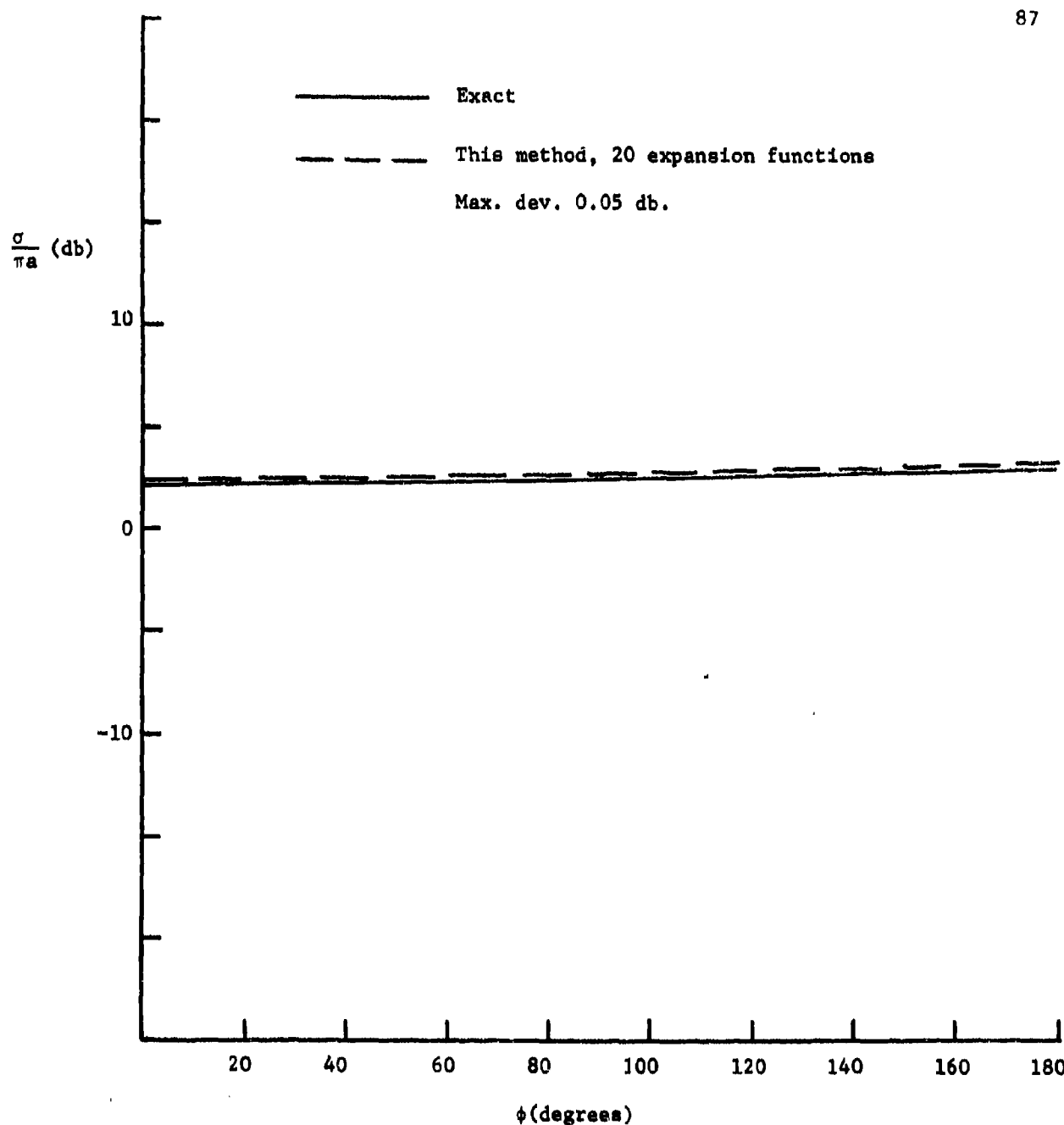


Fig. 4-20. Normalized scattering cross section of a circular cylinder with  $\epsilon_r = 50.0$ ,  $\mu_r = 1.0$ ,  $ka = 0.7$ , parallel polarization (TM).

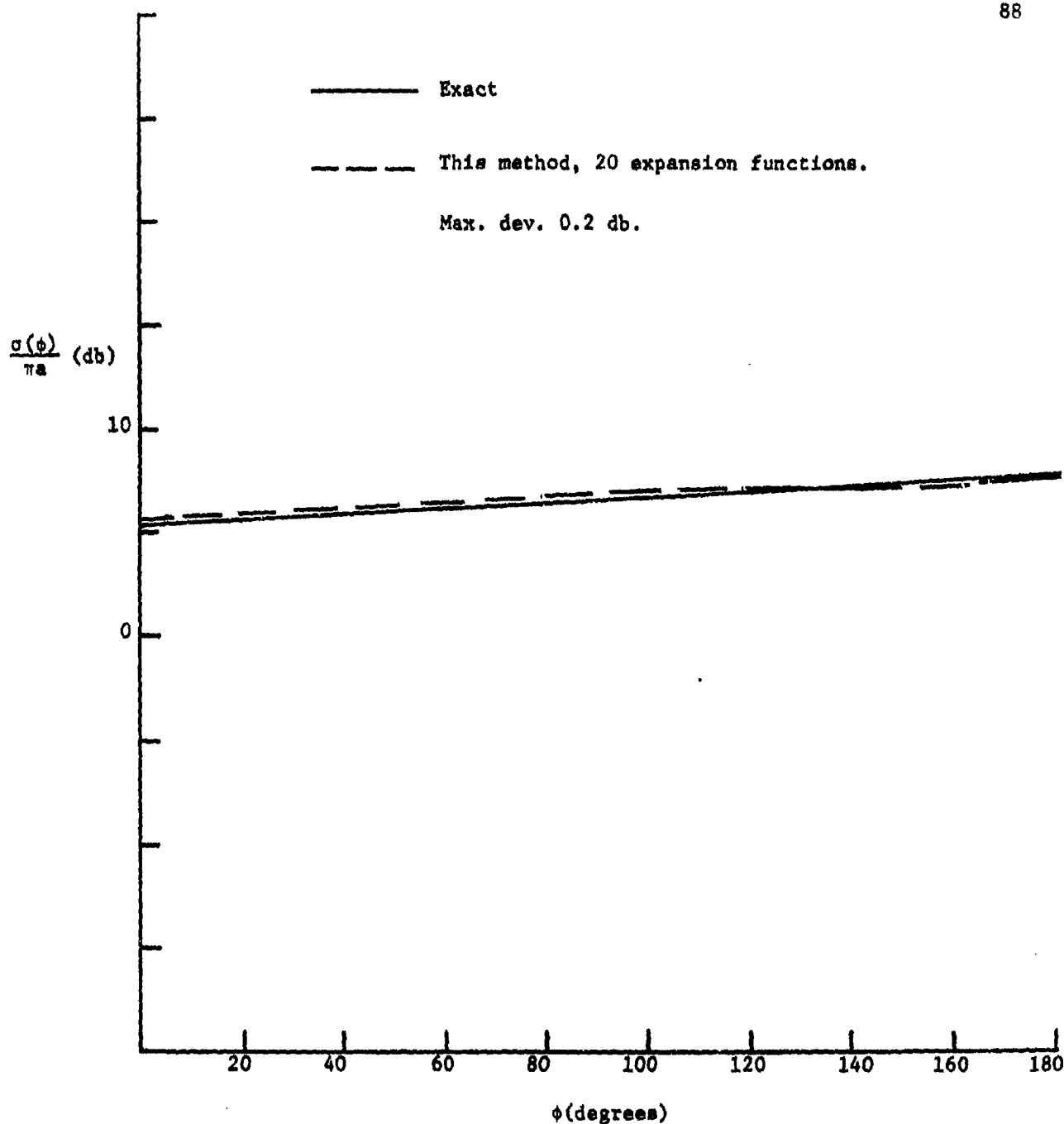


Fig. 4-21. Normalized scattering cross section of a circular material cylinder, with  $\epsilon_r = 4.0$ ,  $\mu_r = 1.0$ ,  $ka = 0.7$  parallel polarization (TM).

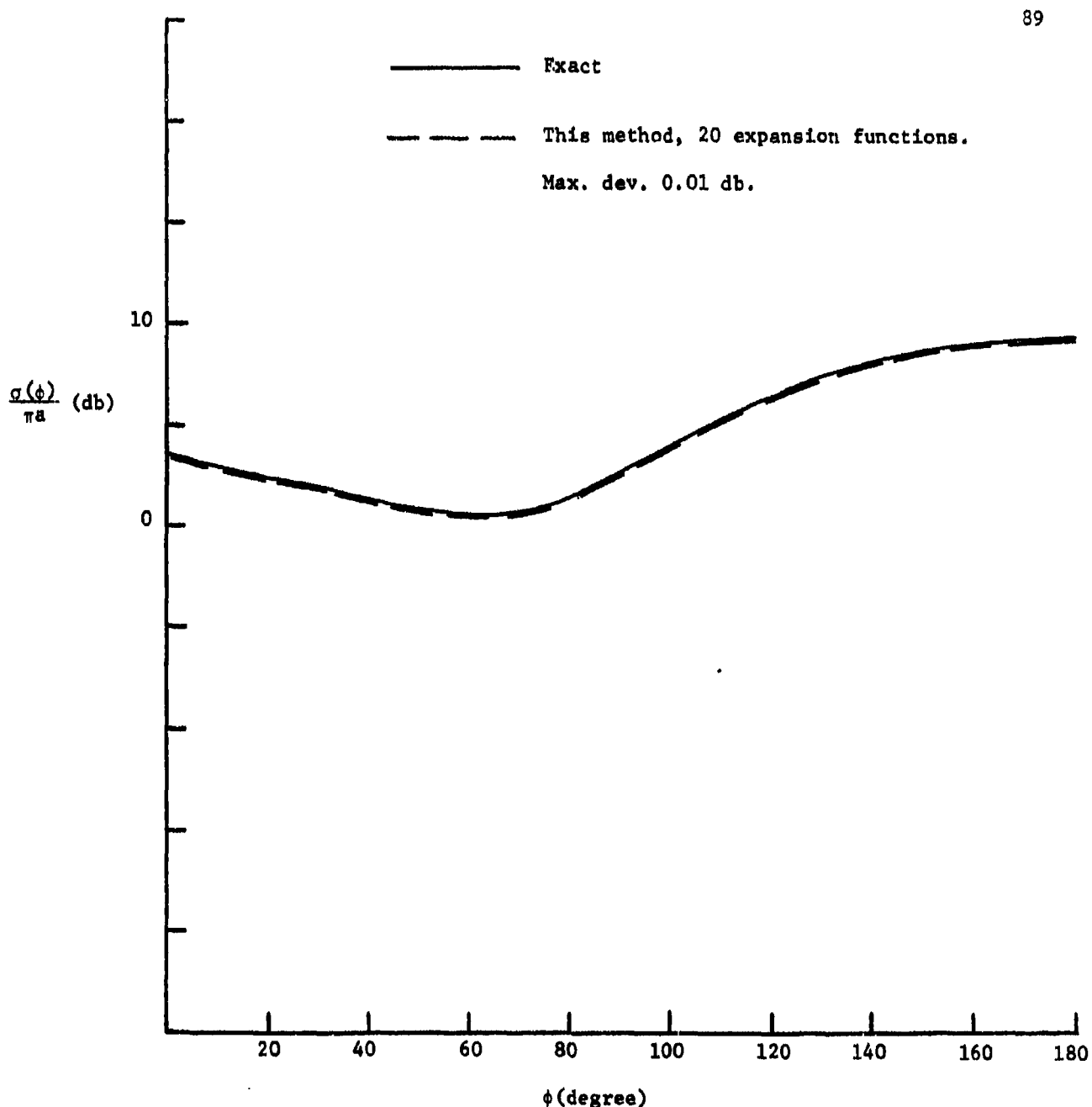


Fig. 22. Normalized scattering cross section of a circular cylinder with  $\epsilon_r = 9.5$ ,  $\mu_r = 1.0$ .

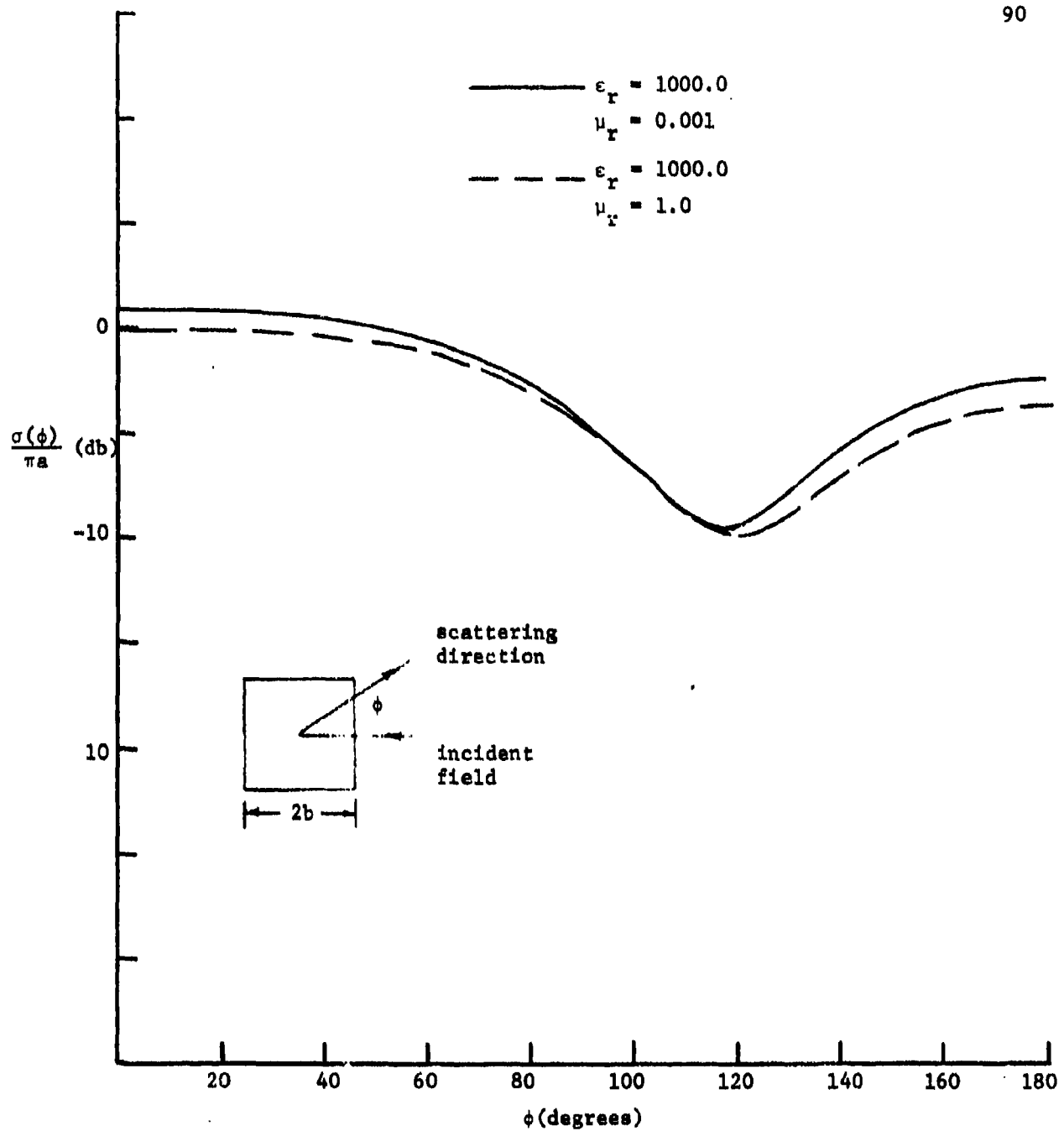


Fig. 4-23. Normalized scattering cross section of a square cylinder with  $kb = 1.4$ , perpendicular polarization (TE).

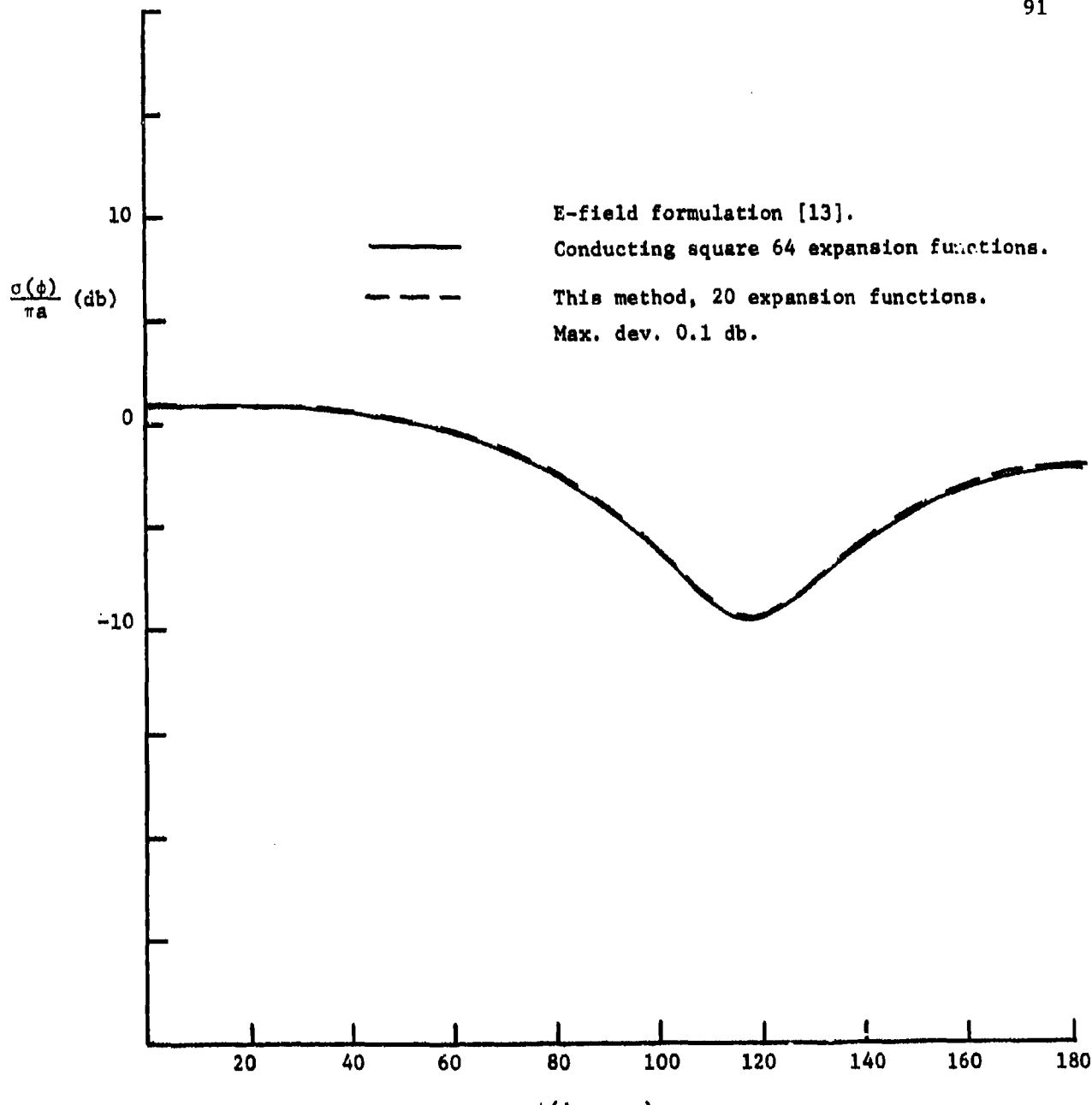


Fig. 4-24. Normalized scattering cross section of a square cylinder with  $\epsilon_r = 10000.0$ ,  $\mu_r = 0.0001$ ,  $kb = 1.4$ , perpendicular polarization (TE).

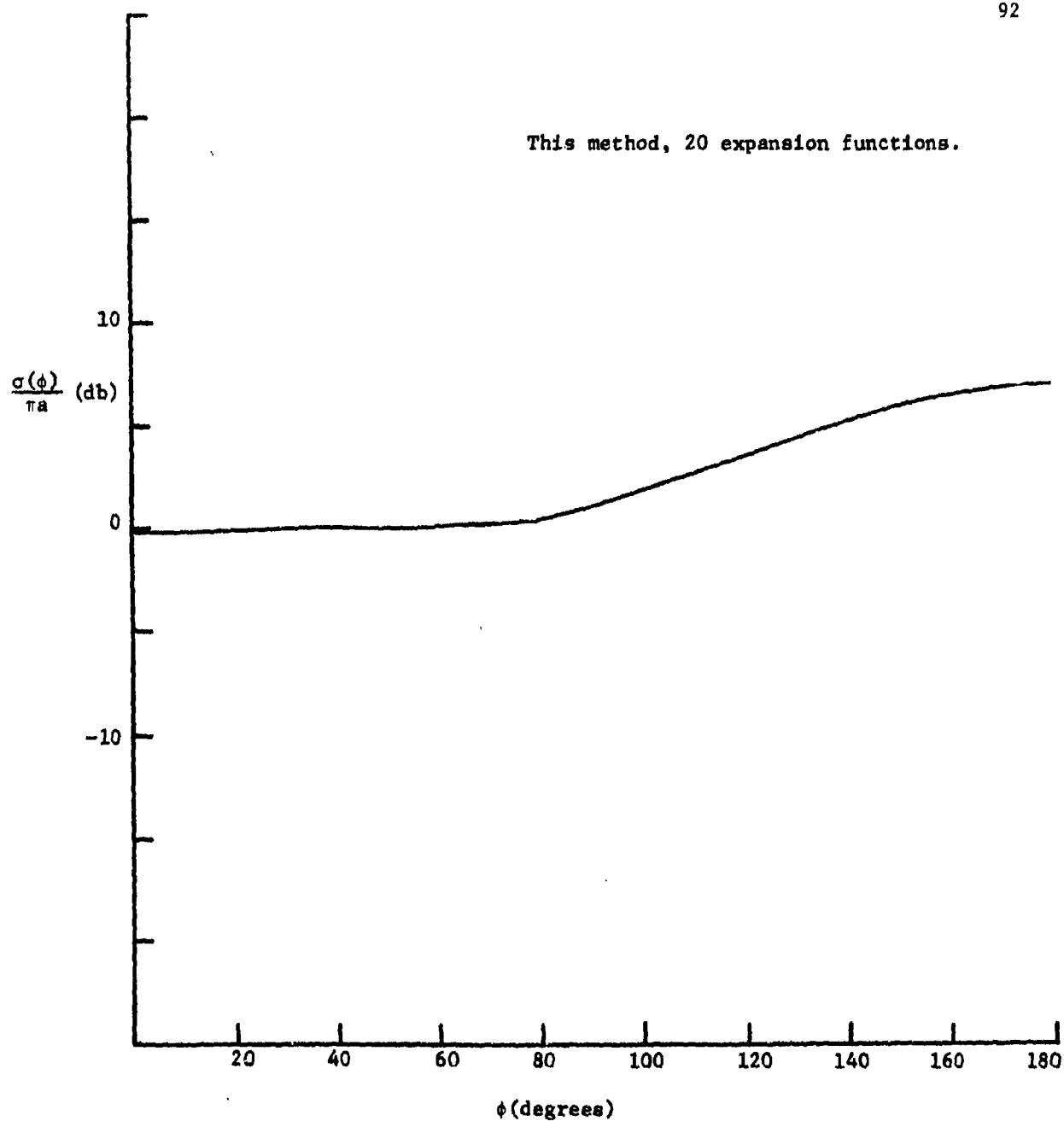


Fig. 4-25. Normalized scattering cross section of a square cylinder with  $\epsilon_r = 9.0$ ,  $\mu_r = 1.0$ ,  $kb = 1.4$ , perpendicular polarization (TE).

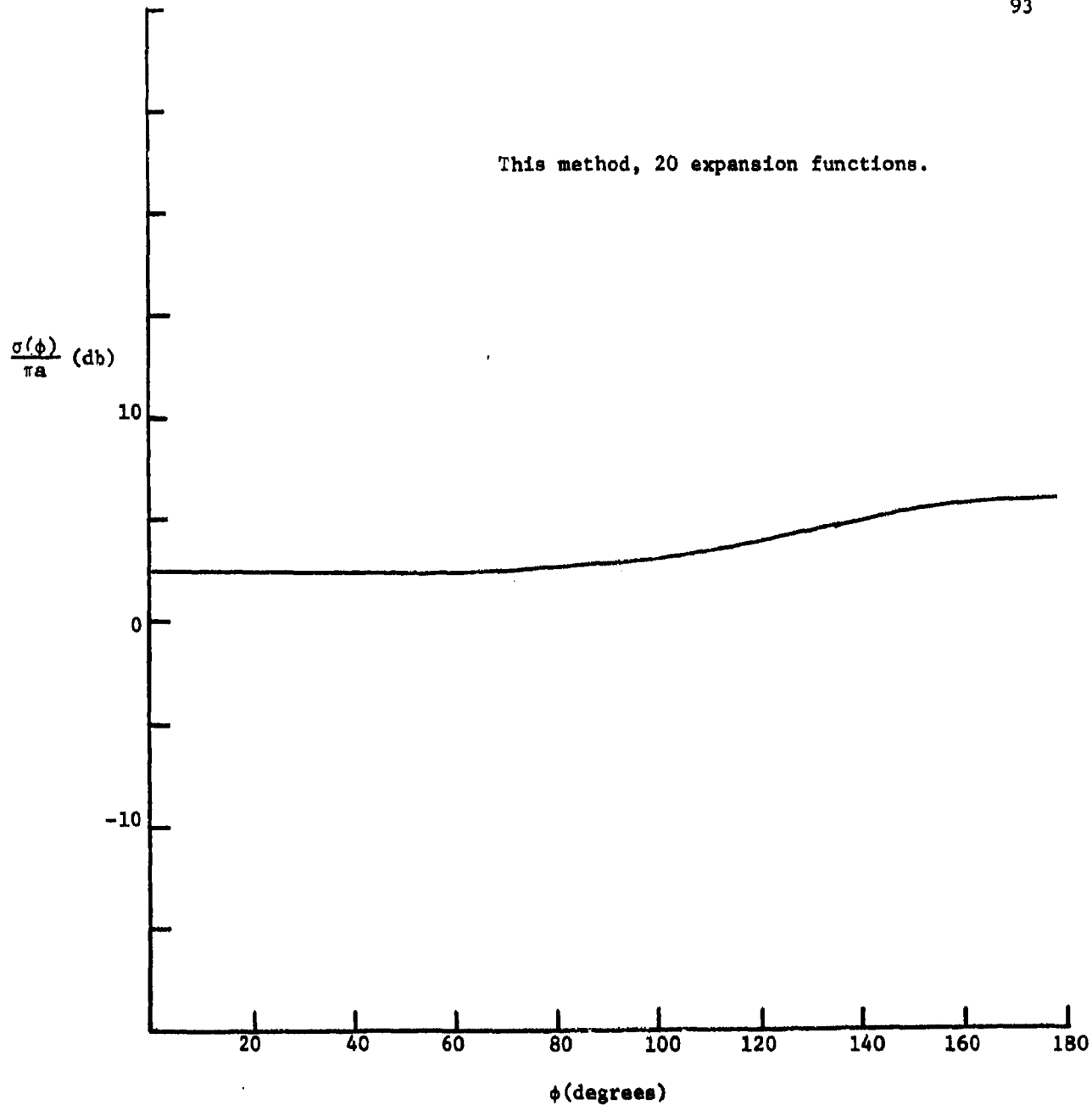


Fig. 4-26. Normalized scattering cross section of a square cylinder with  $\epsilon_r = 100.0$ ,  $\mu_r = 1.0$ ,  $kb = 1.4$ , parallel polarization (TM).

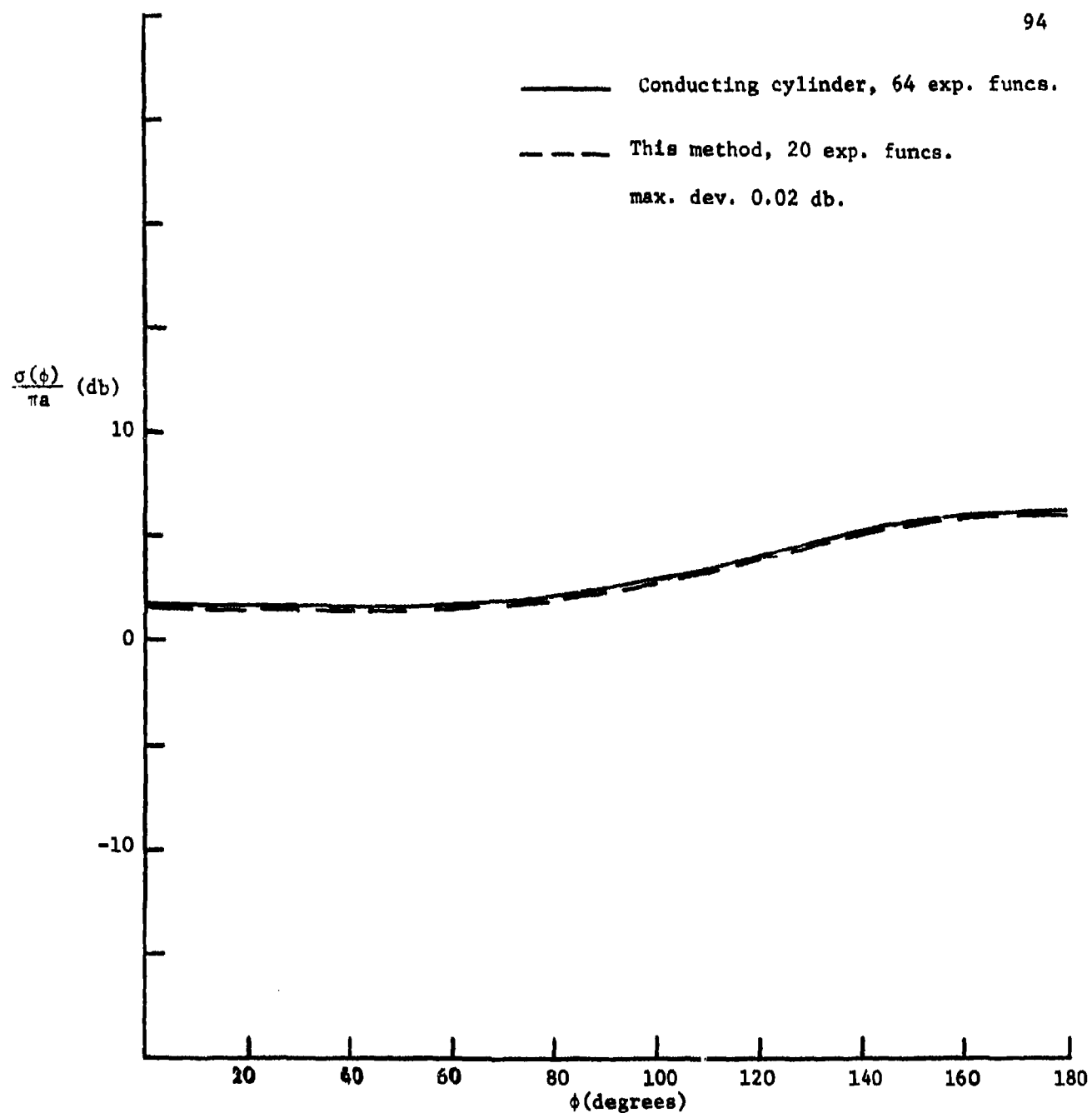


Fig. 4-27. Normalized scattering cross section of a square cylinder with  $\epsilon_r = 10000.0$ ,  $\mu_r = 0.0001$ ,  $kb = 1.4$ , parallel polarization (TM).

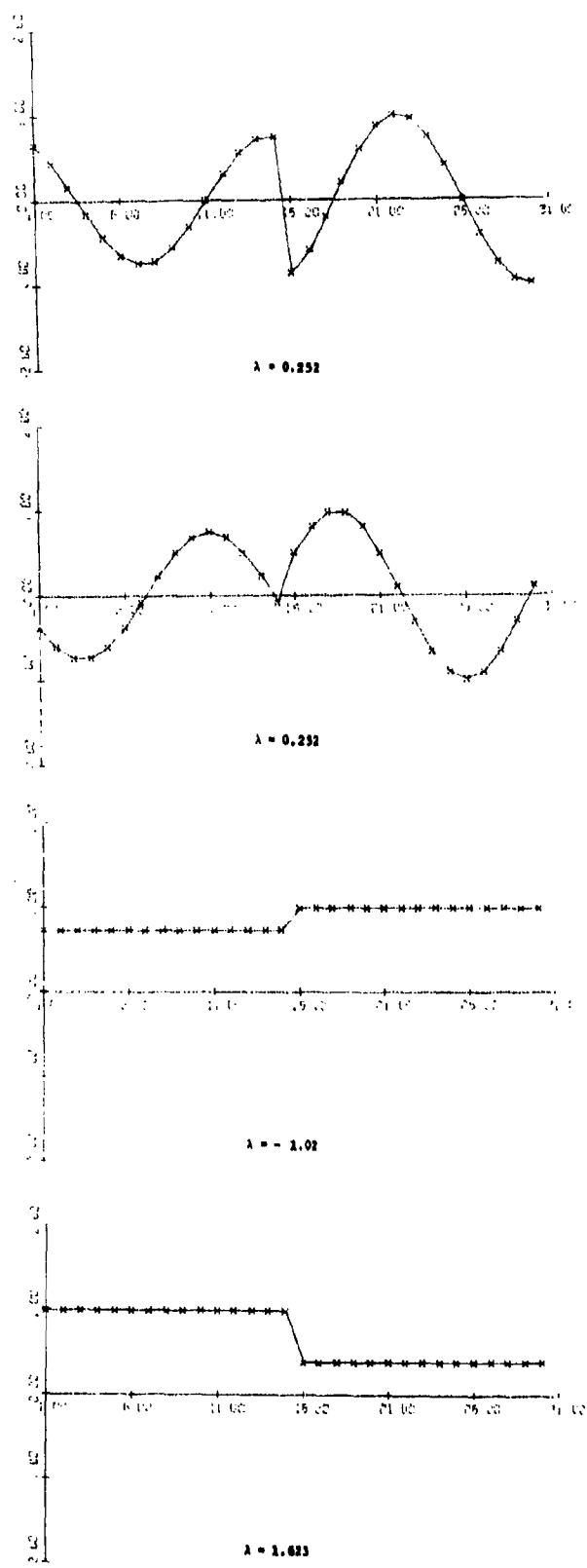


FIG. 4-20. Characteristic currents for a circular cylinder,  $\epsilon_r = 9.5$ ,  $\mu_r = 0.7$ , perpendicular polarization.

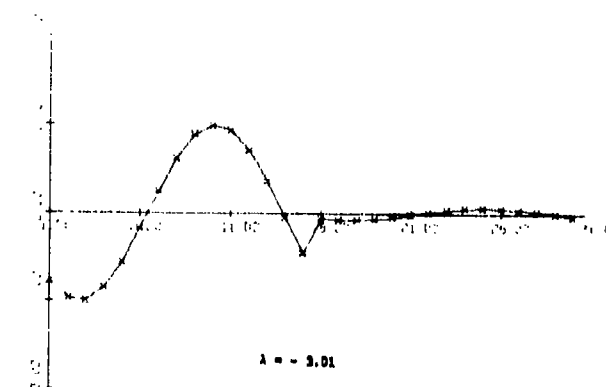
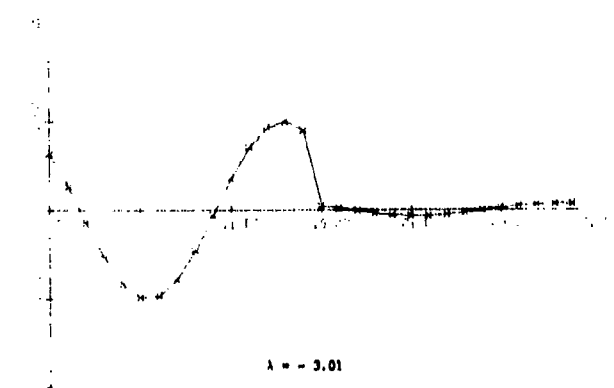
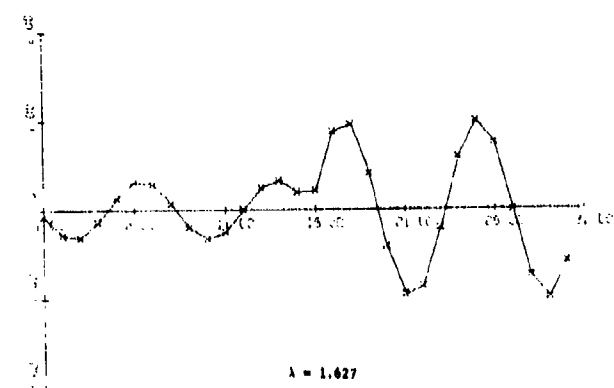
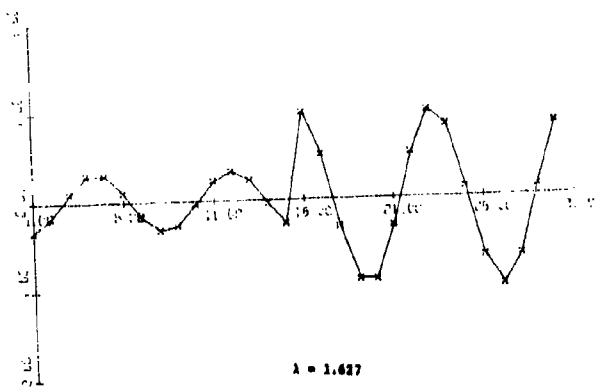
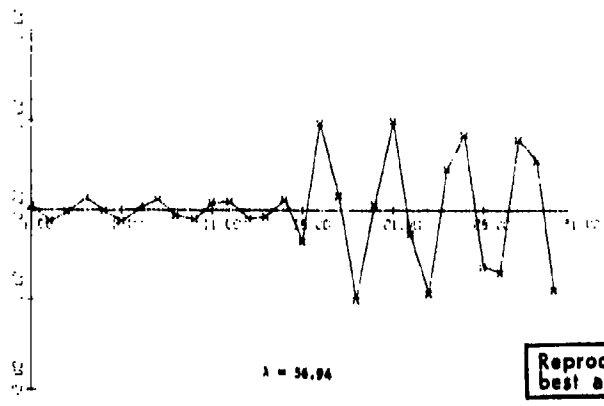
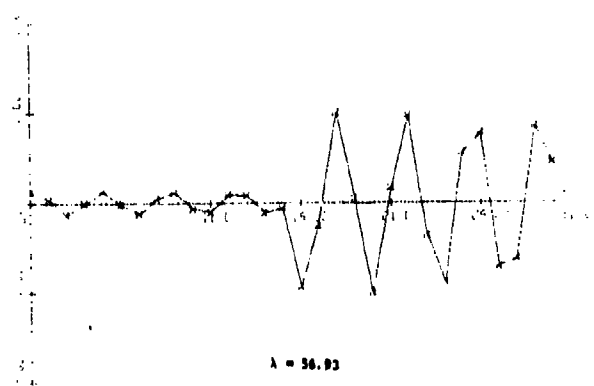
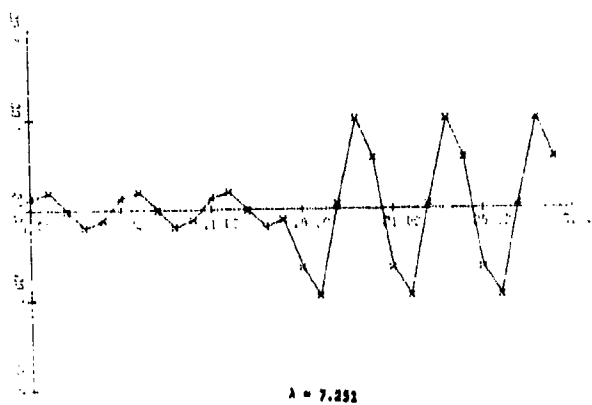
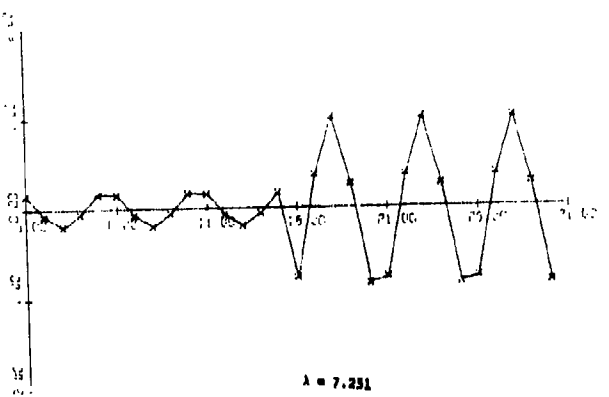


FIG. 4-28 continued



Reproduced from  
best available copy.

Fig. 4-28 continued

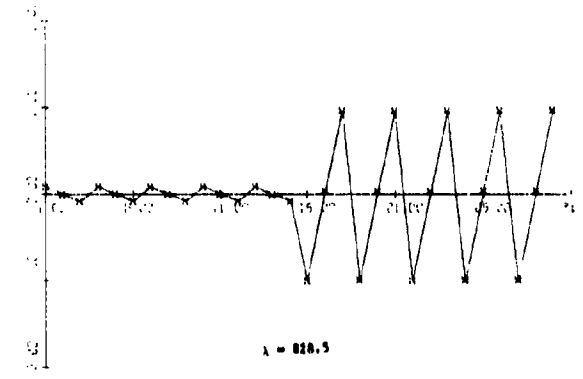
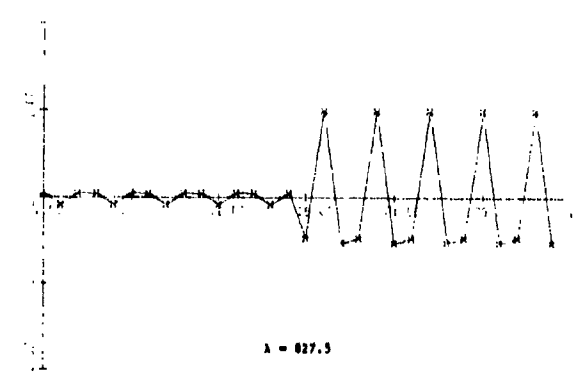
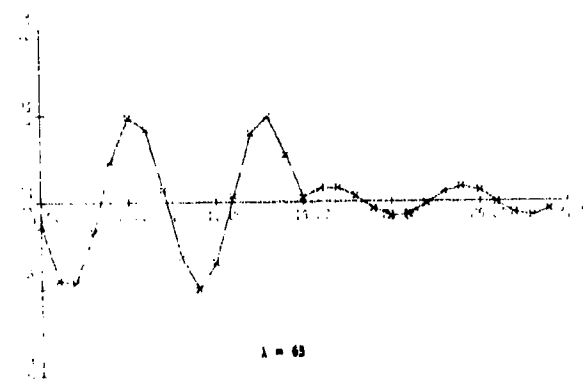
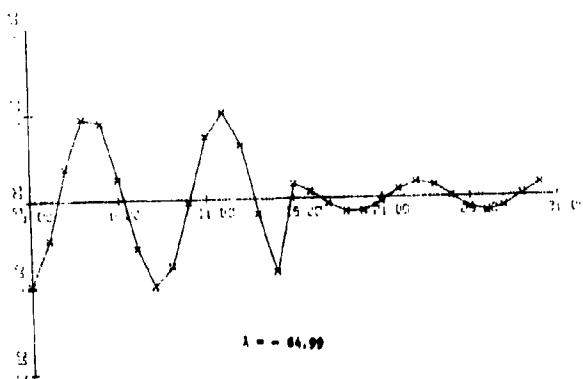
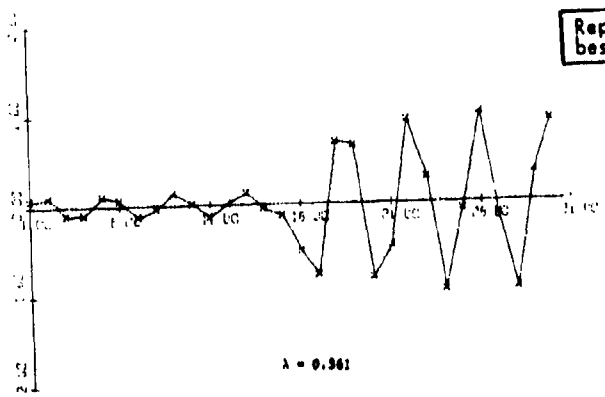
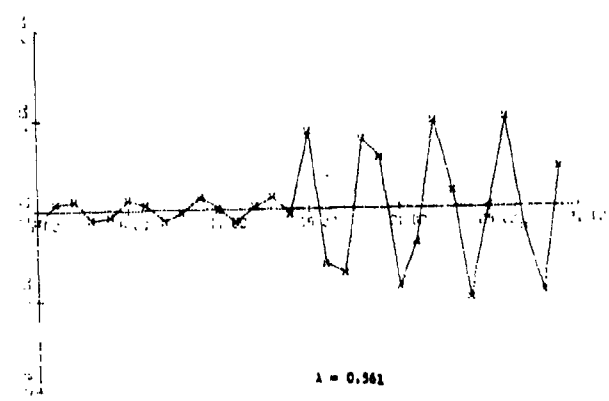
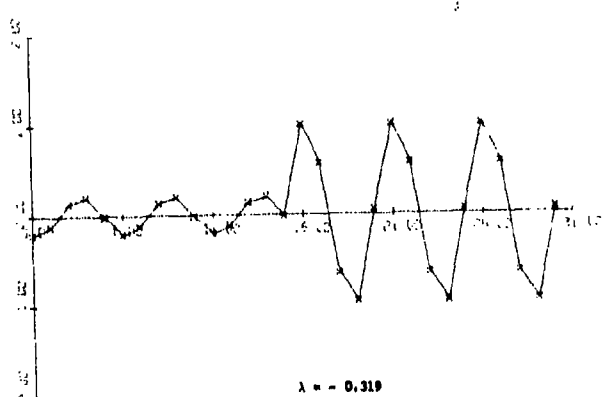
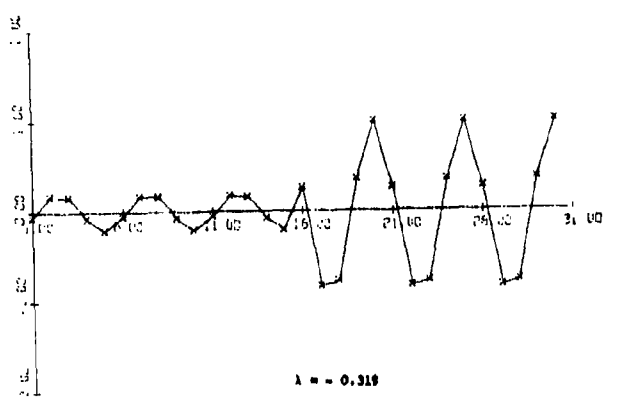


Fig. 4-20 continued.



Reproduced from  
best available copy.

Fig. 4-39. Characteristic currents for a circular cylinder,  $\epsilon_r = 50.0$ ,  
 $ha = 0.7$ , perpendicular polarization.

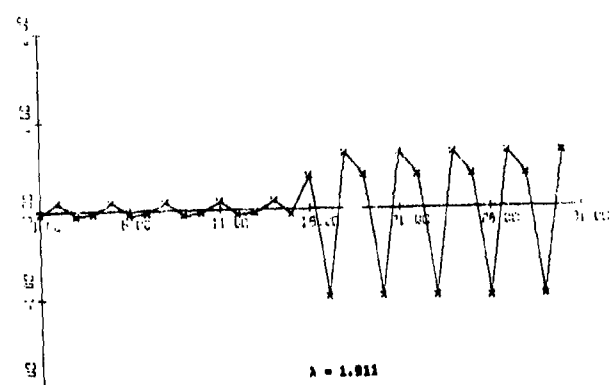
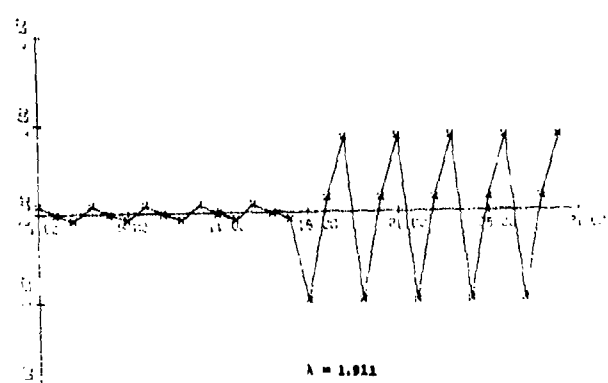
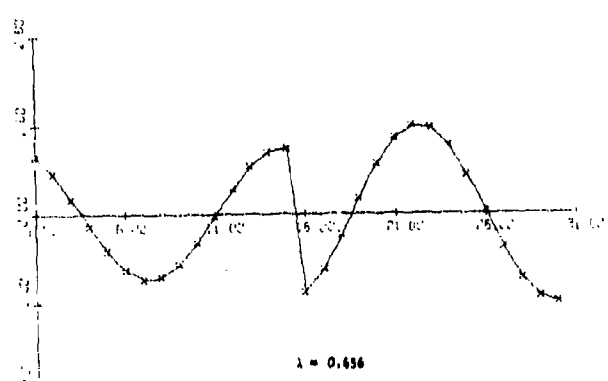
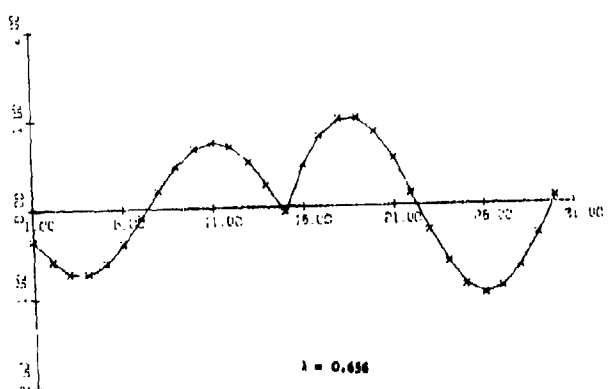


FIG. 4-20. continued.

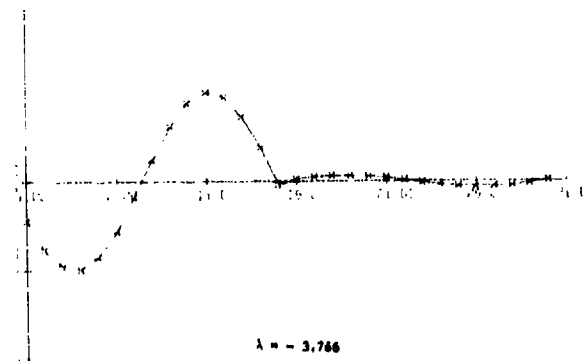
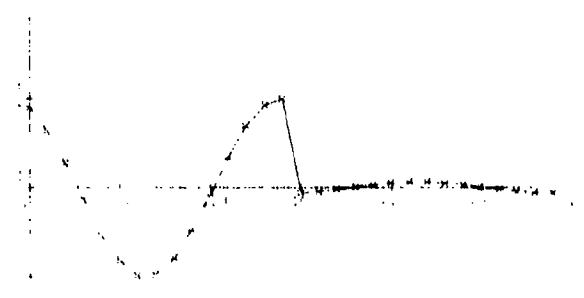
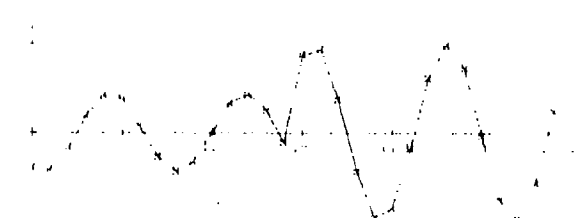
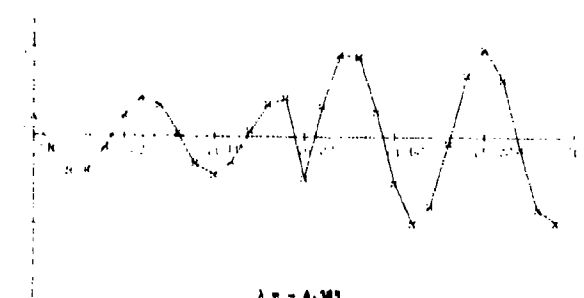
 $\lambda = -3.766$  $\lambda = -3.766$  $\lambda = -4.385$  $\lambda = -4.385$ 

Fig. 4-29, continued.

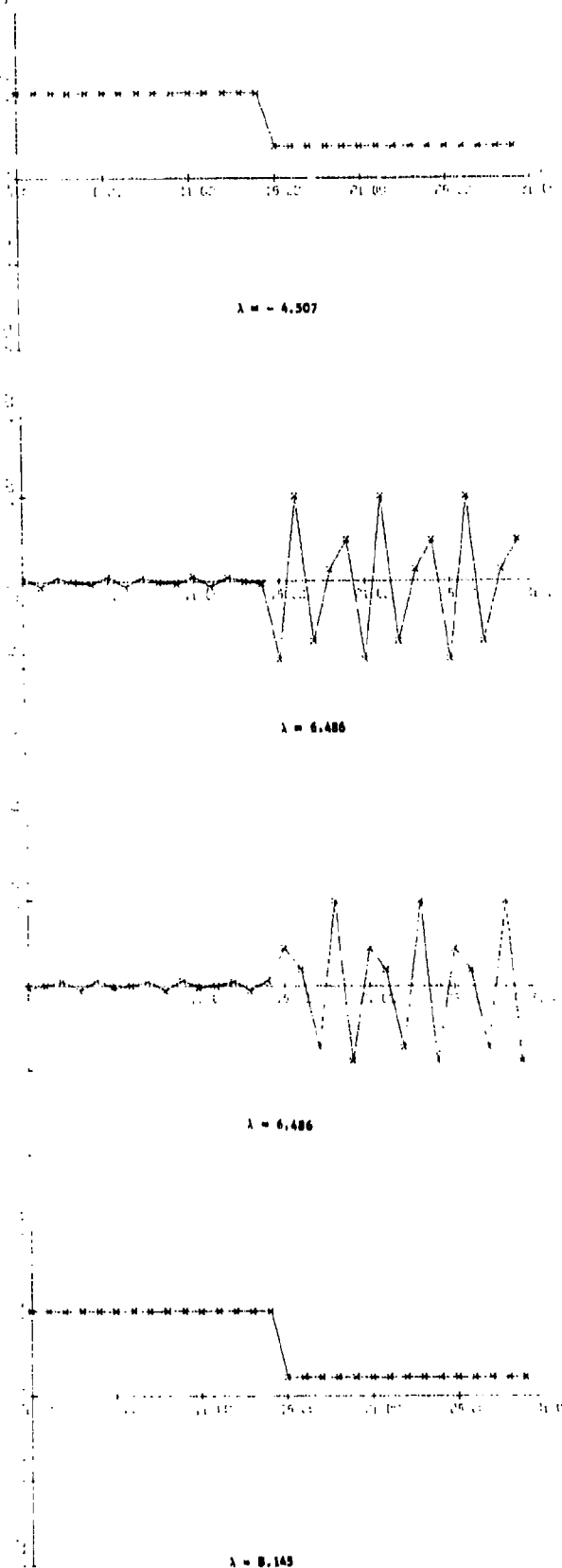


Fig. 4-29. Continued.

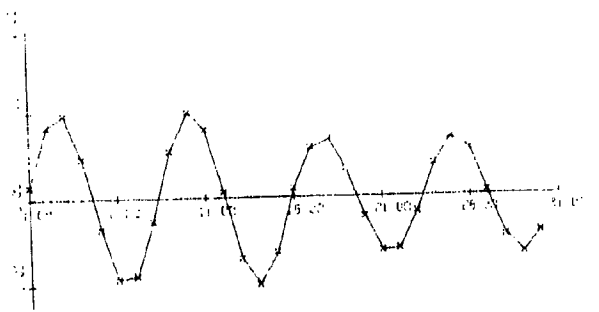
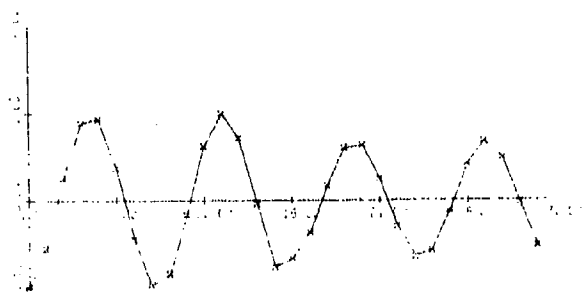
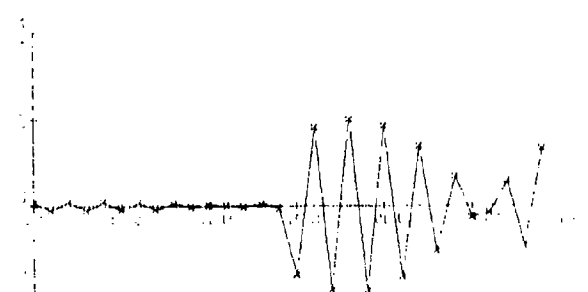
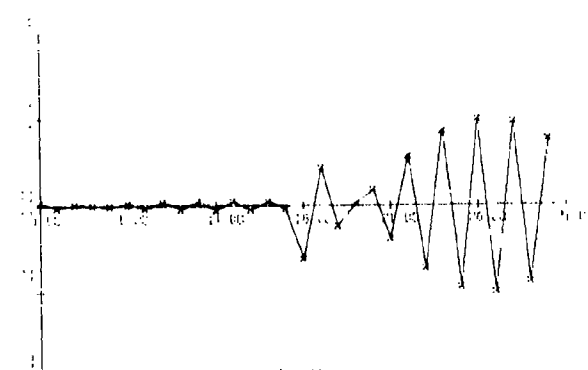
 $\lambda = -29.03$  $\lambda = -29.03$  $\lambda = 36.65$  $\lambda = 36.66$ 

FIG. 4-19. continued.

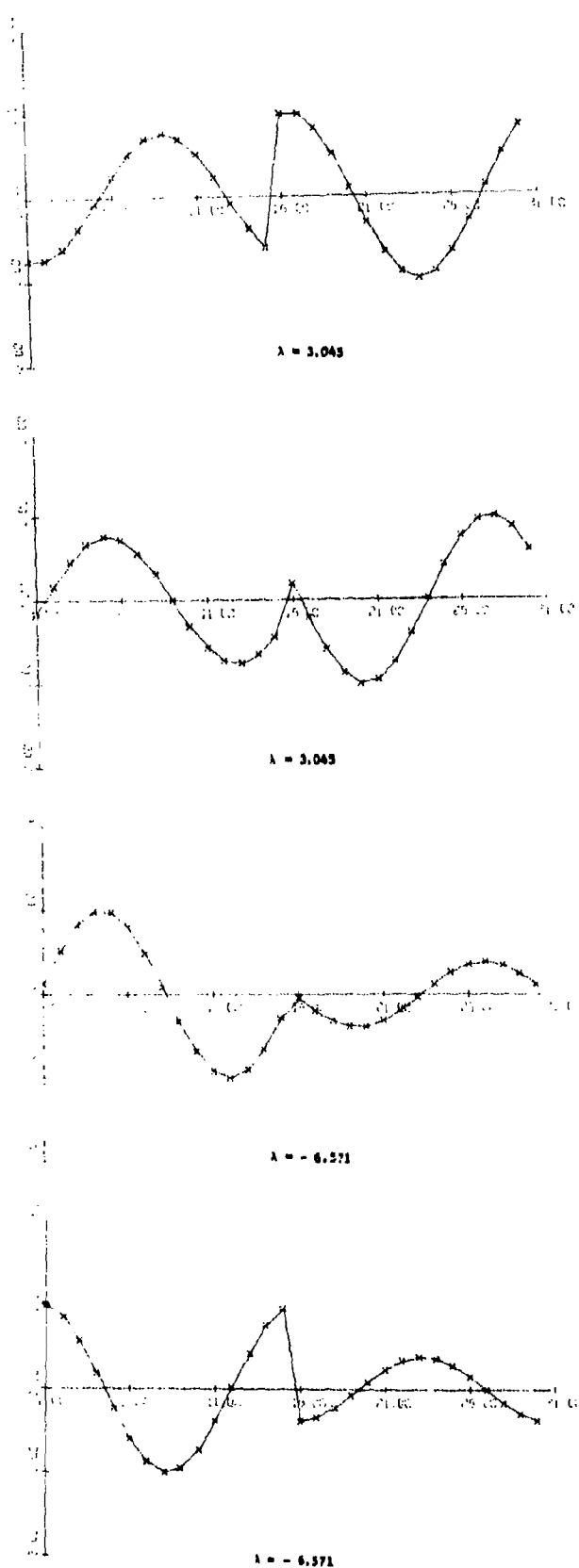


Fig. 4-30. Characteristic currents for a circular cylinder,  $c_2 = 1.36$ ,  $h_2 = 0.7$ , perpendicular polarisation.

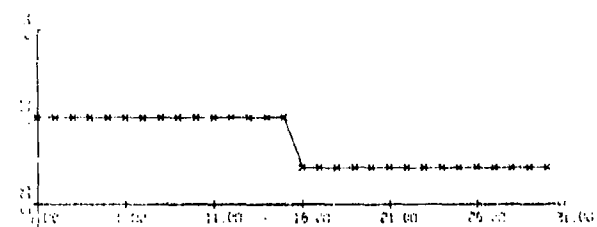
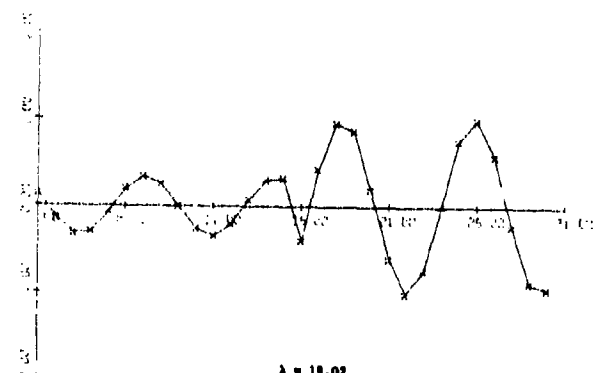
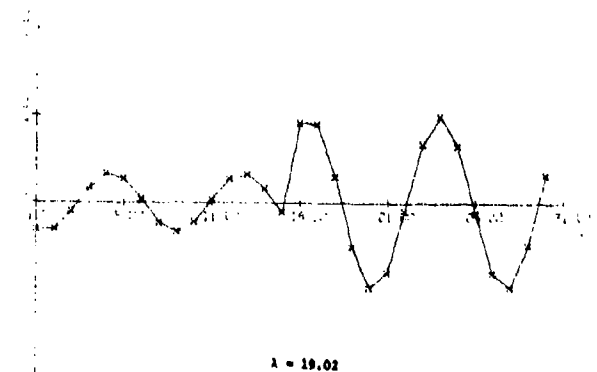
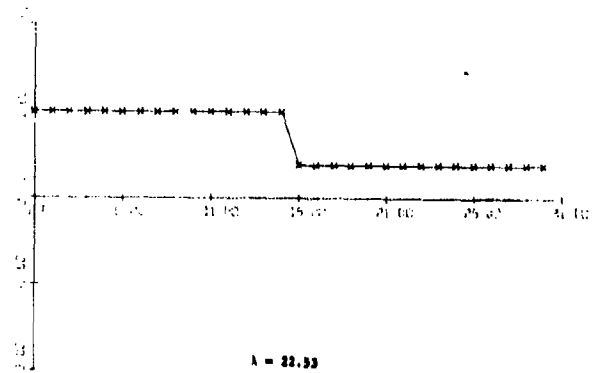
 $\lambda = -16.53$  $\lambda = 19.02$  $\lambda = 19.02$  $\lambda = 22.53$ 

Fig. 4-30. continued.

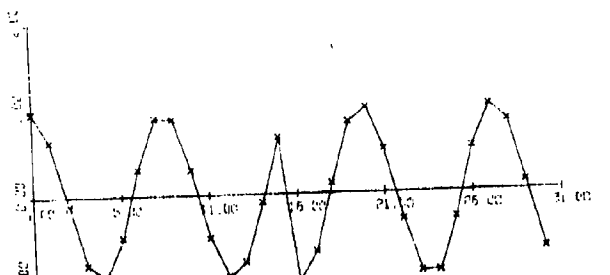
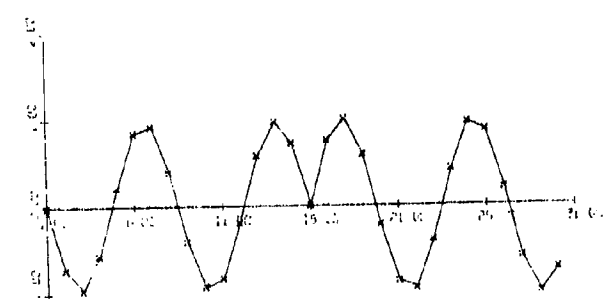
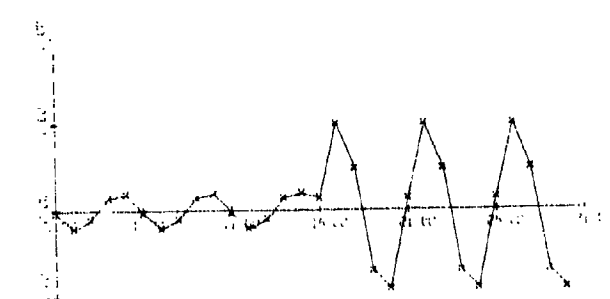
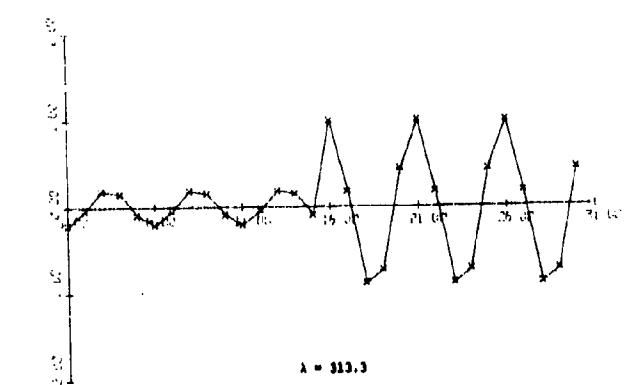

 $\lambda = 341.2$ 

 $\lambda = 341.3$ 

 $\lambda = 313.6$ 

 $\lambda = 313.3$ 

Fig. 4-30. continued.

## CHAPTER 5

## DISCUSSION

A surface formulation is developed for solving two-dimensional electromagnetic scattering problems. A basic theory for characteristic modes of dielectric and magnetic bodies based on the surface formulation is derived. The method of computing characteristic modes can be used for homogeneous material bodies of arbitrary shape provided the body is not electrically large. The characteristic modes of material bodies have most of the properties of those for perfectly conducting bodies, and should find similar uses. The theory presented here is in contrast to that for the volume formulation [4]. The basic difference is that the current in the material body has been treated as equivalent surface currents instead of a volume distribution. The characteristic currents are real and their corresponding eigenvalues are also real. The eigenvectors given by equation (3-73) are those corresponding to the lowest eigenvalues, and they are usually very efficient radiators. Characteristic currents associated with large eigenvalues generally indicate higher order modes which do not radiate very much.

Two ways for computing the scattered fields are given here. The simple material cylinders. The matrix inversion method is easier to use and gives very good results. The characteristic mode method may require slightly longer computing time, but it does provide more insight into the problem. As in the conducting body case, the characteristic mode method should prove to be of value, both theoretically and computationally for scattering and radiation problems. The versatility of characteristic modes has been

adequately demonstrated in analysis and synthesis problems dealing with conducting bodies. The two approaches are based on a surface formulation, and they require the material body to be homogeneous since the unknowns are surface currents. For inhomogeneous bodies the surface formulation is not appropriate, and a volume current distribution must be used which requires sample points inside the scattering body.

## APPENDIX A

## MATRIX ELEMENTS FOR PARALLEL POLARIZATION

For the incident field

$$\tilde{E} = u_z e^{-jk \cdot \tilde{r}_m} \quad (A-1)$$

the following formulas are obtained ( $u_z$  is the axially directed unit vector). The procedures involved are identical to that given in Chapter 2, except that the directions of the surface currents are different.

A.1 Formulas for [Z] Matrix Elements

$$Z_{mn} = -\frac{\omega_0}{4} \sum_{q=1}^4 \sum_{p=1}^4 T_p T_q Z \quad (A-2)$$

where

$$Z = \Delta t_p \Delta t_q H_o^{(2)}(kR_{pq}) \quad (\text{non-coincident intervals})$$

$$= t_p [1 - j \frac{2}{\pi} \log \frac{\gamma k \Delta t_p}{4a}] \quad (\text{coincident intervals})$$

A.2 Formulas for [B] Matrix Elements

$$B_{mn} = -\frac{1}{4} \sum_{q=1}^4 \sum_{p=1}^4 \Delta t_q T_p T_q B \quad (A-3)$$

$$B = -\frac{k_{ii_1}^{(2)}(kR_{pq})}{R_{pq}} [- (x_p - x_q) \Delta y_p + (y_p - y_q) \Delta x_p] \quad (\text{non-coincident intervals})$$

$$= -j2 \quad (\text{coincident intervals})$$

A.3 Formulas for [C] Matrix Elements

$$C_{mn} = -\frac{1}{4} \sum_{q=1}^4 \sum_{p=1}^4 \Delta t_p T_p T_q C \quad (A-4)$$

$$C = -\frac{kH_1^{(2)}(kR_{pq})}{R_{pq}} [ - (y_p - y_q) \Delta x_q + (x_p - x_q) \Delta y_q ]$$

(non-coincident intervals)

$$= -j2 \quad \text{(coincident intervals)}$$

A.4 Formulas for [Y] Matrix Elements

$$Y_{mn} = -\frac{1}{4} \sum_{q=1}^4 \sum_{p=1}^4 \Delta t_p \Delta t_q [ \omega e T_p T_q (u_p \cdot u_q) - \frac{1}{\omega \mu} T_p' T_q' ] Y \quad (A-5)$$

where

$$Y = H_0^{(2)}(k R_{pq}) \quad \text{(non-coincident intervals)}$$

$$= 1 - \frac{2}{\pi} \log \frac{\gamma k \Delta t_p}{4e} \quad \text{(coincident intervals)}$$

A.5 Excitation Matrix Elements

$$v_m^i = \sum_{p=1}^4 T_p \Delta t_p e^{jk(x_{mp} \cos \phi^i + y_{mp} \sin \phi^i)} \quad (A-6)$$

$$I_m^i = -\frac{1}{n} \sum_{p=1}^4 T_p [ -\Delta x \sin \phi^i + \Delta y \cos \phi^i ] e^{jk(x_{mp} \cos \phi^i + y_{mp} \sin \phi^i)} \quad (A-7)$$

## APPENDIX B

### COMPUTER PROGRAMS

B.1 Listing of the program to compute scattering cross sections,  
perpendicular polarisation(TE).



#### N.2 Listing of the program to compute characteristic currents.

```

11=11+1
12=11+0
13=120,X+1,NM
14=X-11,NM
15=(11)+A22*(J11*B22*(K11*A21))
20 CONTINUE
10 CONTINUE
00 FORMAT(1X,A11,I11,F14.7)
00 FORMAT(1D22*222 (INVERSE)/(10IX,F11.6))
11=0
00 R1=1+1,0M
14=(1-J1)*NM,0M
00 R2=1+1,0M
12=1+1+0M
J1=J1+1
13=J1+0
00 R3=K1+1,0M
K1=J2+K
K2=J3+K
14=(J1+1)+(K1+1)+A22*(K1)+A21*(K2)
X1 CONTINUE
R2 CONTINUE
R1 CONTINUE
02=0
00 R4=1+1,0M
03=(J1+1),0M
05=(J1+1),0M
00 R5=1+1,J1
02=J2+1
14=J3+1
K1=J2+K
J2=J3+K
14=(J2+1)+A(K1)+B(K2)
R1 CONTINUE
K1=J2+K+(J2+1)+B(K1)+B(K2)
R1 CONTINUE
R1 CALL EIGEN(R,V,0M,0)
12= CALL EIGEN(R,V,0M,0)
J1=0
00 107,J1,0M
11=J1+1
AMBL1=J1+1,0
107 CONTINUE
00 WRITE(14,51)AMBL1,J1,0M
51 FORMAT(10I10,EIGENVALUES OF THE MATRIX R/(10IX,F14.7))
00 R1=1+1,0M
11=J1+1+0M
14=(J1+1),0M
00 R2=1+1,0M
00 R3=1+0M
12=J3+1
12=(J3+1)+J2+1,0M,0
42 CONTINUE
41 CONTINUE
120
J1=0
00 240,1+1,0M
11=J1+1
00 J1=0
00 250,1+1,0M
11=J1+1
00 J1=J1+1
00 J1=J1+1+1,0M
00 J1=J1+1+1,0M
250 CONTINUE
120
240 CONTINUE
00 WRITE(14,52)1,0M,0
52 FORMAT(10I10,EIGENVALUES OF THE MATRIX R/(10IX,F14.7))
51=0
00 03,1+1,0M
01=1+1,0M
00 04,1+1,0M
12=1+1+1,0M
12=12+1,0
00 05,K1,0M
V1=(K1+1)+0M
02=K1+1
12=12+1+12*(J1+1)+13*(K1)+12*(K2)
45 CONTINUE
44 CONTINUE
43 CONTINUE
K1=J1+1
L1=J1+1
00 260,1+1,0M
00 J1=0,0
00 270,0M+0N
11=L1+1
00 J1=J1+1+1,0M
00 J1=J1+1+1,0M
00 J1=J1+1+1,0M
270 CONTINUE
120
260 CONTINUE
00 WRITE(14,261) (0011),1+1,0M
261 FORMAT(10I10,EIGENVALUES OF THE MATRIX R/(10IX,F14.7))
00 WRITE(14,262) (1211),1+1,0M
262 FORMAT(10I10,EIGENVALUES OF THE MATRIX R/(10IX,F14.7))
467 00 96,1+1,0M
51=0,
01=1+1,0N
14=(1-J1),0NN
17=0
00 97,1+1,0N
02=0,0
F1=J2+0
34=J7-J71
00 98,K1+1,0N
K2=K3+1
K1=K1+1+0N+J7
F1=(J1+1)+(J1+1)+J2+1,0M,0
48 CONTINUE
47 CONTINUE
12=J1+1
12=(J1+1)+0N
00 WRITE(14,141) AMBL1
14=FORMAT(10I10,EIGENVALUES FOR WHICH LAMBDA = 1+011,01
14=FORMAT(10I10,EIGENVALUES FOR WHICH LAMBDA = 1+011,01
00 WRITE(14,401)J11,J12,J13,J14

```





117

**B.4 Listing of the program to compute scattering cross sections  
parallel polarization (M).**

**RETRIBUTIVE JUSTICE**

10. FORMULATE A WORKING ARGUMENT TO SHOW THAT THE BESSEL FUNCTION OF ORDER  $n$  IS ZERO.

FUNCTION (NO. 101)  
EX-CHIEF OF STAFF FOR THE AIR FORCE  
MAY 1951-1955

$f = \text{ABS}(x)$

187,63,3,000-10-1  
8-22-84

**RECEIVED** **SEARCHED** **INDEXED** **SERIALIZED** **FILED**  
**NOV 2 1968**

10. FORMATION OF A NEW STATE IN THE UNION AND THE CONSTITUTIONALITY THEREOF

TO COMPUTE THE COEFFICIENTS OF AN EXPONENTIAL FUNCTION, THAT HAS BEEN EXPRESSED  
IN CALCULATING A HEGMANN FUNCTION OF ORDER ONE ABSOLUTE.

RETURN  
END

**STRUCTURE OF THE  
COMPLEX CLEAVAGE SITE**

#### **DIMENSION (CREDO)**

100-20-10161  
181118

20 CONTINUE  
H1=0

00-10 Mu{+1}

$K \neq M$   
 $K \neq \{M\} \neq K$

STEAMING FISHES FOR 2111 & GESTA MALEIC ACID 2111  
0012-18-M-11

K100141  
A MANAGEMENT SYSTEM FOR THE ENVIRONMENT

18(32+5)1 2,2,6

**ANSWER**

7 CONTINUE  
150H(M)

**ENHANCED  
ENHIGLICH**

**CHARTS**  
**K2 • M1, K**

5.100x6.102)





8.5 Listing of the program to compute scattering cross section from characteristic currents.

```

//YINH-ANG JDN (0639,FF,7,2,900), ICHANGYI, REGION=10K, CLASS=A
// FILE NAME:IV
//CDR,T02P001 DD SYSCONTR
//D01,SYSTIN DD *
$JNA          GMANG
      SUBROUTINE EXMH(PHI,OK)
      COMPLEX CJ
      COMPLEX PP
      COMPLEX VN1
      COMPLEX AJ,EV
      COMMON AJ(9001),EV(301),VN1(301),PV(301),CJ
      COMMON F1(9001),T(801),DX(321),DY(321),YM(321),ML(321)
      COMMON N2,N,NM,JM
      ETA=37A,75D
      N=(N2-1)/2
      CHGCE(PHI)
      SRSIN(PHI)
      L=0
      L=0
      (M) ZDN 13=3,N2=2
      L1=1
      L1=L1
      L1=3-N
      L2=L3-2
      L3=L3-1
      L4=L3-1
      HV(11)=0.
      HV(IJ,IJ)=0.0
      M=2D M=1,I=4
      LL=M+1
      HV(XM(M)+CP*YM(M)*SP)*OK
      DP=(IL(M)+SP)*YM(M)*CH
      C=COS(CP)
      SP=SIN(CP)
      DP=(CP*PC*PEP)+TILL)
      EV(I1,I1)=PP*DP+EV(I1,I1)
      EV(I1,I2)=PP*DLM)+PV(IJ,IJ)
    P10 CONTINUE
      EV(I1,I1)=PP*EV(I1,I1)
      EV(I1,I2)=CJ*EV(IJ,I2)
      L=L+2
    200 CONTINUE
      RETURN
      END
      COMPLEX FC(1301)
      COMPLEX CAMD(1301),VK(1301)
      COMPLEX VN1,CJ,MHD
      COMPLEX AE,AJ,PP
      COMMON AJ(9001),EV(301),VN1(301),EV(301),CJ
      COMMON F1(9001),T(801),DX(321),DY(321),YM(321),ML(321)
      COMMON N2,N,NM,JM

```

```

L=+2
20 CONTINUE
101 FORMAT(0H15.7)
READ(11,201) J,M
201 FORMAT(1X)
WRITE(15,201) J,M
N=J*M*M
READ(11,101) (FC(I,J),I=1,NM)
READ(11,101) (FC(I,J),I=1,NL)
WRITE(15,202) (AM(I,J),I=1,NL)
WRITE(15,201) (FC(I,J),I=1,NM)
WRITE(15,201) (FC(I,J),I=1,NL)
202 FORMAT(0H15.7,1H((1),F14.7)))
203 FORMAT(0H10PNORMKNT/(B1(X,F14.7)))
      DO 50 J=1,M
      J=(J-1)*NM
      DO 60 I=1,NL
      I=(I-1)*NL
      FC(I,J)=FC(I,J)/NM
50 CONTINUE
60 CONTINUE
50 CALL FMXKANS(GK)
      L=0
      DO 100 I=1,NM
      VN(I)=0.0
      DO 110 J=1,NL
      L=L+1
      VN(I)=VN(I)+FC(I,J)*VN(J)
110 CONTINUE
      LL=LN*M
100 CONTINUE
      DO 210 I=1,NM
      VAI(I)=VN(I)*FC(I,I)
210 CONTINUE
      LL=LN*M
      DO 220 J=1,NM
      LL=LN*M
      DO 225 K=1,NL
      L=L+1
      AJ(L)=VAI(I)*FC(I,K)
225 CONTINUE
      AJ(L)=AJ(L)/NM
220 CONTINUE
      DO 230 I=1,NM
      AF(I)=0.0
      DO 235 J=1,NM
      K=(J-1)*NM+1
      AF(I)=AF(I)+AJ(K)
235 CONTINUE
      AF(I)=AF(I)/NM
230 CONTINUE
      WRITE(15,274)
274 FORMAT(//,*1 SCATTERING ANGLE = PMT/(DM*(COS(LN*PI/RAD))**2))
      ANG=0.0
      PN=0.0
      DO 320 I=1,NL
      CALL FMXKANS(GK)
      MN=0.0
      DO 340 J=1,NM
      MN=MN+AJ(J)*AF(I)
      H=DEV(J)*AF(I)+MN
340 CONTINUE
      350 CONTINUE

```

## REFERENCES

1. R. J. Garbacz, "A Generalized Expansion for Radiated and Scattered Fields," Ph.D. Dissertation, Ohio State University, Columbus, 1968.
2. R. F. Harrington and J. R. Mautz, "Theory of Characteristic Modes for Conducting Bodies," IEEE Trans. on Antennas and Propagation, vol. AP-19, No. 5, September 1971.
3. R. F. Harrington and J. R. Mautz, "Computation of Characteristic Modes for Conducting Bodies," IEEE Trans. on Antennas and Propagation, vol. AP-19, No. 5, September 1971.
4. R. F. Harrington, J. R. Mautz, and Y. Chang, "Characteristic Modes for Dielectric and Magnetic Bodies," IEEE Trans. on Antennas and Propagation, vol. AP-20, No. 2, March 1972.
5. R. F. Harrington, Field Computation by Moment Methods, New York: Macmillan, 1968.
6. R. F. Harrington, Time-Harmonic Electromagnetic Fields, New York: McGraw-Hill, 1961.
7. G. T. Ruck, D. E. Barrick, W. D. Stuart, and C. K. Krichbaum, Radar Cross Section Handbook, vol. 1, New York: Plenum Press, 1970.
8. J. R. Mautz and R. F. Harrington, "Radiation and Scattering from Bodies of Revolution," Appl. Sci. Res., vol. 20, June 1969.
9. R. F. Harrington and J. R. Mautz, "Radiation and Scattering from Loaded Bodies of Revolution," Appl. Sci. Res., vol. 26, 1971.
10. R. F. Harrington and J. R. Mautz, "Control of Radar Scattering by Reactive Loading," IEEE Trans. on Antennas and Propagation, vol. AP-20, No. 4, July 1972.
11. R. F. Harrington and J. R. Mautz, "Modal Analysis of Loaded N-port Scatterers," Scientific Report No. 16 on Contract No. F19628-68-C-0180 between Syracuse University and Air Force Cambridge Research Laboratories, AFCRL-72-0179, March 1972.
12. R. F. Harrington and J. R. Mautz, "Synthesis of Loaded N-port Scatterers," Scientific Report No. 17 on Contract No. F19628-68-C-0180 between Syracuse University and Air Force Cambridge Research Laboratories, AFCRL-72-0665, October 1972.
13. R. F. Wallenberg and R. F. Harrington, "Radiation from Apertures in Conducting Cylinders of Arbitrary Cross Section," IEEE Trans. on Antennas and Propagation, vol. AP-17, No. 1, Jan. 1969